IMPROVING POWER SYSTEM SITUATIONAL AWARENESS DURING GEOMAGNETIC DISTURBANCES USING ESTIMATION AND VISUALIZATION

A Dissertation

by

CECILIA ASHLEY KLAUBER

Submitted to the Office of Graduate and Professional Studies of
Texas A&M University
in partial fulfillment of the requirements for the degree of

DOCTOR OF PHILOSOPHY

Chair of Committee,	Thomas J. Overbye
Committee Members,	Katherine Davis
	Timothy A. Davis
	Robert Nevels
Head of Department,	Miroslav Begovic

December 2020

Major Subject: Electrical Engineering

ABSTRACT

Due to the adverse effects of geomagnetic disturbances (GMDs) and geomagnetically induced currents (GICs) on the electric power grid there is increased interest in effective means of monitoring and visualizing such effects. As mitigation plans are now mandated for grid operators and research is being pursued regarding system operations and control during a GMD, the ability to know and understand the current state of the system in real time, especially with respect to GICs, is increasingly needed. To address these challenges, a GIC state estimation method is developed, improved upon, and tested. Additional applications to enhance situational awareness and inform decision making during a GMD are covered, including bad data detection, improvement upon the traditional state estimation methodology, and integration with existing power system analysis and interactive software.

A GIC estimation method is proposed which leverages neutral GIC measurements and available electric field data to estimate the underlying electric field. Distinct from the traditional ac state estimation problem, this dc method leverages the linear relationship between the measurements and newly-defined states for a fast and efficient solution. The performance of the estimator is tested under different scenarios, such as varying measurement error, measurement availability, and granularity of electric field states. The estimator is shown to be an effective means of providing system-wide understanding throughout these scenarios.

The concepts of observability and redundancy are defined for this new estimation method, laying a foundation for an extension to bad data detection. The least absolute value objective is invoked and identification thresholds designed such that outlier data in the measurement set can be detected, identified, and suppressed. Bad measurements are able to be reliably identified, even in the presence of multiple bad data.

The traditional state estimation methods are extended to include GIC modeling, measurements, and states. It is shown to improve the performance in terms of average error and convergence time during a GMD.

Other applications and extensions are explored, including non-Gaussian noise considerations, comparison of available real-time electric field data, and real-time visualization of GICs from real data.

DEDICATION

To my family, for their love and support

ACKNOWLEDGMENTS

This experience pursuing and completing my PhD has been a journey with its ups and downs, and I am so very thankful for all who at some point have supported me.

I am thankful for my advisor and committee chair, Prof. Thomas J. Overbye, for his guidance and vision. His passion for and expertise in power systems is truly an inspiration. I would also like to extend my gratitude to the rest of my committee (Dr. Kate Davis, Dr. Robert Nevels, and Dr. Tim Davis), for their time and insight.

I am grateful to the Team Overbye Research Group and the spirit of collaboration and camaraderie that has been fostered among us. I will miss bouncing around research ideas and taking bubble tea breaks with you all.

I am thankful for the other communities that have been my support network and family over my graduate school years: the University of Illinois Power Group, the Society of Women Engineers, Twin City Bible Church, the Schiblers/TAMU Association of Baptist Students, and anyone else who has enjoyed an evening of board games or trivia with me.

Finally, I will forever be grateful for the love and support of my family. My sisters, for listening to me when times are hard and celebrating with me when times are good. You are both so amazingly talented, thoughtful, and all-around awesome; I am proud to call you my sisters. My parents, for always encouraging and supporting me in the pursuit of my interests. I wouldn't be who I am today without your examples of hard work and love of learning.

CONTRIBUTORS AND FUNDING SOURCES

Contributors

This work was supervised by a dissertation committee consisting of Professor Thomas J. Overbye and Professors Robert Nevels and Katherine Davis of the Department of Electrical and Computer Engineer and Professor Timothy Davis of the Department of Computer Science. All work for the dissertation was completed independently by the student.

Funding Sources

This work is supported in part by the National Science Foundation under a Graduate Research Fellowship and NSF Award Number 1520864. The work was supported in part by the Thomas W. Powell '62 Fellowship from the Department of Electrical and Computer Engineering at Texas A&M University.

TABLE OF CONTENTS

Page

LIST OF FIGURES

FIGURE Page

LIST OF TABLES

TABLE Page

1. INTRODUCTION

1.1 Background

Electricity customers have grown to rely on the consistent and reliable delivery of electric power. For such a large and interconnected system to maintain operability, it is essential that the electric grid be able to withstand and recover from disturbances big and small.

One such possible disruptor is the phenomenon known as geomagnetic disturbances, or GMDs. The resulting changes in the earth's magnetic field can cause geomagnetically induced currents (GICs) which flow in the earth and other conducting paths, such as high voltage transmission lines [1]. As these currents flow in and out of the power system via transformer neutrals they can cause operational disruptions and equipment damage.

An example of the potential harm from these effects is when a GMD shut down the Hydro-Quebec system in March 1989. Millions of people lost power for up to 12 hours because of asset and system failure [2]. In response to the threat that severe GMDs pose to the safe and reliable operation of the electric power grid, the North American Electric Reliability Corporation (NERC) developed Reliability Standard TPL-007-1 [3], requiring potential impact assessments and operational plans from owners and operators of grid assets. Approved by the Federal Energy Regulatory Commission (FERC) in 2016, TPL-007-1 has precipitated increased interest, research, and development in understanding of GMDs and how to better mitigate their impacts on power systems.

To enable the real time response to and mitigation of GMDs by grid operators as described in their assessments, effective tools for GIC monitoring are required. Currently, limited metering and lack of general tools prevent widespread monitoring and situational awareness of GIC flows in the power grid.

In the event of a severe GMD, assets and customers are at risk and without reasonable monitoring tools, use of the appropriate operational and mitigation procedures may not happen. Therefore,

it is of high priority that monitoring techniques are developed which can make the most of the available metering and motivate the installation of additional meters for the dependable and efficient operation of the grid.

1.2 Existing Research and Current Challenges

The potential for GMDs to impact power grid operations have been known for decades and as a result of NERC mandates is receiving increased interest amongst industry professionals and academics alike. To better understand these impacts, improved GIC modeling has been advanced through analysis [4], sensitivity [5], and validation [6]. In addition to vulnerability assessments, mitigation plans are also required of grid operators. Real-time operational mitigation strategies, such as line switching [7, 8] and reactive power support rely on real-time visibility into the current state of the system. Long-term solutions such as the installation of blocking devices [9] also require accurate modeling and are enhanced by measurement availability. Outside of work by Hydro-One [10, 11], few tools for GMD monitoring and management in real time exist.

A common technique in power systems for monitoring is state estimation, by which measurements from the system are used to provide the best-guess (highest probability) estimate of key variables in the system. Commonly this “state" is the voltage magnitude and angle at every bus, from which all other values of interest can be calculated in combination with the system topology. As this technique is highly dependent on an accurate system model to relate measurements to states, the introduction of GICs can lead to estimate error [12]. Therefore, it is imperative that specialized techniques be developed that incorporate or specialize in GIC estimation in the system.

At this time, packages for widespread GIC monitoring and visualization are not widely available or advertised. Real-time mitigation strategies have been under increasing development in recent years, and the development of improved monitoring schemes enables the practical implementation of such strategies in industry. One current challenge is the limited availability of relevant measurements. Just as with traditional state estimation, a minimum number of measurements are required to ensure observability of the system. Therefore, sensitivity analysis to measurement availability and quality should be conducted, as well as means of addressing bad data provided.

The development of relevant tools which leverage available measurements encourages the future installation of additional sensors and communication network, which will continue to improve the results of the proposed estimation methods. Once real-time estimates are made available, how they are used and provided to grid operators, researchers, or students becomes a matter of design and consideration. Additional challenges include integration of GIC estimation or calculation applications with existing softwares and the effective communication and meaningful interpretation of GIC monitoring results.

1.3 Thesis Organization

The main contribution of this work is the development and implementation of an estimator for GIC monitoring and control purposes, which is shown to provide a quick and reliable snapshot of the current system state. The results from GIC estimation are also used as input for an improved GIC-inclusive state estimator and integration with other simulation and control tools. This work enables sensitivity analysis, bad data detection, and placement algorithms for meters as well as visualization applications to further enhance the situational awareness provided to grid operators during a GMD. The tools developed advance GMD monitoring and mitigation research and provide a foundation for additional improvements in realistic simulation of GMDs for operational, educational, and training purposes.

A literature review is provided in Chapter 2. It summarizes GMD effects on the power grid and existing work in power systems state estimation, GIC monitoring and calculation, and GMD mitigation strategies. Chapter 3 provides an overview of GIC modeling and proposes a weighted least squares-based GIC estimation methodology. Due to the linear relationship between electric field and GIC neutral currents, which may be metered in some systems, the resulting optimization problem is linear. Therefore the solution of the estimation problem is analytical and does not have the convergence issues common to power system state estimation methods. A simple example is described to show the mechanics of GIC estimation and how it is superior to mere calculation. In Chapter 4, results of the proposed GIC estimator are demonstrated on a synthetic Texas 2000 bus system under a variety of noise and metering scenarios. The purpose of this section is to

explore the sensitivity of the proposed estimation tool under a variety of circumstances, showing its robustness and reliability under increasingly realistic conditions. In Chapter 5, the concepts of observability and redundancy are defined for GIC estimation and a least absolute value-based formulation designed to improve performance in the presence of bad data. Chapter 6 explores additional monitoring applications, such as providing input to GIC-inclusive state estimation. It also provides a preliminary comparison of currently available real-time electric field data applied to large synthetic cases. In Chapter 7, actual data from the Texas A&M Magnetometer Network is used to estimate electric fields maps which are used to calculate dc line voltages. These are streamed to a power system dynamic simulator software and the current GICs displayed, providing real-time visualization in an interactive environment. Modular integration of the previously developed tools with existing power system software opens up many possibilities for monitoring and control applications. A summary of the contribution of this work and future directions are discussed in Chapter 8.

2. LITERATURE REVIEW AND CONTRIBUTIONS

The motivation and plan for novel GIC monitoring algorithms and tools are presented in this chapter. A more in-depth overview of GMDs and their effect on the electric grid are provided in the first section. A literature review of power systems monitoring tools, specifically state estimation, and the state of the art in terms of real-time GMD and GIC monitoring are presented in the sections which follow. The chapter concludes with a summary of the contributions of the proposed work and applications.

2.1 Geomagnetic Disturbances and Effect on the Electric Grid

GMDs are caused by coronal mass ejection- and solar storm-induced disturbances in earth's magnetic field. Not all solar flare and coronal hole events produce GMDs on the earth, which complicates storm forecasting, and when occurring, the GMD appears 2-5 days after the driving solar event. Solar activity (measured by sunspots per month) follows an 11-year cycle and geomagnetic activity is similarly cyclic, though a major storm can occur at any time during a cycle [13]. The resulting geomagnetic field variations induce low frequency (quasi-dc, less than 1 Hz) electric fields on the earth. The magnitude and direction of these fields depend on the storm, as well as the conductivity of the earth, and geomagnetically induced currents (GICs) are produced by these fields. They flow in the earth and high voltage transmission lines, due to the lines' low dc resistance, as well as metal piping, telecommunication cables and railway infrastructure [14].

From a power systems perspective, the currents enter the system at transformer and substation neutral groundings and it is the resulting effect on the transformers that causes significant issues. These quasi-dc GICs cause half cycle saturation of transformers, by offsetting the expected ac current. Consequently they affect the power grid with harmonics, heating, and reactive power losses [15, 16]. The heating of transformers can lead to transmission asset damage, specifically transformers, which are expensive and time consuming to replace. The resulting reactive power losses contribute to a suboptimal voltage profile and even voltage collapse [17, 18]. These issues

are sources of concern for power system operators and planners. The potential of GMDs to impact power grid operation has been known for decades and is receiving increased recognition as the North American Electric Reliability Corporation (NERC) has mandated vulnerability assessments and mitigation plans from industry [3]. Recent interest has been piqued also by an Executive Order from President Barack Obama, encouraging the coordination of resources and programs to prepare the nation's critical infrastructure for space weather events, like GMDs [19], and a near miss "superstorm" in the summer of 2012 [20].

In efforts to understand and mitigate these impacts, improved GIC modeling and monitoring is being pursued in academia and industry, see [5, 6, 21, 22, 23, 24]. Regarding mitigation, short-term operational strategies will rely on real-time visibility of the current system state [7, 8, 25], while long-term techniques still require accurate modeling and some measurement availability [9]. Beyond [11, 26], few accounts of tools for real-time GMD monitoring and management exist.

Ultimately, the GMD-induced electric fields drive the flowing GICs, the calculation of which has been covered in [13, 27] and is summarized in a future chapter. GIC flows are a function of geoelectric field magnitude, which is related to geomagnetic field by a frequency-dependent transfer function and defined in part by ground conductivity [4]. Spatial variations in this parameter can cause GICs to vary by up to orders of magnitude from one location to another; generally speaking, lower ground conductivity incurs higher surface electric fields which induce larger GICs. There is currently much discussion surrounding the merits of existing conductivity models [28]. Commonly used earth models include

- Uniform earth: earth's conductivity is uniform vertically and laterally
- Layered earth (1D): earth's conductivity is modelled with horizontal layers of differing conductivity and thickness; conductivity does not change horizontally; used for first-order response modeling in a specific region
- Nonuniform earth (3D): earth's conductivity varies vertically and horizontally; in reality, earth does have a complex mixture of conductivity in three dimensions.

A drawback to the adoption of more realistic 3D models is that the computational needs make real-time calculation and prediction unlikely. While 1D approximations are more practical computationally, they do provide more of an average response, not picking up on specific variations in a region. Current research leverages crust and mantle thickness survey data and increasingly available data from projects such as EarthScope [29] to develop and compare models [30, 31]. Future work will continue to explore to what extent these spatial variations influence GIC estimates and the ramifications of different models for offline and online applications. For the purpose of this work, it is be assumed that the driving magnetic field can be measured using magnetometers, of which 6 are now available as part of the Texas A&M University Magnetometer Network, and converted to an electric field measurement in near real-time, the transfer function of which is conductivity model dependent.

2.2 Power Systems Monitoring using Estimation

State estimation for transmission systems is a fundamental power systems tool, enabling nearly real-time system state awareness through established techniques for processing measurement and topology data. The availability and accuracy of this base state is invaluable for system management, providing key inputs for a variety of system security and control methods [32, 33, 34]. Fred Schweppe introduced state estimation in 1968 [34, 35, 36] as a means of processing redundant meter data to produce an estimate of the state of a power system. Today, this basic tool plays an integral role in ensuring secure power system operation and is found in energy management systems (EMS) around the world. In traditional estimation, real-time measurements are procured through the SCADA (supervisory control and data acquisition) system. Input data could include real and reactive power flows, real and reactive power injections, and bus voltages and angles. This data contains errors, which could be the result of noisy channels, analog-digital conversion, and inaccurate calibration. State estimation is the mathematical process that leverages redundancy in the measurement set to find the statistically optimal estimate of the current system state, essentially "cleaning" the error-filled data [37].

Since its inception, the pursuit of robust and reliable state estimation methods has been an area

of research and progress. Numerical ill-conditioning due to differences of weighting factors has caused convergence issues in large systems and been addressed by a variety of matrix transformation methods [38, 39, 40, 41] Other pursuits include improvements in numerical stability, computational efficiency, and implementation complexity [37, 42]. Current research in state estimation focuses on maintaining situational awareness and estimate integrity despite extreme conditions, such as heavy system loading or cyber-attack [43, 44]. While a GMD would certainly constitute an extreme situation, there has yet to be extensive literature on state estimation with GICs in the system.

2.3 GIC Monitoring

At this time, relevant GIC-related measurements that may be of use for real-time GMD mitigation include magnetic field and transformer neutral currents. Magnetometers can provide direct measurement of surface magnetic field disturbances, which can be turned into induced electric field measurements via the previously mentioned model and conductivity dependent transfer functions [45]. During a GMD event, magnetometer stations can take measurements of the changing geomagnetic field and aggregators of this magnetic field data, such as SuperMAG [46], exist, while recent projects have led to the installation of additional meters across the United States and specifically Texas. In the United States, the magnetometer network is generally quite sparse, and interpolation would be used to estimate fields between magnetometer stations. Magnetometer distance from the position of analysis can incur significant uncertainty in electric field response, regardless of the conductivity model used [28]. The new Texas A&M University Magnetometer Network (Fig. 2.1) is now online and the relatively close placement of the meters results in improved observability and can lead to additional advancements in modeling and analysis.

Physically connected to the electric grid, some utilities have installed transformer neutral GIC monitors, such as hall-effect transducers. The purpose of these sensors is often to measure dc current and to inform alert systems. In conjunction with other analysis or aggregation tools, these measurements can be used to provide widespread system awareness.

As traditional power system monitoring methods do not completely capture the GIC model or

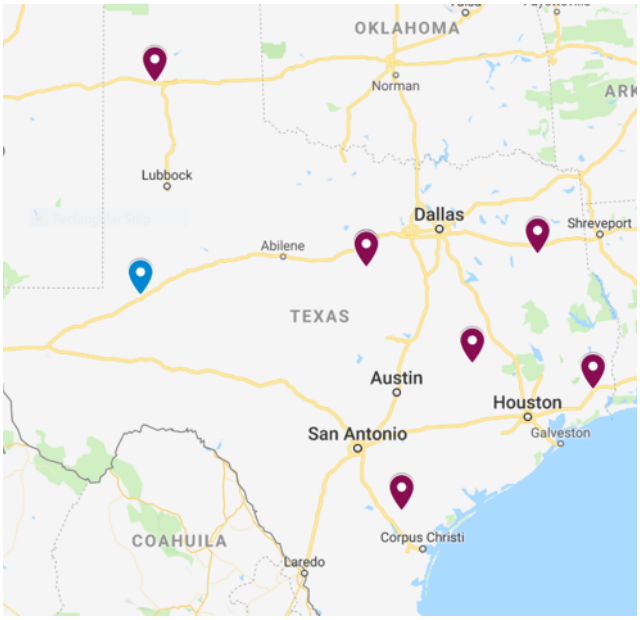

Figure 2.1: Map of recently installed magnetometers in the state of Texas

state of the system during a GMD, it is vital to consider how an incomplete model, one that does not include dc GIC relationships, could incur error. As traditional state estimators do not consider the additional reactive power losses due to GICs in transformers, the estimation may stray from the actual desired solution. This was shown in [12] by using traditional state estimation techniques (weighted least squares) on a large system under a geomagnetic disturbances. "Measurements" were taken from the GIC-inclusive solution of the power flow in a commercially available GIC simulator but the model upon which the estimation algorithm was based did not include GIC models. The result was that the voltage magnitude state average absolute error could be as high as 0.16 per unit, depending on the storm magnitude and number of available measurements. Both the average and the maximum error increased with storm magnitude, which supports the claim that the error is due to lack of GIC modeling.

In [12], the recommendation is that the dc GIC network model needs to be considered in conjunction with the state estimation process. State estimation can only provide the statistically optimal state when the measurements and states are accurately related. Therefore, it is recommended that efforts be undertaken to provide situational awareness from a limited set of GIC-related mea-

surements. On its own, GIC estimates can provide input into monitoring, mitigation, and control algorithms. Alternatively, they can provide reactive power "load" estimates that would enable more accurate ac state estimation results. Either way, the tools developed here will aid in providing insight into a critical phenomenon with currently limited visibility.

The main contribution of this work is the development and testing of a quick and versatile GIC estimation methodology. While there are a number of real-time GIC simulators covered in the literature [47], this *estimator* provides a more accurate snapshot of the GICs flowing through the system by leveraging multiple available GMD-related input types and relying on the measurement redundancy of the near future. In [48] neutral GIC and forecast data was leveraged to inform an early warning system, but has to this date only shown proof of communication network concept and minimal focus on ability to leverage data collection and analysis to inform operators in meaningful and complete ways. The work of this dissertation leverages similar data to provide not just general warnings, but a generally accurate snapshot of what exactly is happening to cause an alarm to go off. In [49] actual neutral GIC and geoelectric field measurements were used to estimate GICs associated with past geomagnetic storms. The methods appear to make many simplifications to the power system model, such that the resulting estimates would be suitable to determine upper limits or run probabilistic studies, but not real time applications. The work of the dissertation utilizes the system model as well as all available measurement data to provide real-time application-ready estimates of the present system GIC state. In [50] electric field estimates are made from neutral GIC measurements, but again they are not intended for real-time applications, instead focusing of model validation. The work of this dissertation uses related methods to estimate electric field while also leveraging real-time magnetic field data. Furthermore, in much of the existing research a uniform magnetic field was assumed, as data is often only available for just one magnetometer. The work of this dissertation considers multiple potential electric field zones, in accordance with recent magnetometer installations in the state of Texas. This enables improved estimates due to the finer granularity of result afforded, providing a better match to realistic spatially varying fields.

In traditional state estimation, bad data detection is considered an integral part of the overarch-

ing state estimation process [37]. In a similar fashion, bad data analysis should be undertaken in the GIC estimation context such that the resulting estimate remains reliable even in the presence of corrupt measurements.

2.4 Contributions

#1. An estimation method for improved visibility of GICs in a system.

The proposed techniques are inspired by traditional state estimation methods but for the purpose of providing widespread understanding of the quasi-dc currents in the system. Considering electric field as the state to be estimated and leveraging available magnetometer and transformer neutral current measurements, a more complete picture of the GMD effects on the power system can be acquired. This work is addressed in Chapter 3.

#2. Sensitivity analysis to measurement noise level and availability, as well as state definition.

Given the uncertainty surrounding measurement noise characteristics and the future of measurement availability, analyzing scenarios while varying these values can provide insight into applicability of the proposed methods under realistic conditions. Additionally, adjusting the granularity with which the states are determined provides future flexibility of the methods as understanding of regional conductivity of the earth is updated. This work is addressed in Chapter 4.

#3. Robust GIC estimation, specifically with respect to bad data and non-Gaussian noise characteristics.

Under realistic circumstances, bad data or measurements with non-Gaussian noise distributions may be present. In Chapter 5, a robust estimation method is developed such that the resulting state estimate is unaffected by unexpected measurement error. This contribution depends on the discussion of the meaning of observability and redundancy for GIC estimation and the consideration of real GIC data and non-Gaussian noise.

#4. Integration with additional monitoring and visualization applications. The proposed tools are not intended to be used in a vacuum, but to be displayed in meaningful ways and integrated with other monitoring and mitigation strategies. Returning to an initial motivating factor, mitigating the error incurred by lack of GIC modeling during traditional estimation, using the results of GIC es-

timation to initialize a GIC-augmented ac state estimation method is demonstrated. Furthermore, tools have been developed to connect the GIC estimation module with commercial power system simulators for additional visualization, analysis, and real-time experimentation. These contributions are proposed and demonstrated in Chapter 6 and 7.

3. MODELING AND ESTIMATING ELECTRIC FIELDS AND GICS *

In this chapter, an estimator for electric fields and GICs is developed. First, modeling of GICs in power systems is reviewed. Traditional state estimation is also briefly covered, as inspiration for the proposed work. A small example is provided to demonstrate the mechanics of this research.

3.1 GIC Modeling

To calculate the GICs flowing in the system, first the induced voltage potentials on the transmission lines are found by integrating the electric field over the length of the line. For a uniform electric field, the (dc) voltage on the line between buses n and m is modeled as

$$V_{nm} = E^N L^N_{nm} + E^E L^E_{nm} \tag{3.1}$$

where E^N and E^E are the northward and eastward components of the electric field vector and L^N_{nm} and L^E_{nm} are the northward and eastward distances of the line between buses n and m. The induced voltages are converted to dc *current* injections by Norton's Equivalent. The total current injection can then be found via Kirchhoff's current law; the resulting vector is give by $\mathbf{I} = \mathbf{HE}$, where $\mathbf{H}$ depends on the length, resistance, and orientation of the lines. For a uniform electric field, $\mathbf{E} \in \mathbb{R}^{2\times 1}$ and $\mathbf{H} \in \mathbb{R}^{(n_b+n_s)\times 2}$, where n_b and n_s are the number of buses and substations in the system, respectively.

For a non-uniform electric field, the system can be divided into k predetermined electric field zones, which could each be experiencing a different electric field. The zones should be defined such that each is an enclosed shape, no zones overlap, and together they cover the entirety of the system geographic footprint. The granularity and boundaries of these electric field zones are to be determined based on regional conductivity, available metering, and expected electric field variation. Expected variation depends on the storm and earth models, but studies have shown that

*Part of this section is reprinted with permission from "A GIC Estimator for Electric Grid Monitoring During Geomagnetic Disturbances," by C. Klauber, K. Shetye, T. J. Overbye, and K. Davis, June 2020, IEEE Transactions on Power Systems, ©2020 IEEE, with permission from IEEE

electric field differences across geographic distances of 200 km can differ by up to two orders of magnitude [31]. Non-uniform electric fields necessitate the creation of a vector $\mathbf{E} \in \mathbb{R}^{2k\times 1}$ of the electric field components. Correspondingly, the distance components L^N_{nm} and L^E_{nm} are separated to represent the portion of the line in each zone. However, $\mathbf{H} \in \mathbb{R}^{(n_b+n_s)\times 2k}$ will still be quite sparse as the voltage induced on a line between two buses usually depends on at most a few electric fields. The dc line voltage calculation of Eq. 3.1 is now the summation of up to $2k$ terms. An example of this can be seen in Fig. 3.1, where Eq. 3.1 is

$$V_{12} = E^N_2 L^N_{12} + E^E_2 L^E_{12} \tag{3.2}$$

for the red line that lies completely in zone 2, and

$$V_{23} = E^N_2 L^N_{23'} + E^E_2 L^E_{23'} + E^N_3 L^N_{23''} + E^E_3 L^E_{23''} \tag{3.3}$$

for the green line that lies in zones 2 and 3. Furthermore, a disturbance with non-linear magnitude and uniform direction could be considered, in which case $\mathbf{E}$ would have length $k+1$, i.e., k magnitudes and one direction.

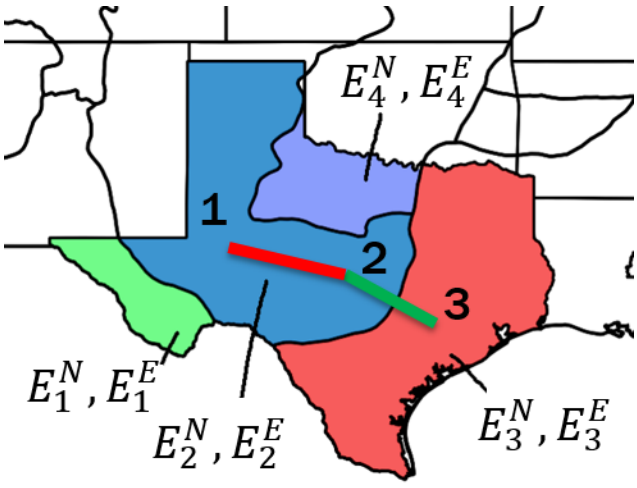

Figure 3.1: Example of determining L_{nm} when a line crosses multiple zone regions

Whether uniform or non-uniform electric fields are used, the dc voltage (V_n) at a bus or substation neutral is determined by solving the dc network described in [16],

$$\mathbf{V} = \mathbf{G}^{-1}\mathbf{I} = \mathbf{G}^{-1}\mathbf{H}\mathbf{E} \tag{3.4}$$

where $\mathbf{G}$ is a sparse square matrix of conductance values augmented to include substation grounding resistances values. Matrix $\mathbf{G}$ is much like the bus admittance matrix in power flow analysis, with dimensions of $(n_b + n_s) \times (n_b + n_s)$.

The GIC flows from node n to node m are determined by

$$I_{nm} = g_{nm}(V_n - V_m) \tag{3.5}$$

where g_{mn} is the connecting line conductance from $\mathbf{G}$. The effective GIC, $\mathcal{I}_t$, is the effective per phase current depending on transformer t type and configuration. For simple cases, such as for GSU transformers, $\mathcal{I}_t$ is merely the current in the grounded (high-side) winding. Otherwise $\mathcal{I}_t$ depends on the current in both coils [16]. According to [5],

$$\mathcal{I}_t = \left| I_{H,t} + \frac{I_{L,t}}{a_t} \right| \tag{3.6}$$

where $I_{H,t}$ is the per phase GIC going into the high side winding, the series winding for an autotransformer, $I_{L,t}$ is the per phase GIC going into the low side of the transformer, and a_t is the transformer turns ratio. In matrix form, (3.6) for all transformers is given by

$$\boldsymbol{\mathcal{I}} = \left| \mathbf{\Phi}\mathbf{G}^{-1}\mathbf{H}\mathbf{E} \right| \tag{3.7}$$

where $\mathbf{\Phi}$ is a sparse matrix with entries consisting of substation and transformer conductances. GIC flows through a transformer increase its reactive power absorption. Importantly, this reactive power loss is the key link between the dc and ac power systems. The additional reactive power

loss for transformer t in Mvar is dependent on the transformer core model, GICs, and voltage. It is given by

$$Q_{loss,t} = f(V_{pu,t}, \mathcal{I}_t) \tag{3.8}$$

where $V_{pu,t}$ is the per unit ac terminal voltage for transformer t, and $f(\square)$ is a nonlinear expression specific to the transformer and dependent on the current conditions [51]. While the nonlinear model is increasingly encouraged, a linear expression has been often assumed [52]:

$$Q_{loss,t} = k_t V_{pu,t} \mathcal{I}_t \tag{3.9}$$

where k_t is a transformer dependent constant. The losses due to GICs in the dc network affect the ac network by drawing additional reactive power, lowering the system voltage profile, and it is important that they are appropriately modeled, depending on the application.

It is also useful to define the relationship between transformer neutral currents, which are actually metered, and electric fields. Let $\boldsymbol{\mathcal{I}}_n$ be the vector of transformer neutral GIC currents and $\boldsymbol{\Phi}_n$ also be a sparse matrix with transformer conductance entries, then

$$\boldsymbol{\mathcal{I}}_n = \boldsymbol{\Phi}_n \mathbf{G}^{-1} \mathbf{H} \mathbf{E} \tag{3.10}$$

By modeling and monitoring the dc network, previously unavailable insight into GIC flows and the resulting ac network changes can assist grid operators during geomagnetic disturbances.

3.2 Traditional State Estimation Methods

Traditional state estimation programs utilize system measurements and topology to provide awareness for real-time monitoring. Typical frameworks are formulated as overdetermined systems of nonlinear equations and solved as weighted least squares (WLS) problems [33]. The state vector $\mathbf{x}$ is defined to be the voltage magnitude and angle at every bus in the system and a measurement vector $\mathbf{z}$ can consist of real and reactive power flows and injections, voltage magnitude and angle differences, current flows and injections, and even transformer turns ratios and phase shift angles,

when available. A measurement model relating the states $\mathbf{x}$ to the measurements $\mathbf{z}$ for measurement i is given by

$$z_i = h_i(\mathbf{x}) + e_i. \tag{3.11}$$

The relationship between the ith measurement and the states $\mathbf{x}$ is modeled by the function $h_i(\square)$, which is nonlinear and non-convex, while e_i is the measurement error, assumed to normal with zero mean and variance σ_i^2. WLS state estimation is set up as a quadratic optimization problem with equality/inequality constraints which will minimize the weighted total of the squares of the measurement residuals. More accurate measurements are given more weight and under certain assumptions WLS is also the maximum likelihood method. For power system state estimation, the problem is solved by iterative methods, due to the nonlinearity of the power flow equations. Convergence issues and state initial guess dependence are known challenges that can arise when using iterative methods. There exists a large collection of work addressing these issues [53, 54], though such issues will not be a problem for the GIC estimator proposed in Section 3.3 due to the linearity of (3.10).

3.3 GIC Estimation Methods

In the state estimation research space, linear estimators have been introduced in part thanks to increasing installations of phasor measurement units [55, 56, 57]. With sufficient metering the traditional states are observable from these measurements when defined in the complex plane and therefore related to the available measurements by a linear measurement model. For GIC estimation, the linear relationship of (3.10) also enables a linear estimator with similar benefits such as an iterative-free solution.

The states shall be the underlying electric field, $\mathbf{E}$, specifically the northward and eastward components of each predetermined electric field zone. Recall, each zone is an enclosed shape such that no zones overlap and together they cover the entirety of the geographic footprint of the system. Analogous to the traditional estimator, with this knowledge (the underlying state, $\mathbf{E}$) and an understanding of the system topology one can calculate all other values of interest pertaining

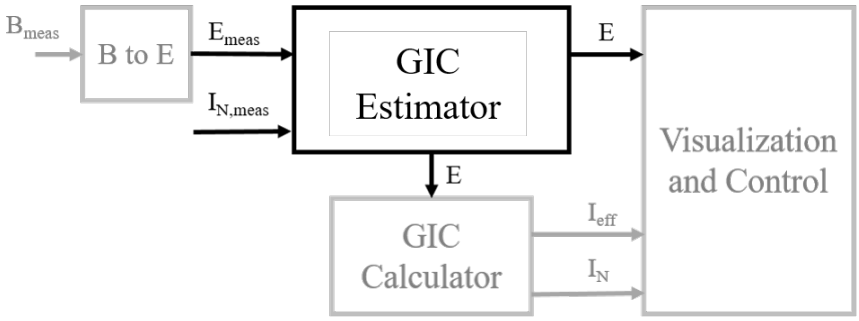

Figure 3.2: GIC estimation in the context of a broader GMD monitoring and mitigation scheme for power grid operations. Reprinted with permission from [61]

to the GMD effect on the power system, namely effective GICs, reactive power losses, and potentially transformer heating effects. Available measurements may include electric field estimates **E** (calculated from magnetometer magnetic field measurements **B**) and GIC neutral currents from transformers, as illustrated in Fig. 3.2. Depending on the granularity of available magnetometer measurements and calculated **E** therein, gaps in input **E** are provided via interpolation [58, 59]. The **B** to **E** conversion uses ground conductivity models to convert magnetic field data to electric field data. These models are derived from magnetotelluric study results and geological data and are available from the United State Geological Survey [60]. The initial models are expected to change with future assessments. Here it will be assumed that the ground model is known such that a **B** measurement can be mapped to an **E** measurement prior to integration with the GIC estimator. The diagram also shows how the resulting states provide valuable inputs for GIC calculators or potential visualization and control tools. Eq. 3.11 in matrix form for GIC estimation is given by

$$\mathbf{z} = \mathbf{h}\mathbf{x} + \mathbf{e} \tag{3.12}$$

where

$$\mathbf{h} = \begin{bmatrix} \mathbf{I}_{j\times 2k} \\ \{\mathbf{\Phi}\mathbf{G}^{-1}\mathbf{H}\}_{l\cdot} \end{bmatrix} \tag{3.13}$$

The identity matrix $\mathbf{I}$ has length corresponding to the number of state measurements, j, and width

equal to two times the number of states, or the length of $\mathbf{E}$, $2k$. The l rows of $\{\mathbf{\Phi G}^{-1}\mathbf{H}\}$ corresponding to the available $\mathcal{I}_n$ measurements. The resulting linear least squares state estimation optimization problem is as follows:

$$\min \quad (\mathbf{z}-\mathbf{hx})^T\mathbf{R}^{-1}(\mathbf{z}-\mathbf{hx}) \tag{3.14}$$

where $\mathbf{R}$ is the measurement error covariance matrix. The weight matrix, $\mathbf{R}^{-1}$, has diagonal elements $R_i^{-1} = 1/\sigma_i^2$. In traditional estimation, iterative methods are invoked to solve for the states, $\mathbf{x}$. Due to the linear nature of GIC systems, an analytical solution exists without need for iterating,

$$\mathbf{x} = [\mathbf{h}^T\mathbf{R}^{-1}\mathbf{h}]^{-1}\mathbf{h}^T\mathbf{R}^{-1}\mathbf{z}. \tag{3.15}$$

Therefore, solving for the GIC estimate is extremely quick; Eq. 3.15 requires simple matrix multiplication and $\mathbf{G}^{-1}$ is never explicitly inverted but solved using sparse matrix methods. Even then, the most computational taxing component, $\mathbf{G}^{-1}$, does not need to be found unless the system topology changes. As with traditional estimation, the proposed linear GIC estimator requires sufficient metering for redundancy and observability. Redundancy enables better estimates and the ability to filter out noisy or bad measurements. Observability is required to even obtain a solution. The results which follow demonstrate the estimate improvement with increased metering and the minimum metering required for observability and meaningful results is explored in a future chapter.

To validate this methodology, a synthetic GMD event will be applied to a test network. "Metered" measurements will be taken from the GIC solution and synthetic noise added. The underlying electric field state will be estimated and compared to the known driving electric field. Additionally, comparison between actual GIC neutral current values and values calculated from the estimate will be made. This will show the error that propagates in the presence of estimation error and the effect it might have on operating procedures. Overall, the proposed GIC estimator will provide previously unavailable situational awareness to grid operators during a GMD that will

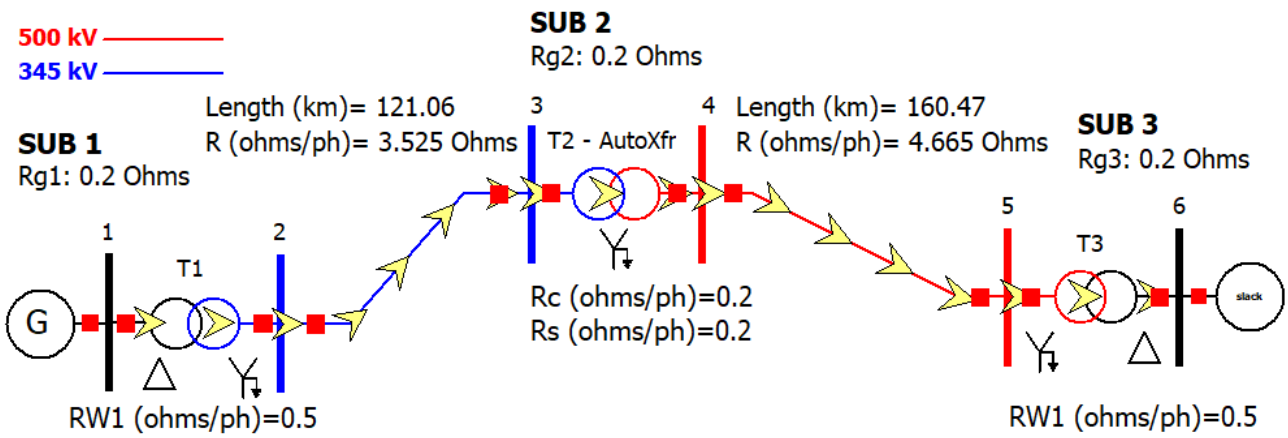

Figure 3.3: Oneline for GIC estimation example with 6 buses and 3 substations. Reprinted with permission from [61]

enable improved response to and mitigation of GICs.

3.4 A Simple Example

A simple example will show how the proposed method works and the system understanding improvement enabled by incorporating additional measurements. Consider the 6-bus system in Fig. 3.3 and assume there is an underlying spatially-varying electric field such that the left half of the system is experiencing a field with a particular magnitude while the right half experiences a different magnitude. The direction and size of the yellow arrows superimposed on the transmission lines visualize the direction and magnitude of the resulting GIC flow. Assume there is one magnetometer installed on the right side of Fig. 3.3 from which the electric field in the region can be estimated, with decreasing certainty the furter the value is applied from the magnetometer site. If no other measurements were available, someone who wanted an idea of GIC flows or reactive power losses in the area could calculate $\mathcal{I}_n$ using (3.10). The resulting neutral current calculation results are available in Table 3.1, along with the actual values provided by a power flow simulator. The sign of the neutral current value indicates the direction of the current flow, with a positive value indicating amps flowing from the system into the neutral. A negative number indicates current flowing from the neutral into the system.

Table 3.1: Actual, calculated, and estimated neutral currents for a GIC calculation/estimation example. Reprinted with permission from [61]

	Neutral Current (A)		
	T1	T2	T3
Actual	-297.8	129.4	168.4
Calculated	-271.9	106.4	167.2
Estimated	-299.9	130.8	171.3

Because there is a different underlying field on the left side of the system, there is some error in the GIC calculation results. This reiterates that with magnetometer measurements alone, neutral currents can be calculated, but data error is not able to be filtered out and higher granularity of states is not able to be achieved.

Now consider an available GIC neutral current measurement at Transformer 1 (T1) with a value of -300 A. This transformer has the highest magnitude current in the system and is likely monitored for this reason. Assuming this information can be aggregated with the electric field and topology information, GIC estimation is run to estimate the electric field of both the left and right sides of the system as separate states. It is assumed that the neutral current measurement is more heavily weighted than the electric field information, for which the weight is stronger on the right side than the left. This is consistent with the idea that confidence in electric field data is higher closer to the magnetometer data from which it is derived. The neutral current calculations resulting from the estimate are also shown in Table 3.1. Note that with just the two measurements but without the GIC estimator, the current in T3 can be calculated and the measurement at T1 can override the wrong value calculated from the electric field measurement, but the current at T2 will have sizeable error without additional analysis. As seen in Table 3.1, adding additional measurements or incorporating all available information into a tool like GIC estimation allows for a better understanding of $\mathcal{I}_n$ across the system, not just where values are metered. The chapter that follows provides more sophisticated analysis of the proposed methodology.

4. GIC ESTIMATION RESULTS *

In this chapter, results of the GIC estimation methodology are presented for various cases set on the 2000-bus Texas system and various measurement and state definition scenarios. An overview of potential results and basic visualizations as well as sensitivity to measurement availability and quality. The results show that the estimator performance improves with additional metering and less noisy measurement data. Sensitivity to state estimate granularity is less conclusive, and is likely to be system and geography dependent in practice. Additional research and exploration to improve estimator performance and realism are provided in the next chapter.

4.1 Test Case

For the purpose of demonstration, the proposed GIC estimation method is tested on a 2000-bus synthetic system set on the footprint of the state of Texas [62]. The system contains voltages ranging from 13.2 kV to 500 kV, nominal, and over 850 transformers, almost half of which are autotransformers. When electric field information is provided, GICs can be calculated in the system as the case, shown in Fig. 4.1, contains the necessary substation, transformer, and geographic data. The electric field is first assumed to be uniform within the 1D earth resistivity model regional zones shown in Fig. 4.2. In reality, the actual electric field variation across the region could be more complicated, which future examples address. In the future, the recent magnetometer installations in the state of Texas may be able to provide further insight into the conductivity patterns of the region, and thus the appropriate delineation of electric field zones to be used as states.

4.1.1 Synthetic GIC Neutral Current Measurements

To generate artificially noisy measurements for use with the estimator, a subset of the GIC neutral current results are selected and random Gaussian noise is superimposed with varying variance. The actual noise characteristic of the relevant measurements touched upon in a future sec-

*Part of this section is reprinted with permission from “A GIC Estimator for Electric Grid Monitoring During Geomagnetic Disturbances," by C. Klauber, K. Shetye, T. J. Overbye, and K. Davis, June 2020, IEEE Transactions on Power Systems, ©2020 IEEE, with permission from IEEE

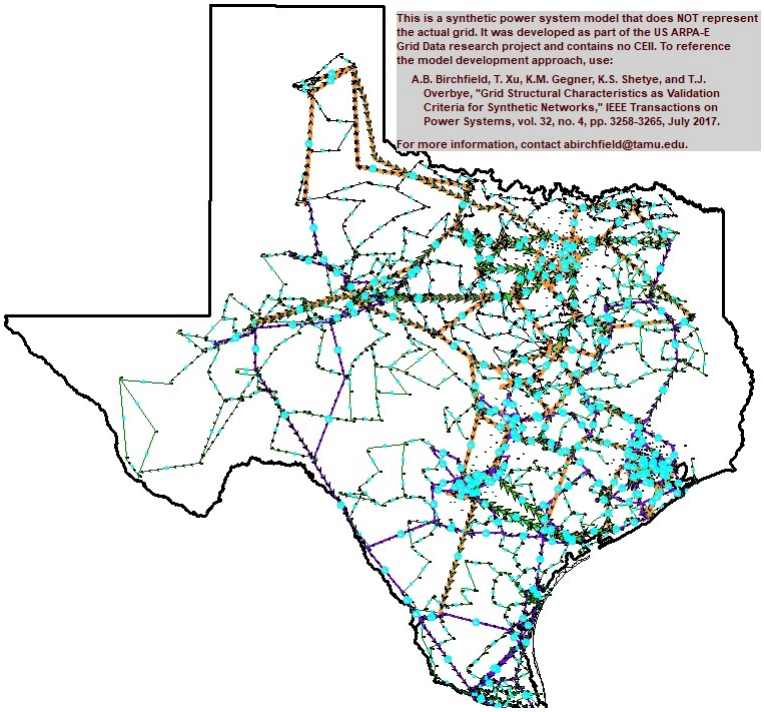

Figure 4.1: Texas 2000 bus synthetic case oneline diagram. Reprinted with permission from [61]

tion, but studying the method's sensitivity to various levels of noise provides proof of concept for the proposed methodology. In the following simulations, the installation locations of "measured" transformers is randomly chosen such that the pre-defined number of measurements is met with a balanced distribution of meters in each of the resistivity zones. In these studies, the number of such measurements spans from 0 to 100.

4.1.2 Synthetic Electric Field Measurements

Six synthetic magnetic field meters are placed to emulate the number recently installed for the Texas A&M University Magnetometer Network. The location of the field meters is chosen to provide visibility in each of the regional resistivity zones and redundancy in the larger zones (by area). To generate synthetic electric field "measurements," the electric field information which was applied to the system to simulate a GMD is exported. Specifically it is saved at the locations of the synthetic magnetometers and random Gaussian noise is superimposed with varying variance. The actual process of determining geoelectric field from magnetic field measurements from mag-

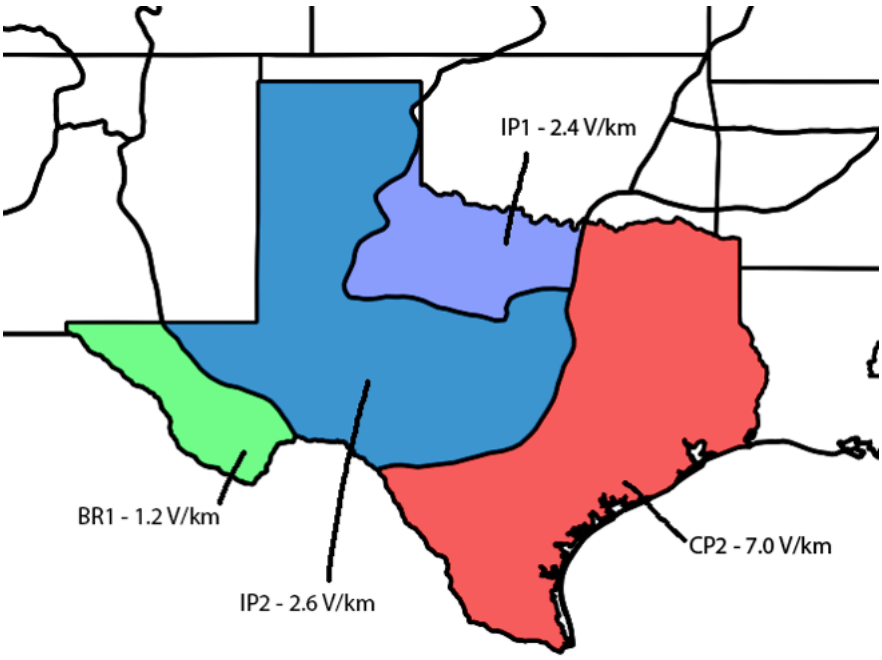

Figure 4.2: Regional resistivity zones in the state of Texas (figure by Jennifer Gannon). Reprinted with permission from [61]

netometers is covered in other literature [13] and it is assumed that it can be carried out online. Since the underlying electric field state is known, the sensitivity of the GIC estimator to realistic conditions can be explored by comparing the estimated and actual states in different scenarios. The conditions covered here include varying of measurement noise and number of measurements.

4.1.3 Preliminary Results

The first result (Fig. 4.3) shows a potential situational awareness scheme provided to grid operators using GIC estimation. For this particular instance, there is a limited set of 6 magnetometer and 16 transformer measurements, denoted by diamonds. Hence from 22 measurements the northward and eastward electric field components in the four resistivity zones (8 states) are estimated and the resulting GICs across the system calculated. Without comparable monitoring tools or metering all 800+ transformers in the system, it would not be known that 8 substations in the system have transformers with effective GICs over 50 A, denoted by red circles, or which transformers are at risk of having high GICs, denoted by yellow circles. Comparing these estimated results to

the known actual values gives Table 4.1. The resulting maximum and mean error (in V/km) are reasonable, given noisy measurements, and the effective GIC results which follow are reasonable relative to the magnitude of the actual signals. Initial studies (not shown) demonstrate that the estimate error does not seem to be dependent on storm size or direction.

Table 4.1: Average and maximum electric field and effective GIC estimation error. Reprinted with permission from [61]

	Electric Field (V/km)	Effective GICs (A/phase)
Mean Error	0.0605	0.2210
Max Error	0.1510	1.9911

4.2 Sensitivity to Realistic Conditions

By varying the error superimposed on the synthesized measurements and the spatial variation of the electric field states, further insight into the practicality of the GIC estimation method is explored. This ensures that the proposed methods can be applicable in realistic situations.

4.2.1 Electric Field Estimate Error

Determining the estimator's sensitivity to noise in the electric field input is valuable to understanding the practical usefulness of the tool under realistic conditions. Procuring these electric field estimates involves converting magnetic field data, likely from a magnetometer, into electric field data, using ground conductivity models. Error can be introduced both from noise in the magnetometer measurement and the conductivity transfer function. As has been discussed, the reliability of the result is dependent on the accuracy of the model, which holds for the magnetic to electric field conversion. Here, the estimator's robustness to this variance is shown in Fig. 4.4. For the given storm represented by a uniform electric field (2 V/km east, 2 V/km N) the noise applied to the electric field is varied. Holding the number of electric field inputs, GIC neutral current

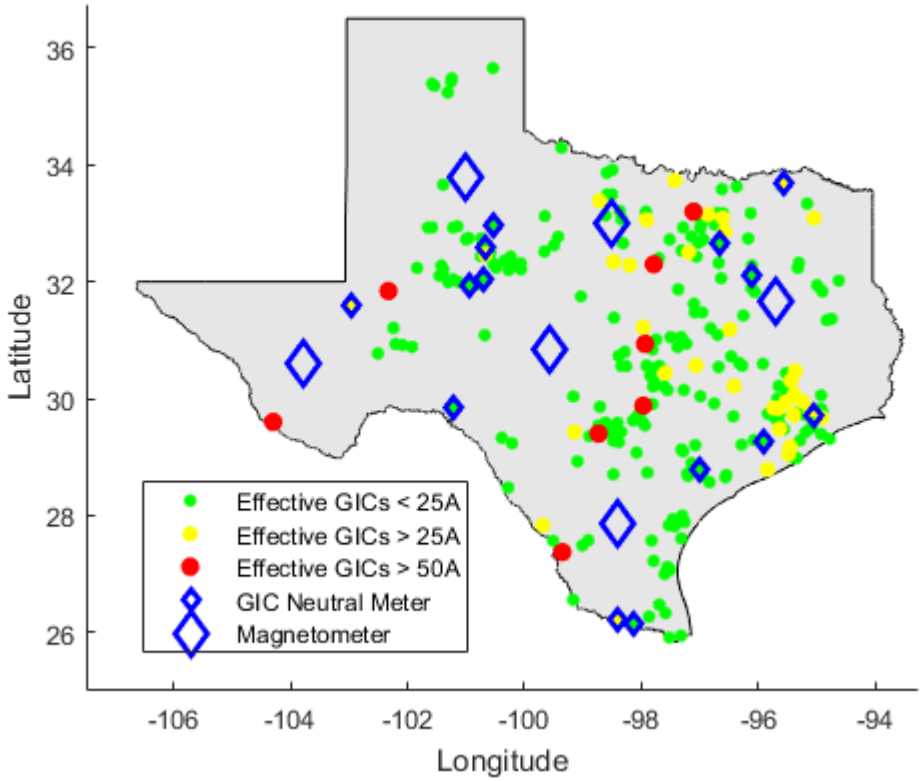

Figure 4.3: Situational awareness visualization for all transformers in the system (circles) from a limited set of measurements (diamonds) consisting of 6 magnetometers and 16 transformer neutral currents. Reprinted with permission from [61]

measurements, and states to be estimated consistent with the previous scenario, the resulting electric field estimate deviations are averaged over 1000 Monte Carlo simulations at each noise level. Fig. 4.4 shows that while extremely noisy or low confidence inputs may produce less-than desired results, generally the estimator still provides useful results for grid operators. Nevertheless, the improvements due to better inputs motivate data quality standards for magnetometer installations and model accuracy standards for the online conversion from magnetic to electric field inputs. Additional work considering estimator sensitivity to non-Gaussian noise characteristics is presented in a later section.

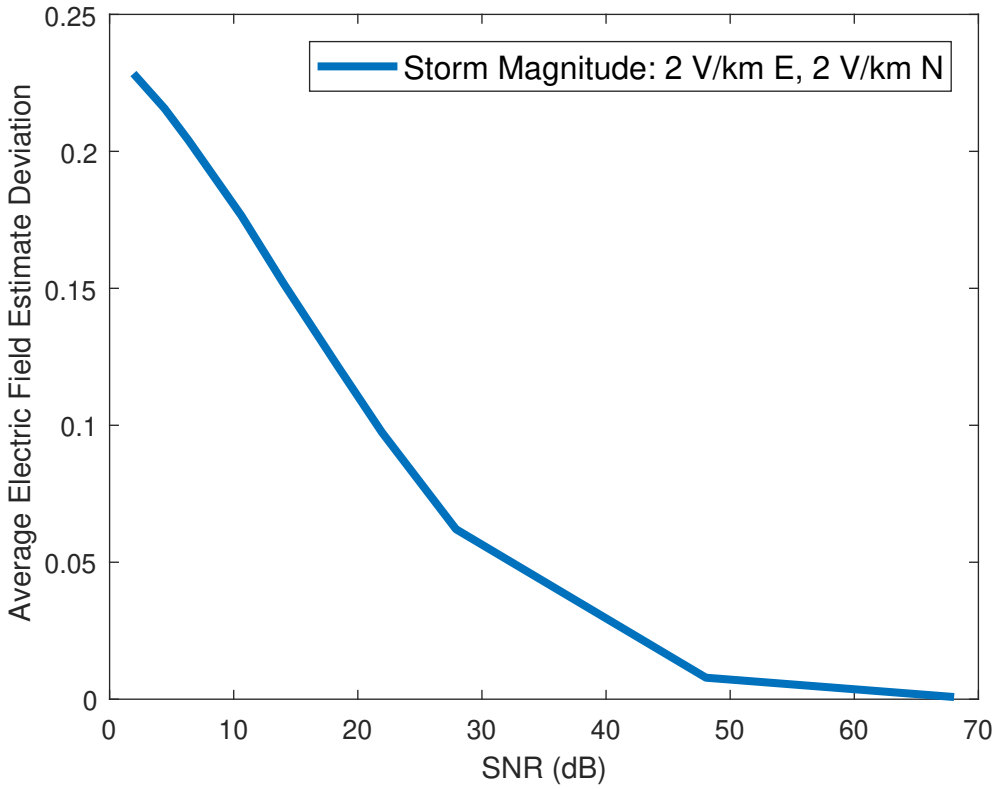

Figure 4.4: Average electric field deviation (from 2 V/km) decreases as the noise of the electric field estimate (used as input) decreases. Reprinted with permission from [61]

4.2.2 Measurement Availability

While GIC neutral current measurements are not currently very common, with developments like the proposed GIC estimator and increasing availability of magnetic field measurements, future installations are increasingly motivated. As more applications are developed and their benefits made known, additional investments in metering become more viable. As with the original scenario, the same same states are estimated using the same electric field inputs. But in these scenarios, the number of available GIC measurements are varied. Fig. 4.5 shows the absolute value of the deviation between the estimated and actual electric field averaged over 1000 Monte Carlo simulations while varying the number of GIC neutral current measurements available, randomly placed. It shows that as more GIC measurements are made available (out of a possible 861, for this par-

ticular case), the resulting electric field estimation becomes more accurate. This is to be expected as similar results are found in mainstream state estimation literature as increased observability not only enables improved results, but also the ability to filter measurement noise and perform bad data detection. It should be noted that the greatest improvement in average electric field estimate deviation (denoted by the steep slope) is found amongst the first 20% or so measurements. While additional measurements do make a difference, for an already highly visible system it may not be cost effective to invest in additional meters for such a minuscule improvement, at that point. Additionally, these results would vary with differently defined electric field states, i.e. more measurements are required to estimate the electric field with finer granularity well, which is covered in the next subsection. Continuing research on observability for GIC estimation methods will open interesting research questions as well as provide practical tools for electric utilities considering new metering installations.

While for this analysis GIC measurements were placed randomly, that is not representative of metering on the actual grid. It is likely that transformers at risk for high GICs would be metered over smaller or low-risk transformers. When considering the more realistic scenario of measurement placement favoring high risk transformers or a more strategic algorithm aiming for geographically balanced metering, it is expected that the average electric field magnitude error would be lower than if the measurements were placed randomly, due to improved redundancy and guaranteed observability. These concepts are covered in more depth in Chapter 5. At a minimum, due to each state (electric field in a predefined zone) having two parts, an eastward and a northward component, for a zone to be observable without any electric field input there must be at least two GIC measurements in or near that zone. Therefore, the number of available GIC measurements is a limiting factor to the number of electric field zones that can be estimated.

4.2.3 Granularity of Electric Field Zones

Recovering and estimating electric fields zones with higher granularity (more zones in the same space) is of interest because it is realistic to realize that the electric field may vary spatially more than is modeled by the regional resistivity zones. Estimating smaller, and thus more, zones

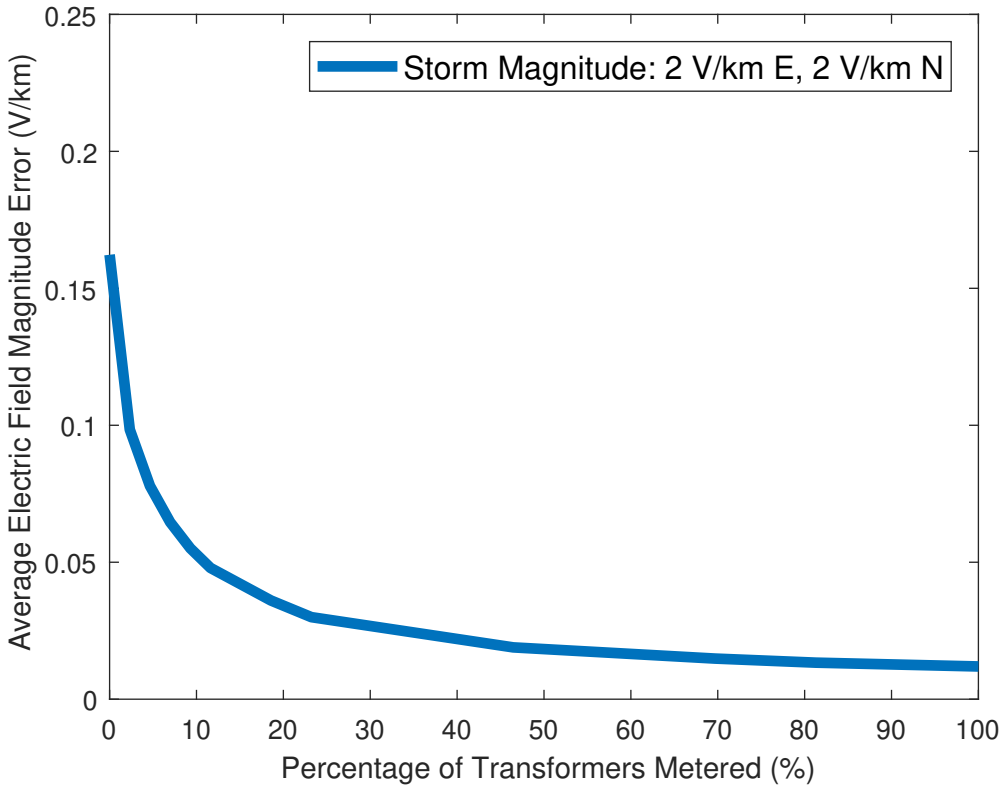

Figure 4.5: Average electric field magnitude error decreases as the number of available GIC neutral measurements increases. Reprinted with permission from [61]

requires additional metering to maintain observability. With limited available magnetometer measurements, the usage of electric field "pseudomeasurements" may be utilized. In this situation, a pseudomeasurement is provided by the nearest magnetometer in the same regional conductivity area. To illustrate the estimation of more electric field zones on the same geographic footprint, an input electric field with higher granularity is created, such that the electric field is varying every 2 degrees latitude and longitude. In this example, the electric field magnitude and angle will be estimated for 20 distinct zones, where the zones to be estimated are defined along the boundaries of a square grid. Along the perimeter of the system zones may be widened or lengthened by up to 0.25° to prevent the creation of an additional zone that would likely have limited measurement visibility due to its smaller area. These zones and their normalized electric field magnitude for a hypothetical snapshot in time are shown in Fig. 4.6. Given limited metering, pseudomeasurements

are used in zones not directly metered. These values are determined by proximity to actual meters and influenced by the regional resistivity zones. Fig. 4.7 shows the pseudomeasurements and measurements used as input. The objective of the estimator is to recover the 20 zones/states as seen in Fig. 4.6.

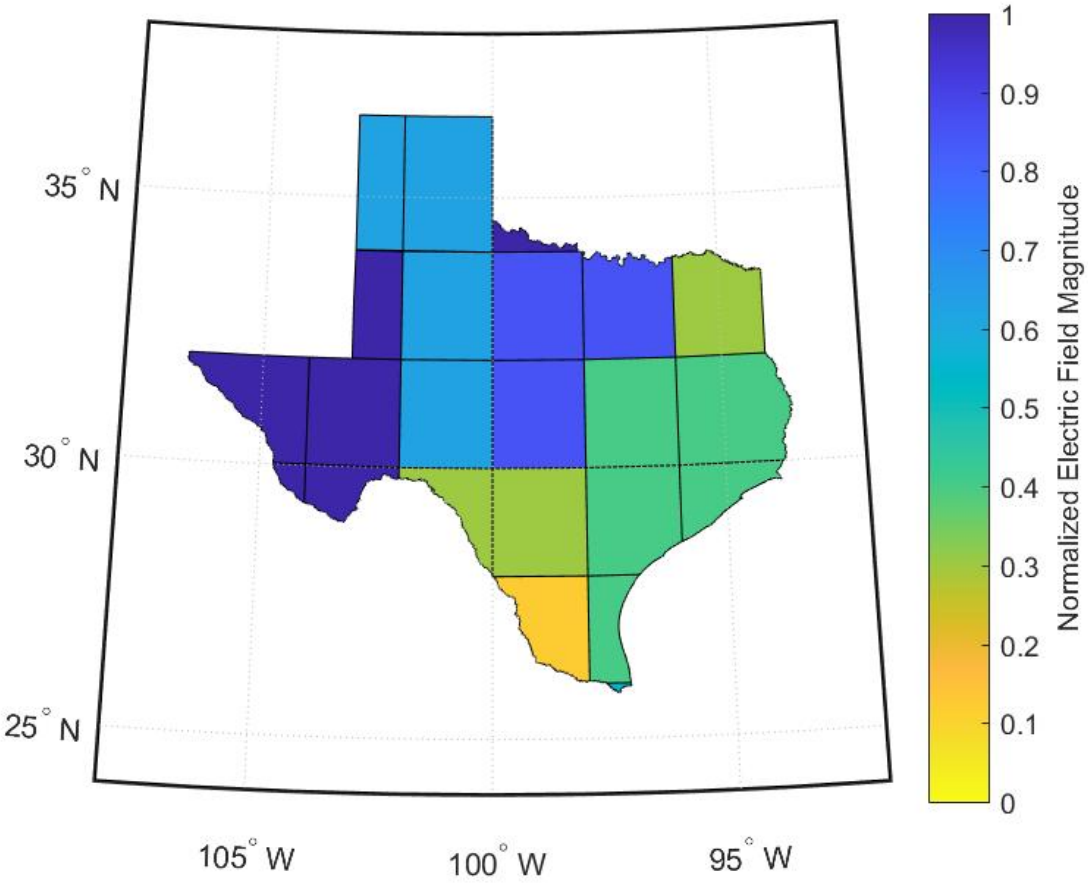

Figure 4.6: An electric field with more spatial variation. In this example, the estimator will recover 20 zones, as opposed to just 4 in Fig. 4.2. Reprinted with permission from [61]

The absolute error for both electric field magnitude and angle estimates, averaged over 1000 Monte Carlo simulations, is shown in Fig. 4.8 for increasing penetration of transformer neutral metering. This is compared to the error of the noisy pseudomeasurements that have not been

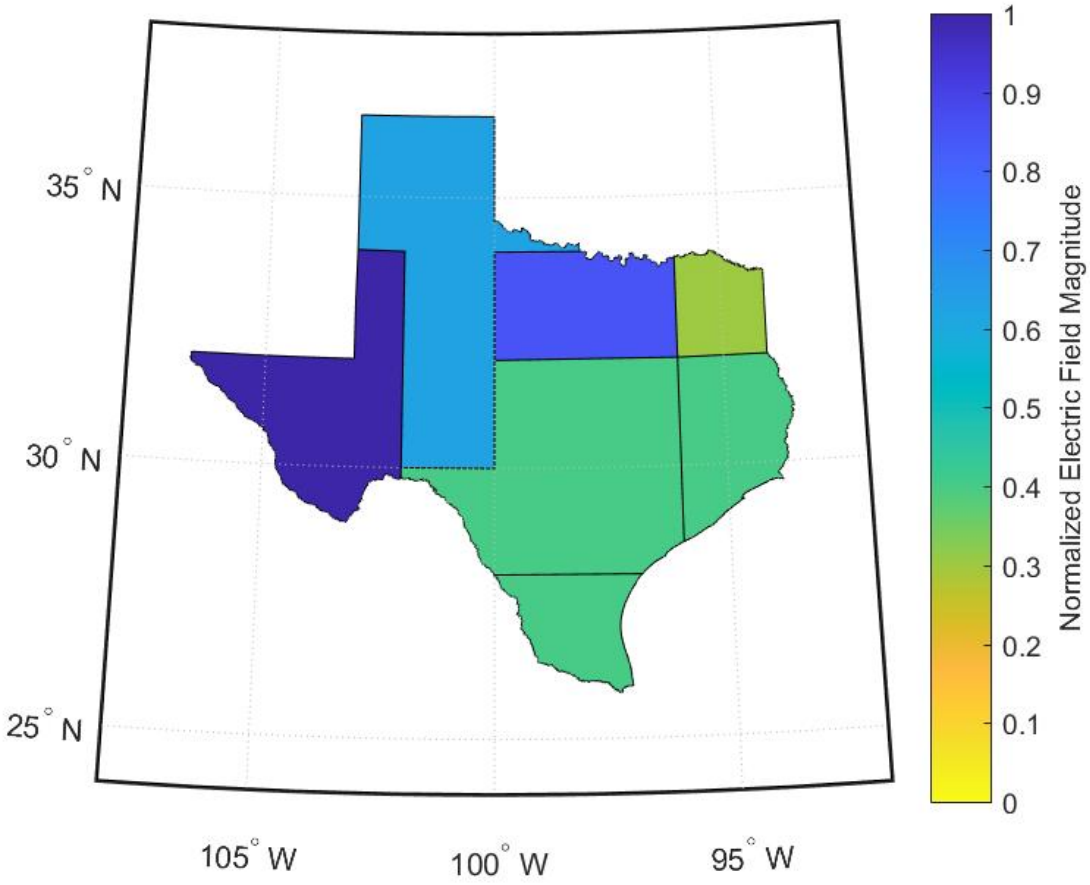

Figure 4.7: Using 7 electric field inputs, this figure shows the electric field "pseudomeasurements" for zones without a magnetometer. Reprinted with permission from [61]

filtered by an estimation process or augmented with additional metering. Note that the error in Fig. 4.8 is greater than that in Fig. 4.5. This is due to the fact that, in this example, the underlying electric field is more spatially varying and thus more states are being estimated from roughly the same amount of data. As more meters are installed in a particular area, future research will provide more insight into the spatially varying properties of electric fields in that region and inform estimator design decisions with respect to estimation specificity.

Initial insight on the trade-offs between estimating more or fewer zones indicates that increasing the number of zones can better match the spatial variability of a realistic geomagnetic storm that results in highly variable electric fields. Granted, this is dependent on there being sufficient

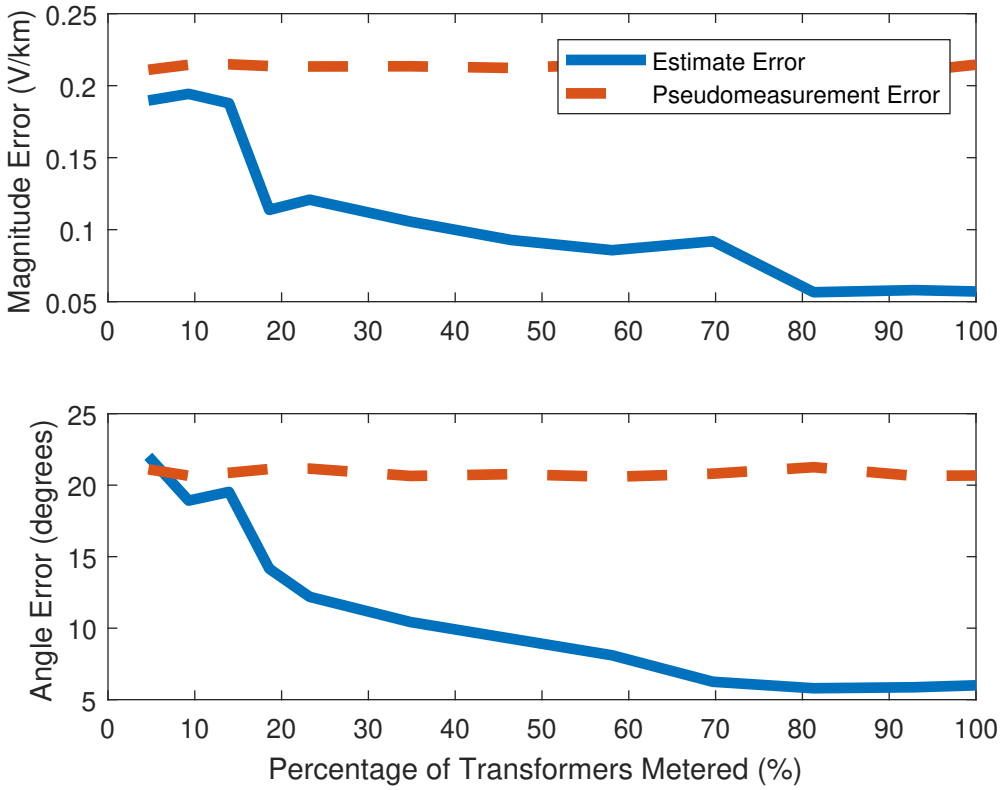

Figure 4.8: Average absolute error for electric field magnitude and angle when estimating 20 zones with 7 magnetometers. Reprinted with permission from [61]

metering to estimate all defined zones with reasonable accuracy. As seen in Fig. 4.9, for less than 30% of transformers (randomly) metered and the same 7 electric field inputs, estimating 12 zones provides better results than estimating 20 zones. This is due to the higher input needs of estimating more states. For future applications, designing the states, and thus the measurement vector, will be dependent on the system and the available metering infrastructure. Offline studies can be used to analyze what level of state granularity might fit the needs of the system operators best.

4.2.4 Additional Practical Considerations of Results

In practice, the estimated electric field states would be used to calculate GICs flowing through the system, which could be fed to some display providing situational awareness to grid operators. Effective GICs across the system are a powerful input to a variety of mitigation algorithms; hence an accurate estimate compared to merely considering the measured values could be the difference

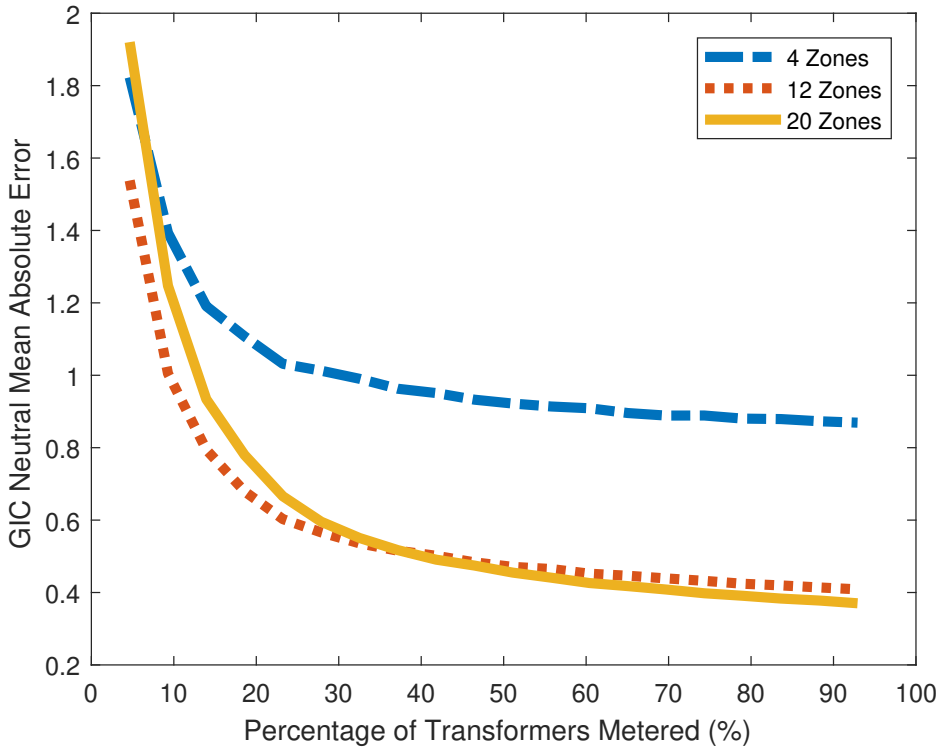

Figure 4.9: GIC neutral mean absolute error for different number of zones with increasing transformer metering penetration. Reprinted with permission from [61]

between taking the optimal action to mitigate GMD damage and taking actions that don't help or make the situation worse. It would also be useful to have alarms tied to these values which would trigger for currents high enough to warrant closer consideration from grid operators. To validate the GIC estimation method under the application of high current alarms, a warning threshold of 50 A is set and the effective GICs across the system calculated from both the input "measurements" and the estimated states. Over 200 Monte Carlo simulations, the number of times that either technique produces a false alarm or fail to recognize a high current transformer is recorded and shown in Fig. 4.10. Without estimation, an average of two false positives and one missed alarm are encountered per simulation, regardless of the number of (random) available GIC measurements. With sufficient metering (about 15 GIC neutral meters for this scenario) and estimation abilities, the potential of encountering an alarm error drops to less than once each per estimation run, and decreases with more measurements. On average, using GIC estimation does not create alarm errors that do not

already exist as a result of just the electric field inputs. This confirms that GIC estimation is a value-added process that is low risk in addition to low effort.

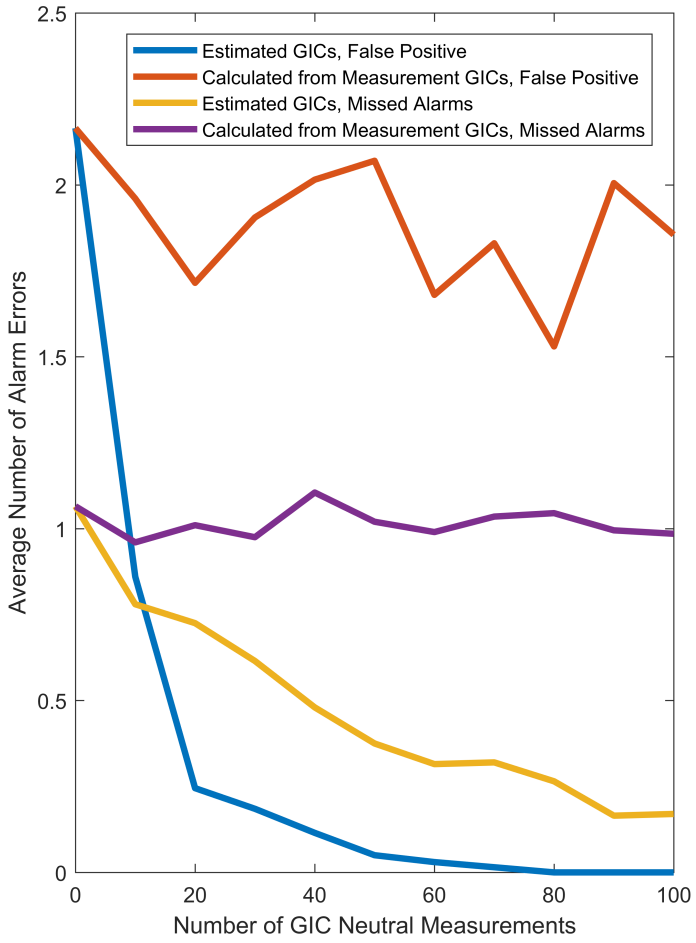

Figure 4.10: Number of false or missed alarms (50 A threshold) from measurements versus estimates. Reprinted with permission from [61]

A common concern with state estimation algorithms is computational efficiency and run time. Because of the linear nature of GICs, this is not an issue for GIC estimation. In practice, the bigger barrier to generating estimates quickly lies in measurement latency. The estimation problem itself takes less than 0.0005 seconds using MATLAB on a PC with a processor Intel(R) Xeon(R) E5-

1650 @ 3.6 GHz. The most computationally expensive part is the inverse in (3.15), which can become intensive as matrix size increases if no special matrix properties are exploited. Fortunately the size of the matrix is two times the number of electric field areas, which would be limited by available meters and the impracticability of too many zones.

In these chapters, a WLS-based GIC estimation has been motivated, designed, and tested. Under a variety of increasingly realistic scenarios, the method proves to be efficient and effective. In the next chapter, GIC estimation is extended to include bad data detection and consideration of measurement placement and noise characteristics.

5. BAD DATA DETECTION AND MEASUREMENT NOISE FOR GIC ESTIMATION

State estimation is expected to leverage measurements and the system model to provide a reliable data set for other monitoring, assessment, and control functions, and it is reasonable to include the detection of measurements errors among the expected functionalities. Detecting, identifying, and eliminating expected and outlying measurement error when possible is crucial to providing a trustworthy system state. In this chapter the discussion will be focused on bad data analysis and the advanced state estimation functionality required to identify, detect, and minimize the effect of bad data. To this end, the concepts of observability and redundancy are introduced and a least absolute deviation estimation scheme developed and tested. Measurements with other non-Gaussian error characteristics are considered as well.

5.1 Background

To maintain estimate quality, comprehensive state estimation algorithms might have the capability to handle one or more of the following error types:

- Measurement Error: these random errors exist due to meter accuracy and analog-digital conversion and communication; this can be filtered out in the estimation process especially when the random error follows a Gaussian distribution
- Parameter Error: these errors are the result of model parameter uncertainty; for GIC estimation this is likely to be uncertainty in substation grounding resistance or transformer winding values
- Bad Data: these larger measurement errors are caused by meter bias, meter failure, or cyber attack
- Topology Error: these errors exist due to wrong connectivity information

Bad data detection includes detecting, identifying, and eliminating the effects of measurements with gross errors which can sway the resulting estimate. These potentially incorrect results can lead

to wrongly informed decisions in extreme cases [40]. The WLS estimation model as described in Chapter 3 is based on an assumption about the measurement error probability distribution, namely that it is Gaussian with zero mean and known variance. In the presence of bad data, the Gaussian assumption upon which the model is built is invalidated.

There are two main strategies for dealing with bad data in state estimation [33, 63]:

- Post-process the results of WLS state estimation to detect and identify bad data
- Replace the WLS state estimator with a more robust estimator

Regardless of method, desirable outcomes include the ability to correctly locate and remove or minimize the effects of the bad data on the state estimate with realistic implementation requirements and reasonable computation time.

Post-processing methods often rely on observing the difference between the measured values and values calculated from the estimated state. Also known as the residual, the measurement corresponding to the largest, often weighted or normalized, residual is eliminated as bad data and the estimation/detection/identification process repeated [64, 65]. Drawbacks of this method include heavy computational burden and potential loss of observability and ability to detect with loss of measurements. Where the residual test looks at the residuals from a global perspectives, hypothesis testing methods using statistical criterion specific to each suspect measurement [66]. Using these methods most bad data can be identified and removed within a few steps.

Alternatively, a more robust estimator can be chosen, specifically one that is less sensitive to deviations from the underlying assumptions. This group of methods are united by nonquadratic criteria where the identification and elimination of bad data is inherently part of the state estimation process itself [67]. Potential drawbacks of these methods include slower convergence and risk of wrong identification.

The contribution of this chapter is leveraging a robust estimation method to detect, identity, and minimize the effects of bad data on GIC estimation. The robustness of a least absolute value-based (LAV) formulation compared to the WLS method proposed in previous work will be shown in the

GIC estimation context, as well as results which show the suitability of the proposed method to detect and deal with bad data using a variety of simulations set on the synthetic Texas 2000 bus case. To enable these methods, a novel discussion on the concept of observability with respect to GIC estimation is also provided. Lastly, to further explore GIC estimation beyond the Gaussian noise assumption, the estimator response to a noise distribution motivated by analysis of real GIC data is demonstrated.

5.2 Observability and Redundancy for GIC Estimation

In this section, the concepts of observability and redundancy are considered for the proposed GIC estimation formulation. These ideas are fundamental definitions for traditional state estimation, and are also foundational to the development and application of estimation methods for GIC visibility. Defining and understanding these concepts enables functionality such as measurement placement and bad data detection, covered in this and the following subsections.

The concept of observability is well-established in the state estimation literature and considered a necessary component of any state estimation program [68, 69, 70]. The gist of the concept is that there exists a sufficient number and distribution of measurements mathematically required to estimate the desired states. Having an overdetermined system, more measurements than states, contributes to observability but is not alone sufficient. As with traditional estimation, a full column rank measurement matrix implies that the states can be uniquely acquired. Therefore, for GIC estimation a full rank matrix $\mathbf{h}$ is a necessary condition for observability. This can be easily checked using Gaussian elimination for small systems and singular value decomposition (SVD) or QR factorization more generally.

Electric field pseudomeasurements and interpolation can be leveraged to provide a full, though approximate, set of input states. For that reason, it is rare for a system to not be observable as defined above. Therefore, a more stringent observability criterion is also defined where observability is achieved when the set of GIC current measurements alone is sufficient to determine the system state. Specifically,

$$\{\mathbf{\Phi G}^{-1}\mathbf{H}\}_l \tag{5.1}$$

must be full rank. While the hardware requirements are greater (at least twice as many GIC neutral current meters as states desired to be estimated), this perspective is less sensitive to uncertainty or errors in electric field input. Ensuring this type of observability is even more important in regions that rely on interpolation because of lack of local magnetometers or have more uncertainty in their conductivity profile.

One unique consideration for GIC estimation is that observability is not only system dependent, but also state definition dependent. In traditional estimation the states (voltage magnitude and angle) are clearly defined. For GIC estimation the states, the boundaries of the electric field zones, can be redefined in a nearly infinite number of ways. Hence, a system may be observable for a particular set of defined states or be made observable using differently defined states. It should be remembered that it cannot be known how much the underlying field actually varies with the existing available instrumentation and that these boundary definitions are based on assumptions.

For GIC estimation, critical measurements are defined as those which if removed from the measurement set render the system unobservable in the stricter sense for the given states. Measurements not considered critical are redundant and redundancy in the measurement set is necessary to be able to identify bad data. Bad data in critical measurements cannot be detected or removed. A simple redundancy metric can be defined, where

$$\mathcal{R} = \frac{\text{number of measurements}}{\text{number of states}} \tag{5.2}$$

. Generally, higher redundancy and lower noise will result in more accurate estimates [71]. In GIC estimation states can be combined, which increases redundancy by decreasing the number of states, but at the loss of estimate granularity. This trade off is a design consideration unique to the GIC estimation formulation.

Lastly, SVD can be used to identify unobservable states and inform future meter installations. Additionally, one unique benefit of the dependence of GIC estimation observability on state definition is that observability can be achieved without time or money by redefining zone boundaries.

With the concepts of observability and redundancy defined, the topic of measurement placement logically follows. While the analysis of Chapter 4 was based on random measurement placement, in practice GIC meters are placed due to a variety of technical and financial reasons. Two measurement placement algorithms are described in this section, representing more realistic and aspirational measurement sets than random for simulation use. They can also be modified to guide in the placement of additional meters for additional redundancy.

The first measurement placement algorithm is risk based. The sites are ranked based on maximum effective GIC current when a uniform electric field is applied to the system in the worst direction for that particular transformer. The p highest locations are chosen to have a meter placed there, where p is the number of meters to be placed as decided on by the system or scenario designer. This method aligns with the likelihood that on real systems meters will be installed at high risk transformers, where risk is determined based on extensive studies which determine which are likely to experience the greatest GIC loading. With this method GIC strict observability and redundancy are not guaranteed but can be achieved with sufficiently large p.

The second placement plan prioritizes balanced geographic placement across predefined zones. The transformers are similarly ranked and placed by high currents, but an additional meter cannot be placed within the same zone until all other zones have the same number of meters. If there are no more transformers to meter within a particular zone, a transformer at one end of the longest line passing through the zone is metered next. When there are no more lines to meter, that zone is as observable as it can be and will be skipped in the algorithm. This meter placement scheme can guarantee strict observability for $p > 2k$, where k is the number of zones and as long as no zones were skipped due to maxing out of available measurement locations related to a particular zone.

For the simulations using the Texas 2000 case which follow, $k = 20$ and $p = 60$. There is basic observability due to the use of electric field measurements and pseudomeasurements, where needed, for the full footprint of the study system. Furthermore, strict observability is achieved as well using both measurement placement schemes and $p = 60$. The risk based placement is show in Fig. 5.1. Even though there are not necessarily meters placed in every zone, the system can still

be observable due to lines incident to the meters passing through the meter-less zones.

Using the geographically-based scheme a minimum of 40 GIC neutral current measurements can provide full current-based observability. Meanwhile, the risk based scheme required at least 50 measurements to be current-based observable. For either scheme, additional measurements help provide the redundancy required to leverage bad data detection.

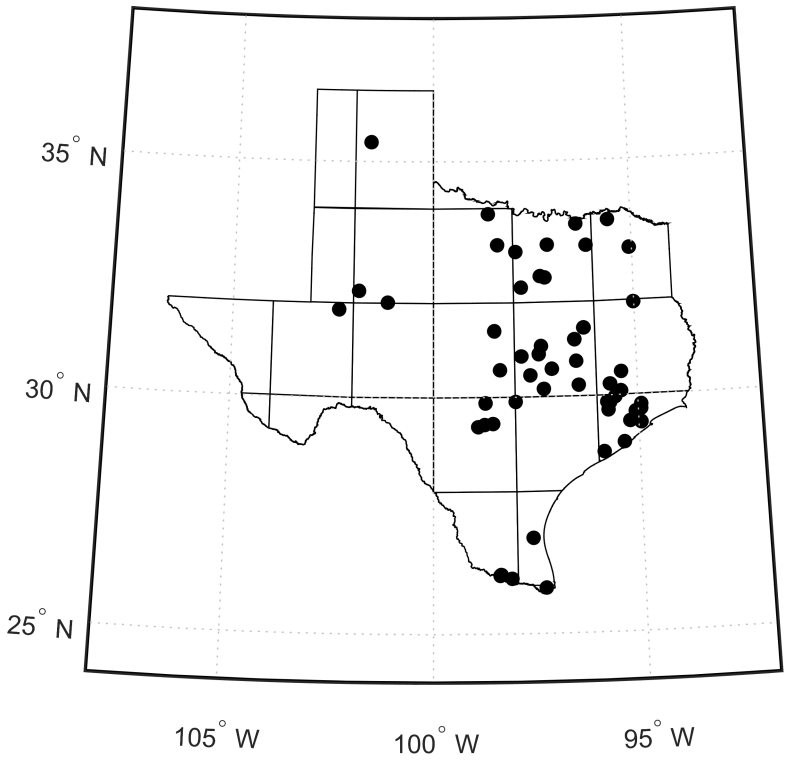

Figure 5.1: Placement of 60 meters for 20 zones using the risk-based measurement placement scheme

With observability for GIC estimation described, as well as the other relevant concepts of redundancy and measurement placement explored, there is a sufficient foundation to consider the bad data detection problem. With sufficient redundancy through appropriate measurement placement, outlier GIC data can be detected and identified as such using the methods provided in the

next subsection.

5.3 Bad Data Detection Methods using Least Absolute Value

If there is an error with a particular or a number of GIC neutral current measurements, it can sway the electric field estimate away from the true value. As the electric field estimates drift from reality in a particular region(s) all resulting GIC currents in that region are affected. Because these values can be used for operator situational awareness and as input to analysis tools for decision making, it is imperative that the estimate is unaffected by bad data. Because of the WLS methods' known sensitivity to bad data, it is difficult to detect and certainly identify the bad data in the measurement set. Therefore, the least absolute value (LAV) method, a more robust estimation approach, is commonly invoked. The major difference being the use of the 1-norm instead of the 2-norm (Euclidean norm) to minimize the difference between the measured and estimated values. While the WLS method has a closed-form solution and can be efficiently computed, there is no closed-form solution for the LAV estimation approach. The problem can be converted to a linear program and maintains low computational complexity when using one of the many available efficient solvers.

The LAV approach, or minimization of the sum of absolute deviations between sets of predictions and observations, also starts with the measurement model at a moment in time presented in (3.11). Consider the form

$$\epsilon_i = z_i - h_i \mathbf{x}. \tag{5.3}$$

where the ith observation is denoted by i, the deviation is given by the real value ϵ_i and the measurement (observed) value is z_i. Like previously formulated, the matrix $\mathbf{h}$ represents the relationship between the measurements and states and h_i is the row of $\mathbf{h}$ that corresponds with the ith

observation. The minimization of the summation of the absolute deviations for all ϵ_i is:

$$\begin{aligned} \min_{\mathbf{x}} \quad & \sum_i |\epsilon_i| \\ \text{s.t.} \quad & \epsilon_i + h_i \mathbf{x} = z_i \; \forall i \\ & \epsilon_i \in \mathcal{R} \end{aligned} \tag{5.4}$$

The problem is not yet a linear program (LP) due to the nonlinearity of the absolute value function. Common methods for transforming the LAV problem into an LP include bounding, using the dual, and variable splitting, which will be used here. Variable splitting involves the introduction of the non-negative auxiliary variables ϵ_i^+ and ϵ_i^- such that

$$\epsilon_i = \epsilon_i^+ - \epsilon_i^-. \tag{5.5}$$

The absolute value objective can be represented as the sum of two variables, $\epsilon_i^+ + \epsilon_i^-$, as long as the product of the two variables is zero, i.e., $\epsilon_i^+ \times \epsilon_i^- = 0$. This results in the LP

$$\begin{aligned} \min_{\mathbf{x}} \quad & \sum_i (\epsilon_i^+ + \epsilon_i^-) \\ \text{s.t.} \quad & \epsilon_i^+ - \epsilon_i^- + h_i \mathbf{x} = z_i \; \forall i \\ & \epsilon_i^+, \epsilon_i^- \geq 0 \end{aligned} \tag{5.6}$$

where the nonlinear product constraint is dropped because the minimization of the sum of the terms implies that at least one of the terms must be zero. Now as an LP, the LAV problem can be efficiently solved using any of a host of publicly available linear solvers, such as those found in the SciPy package for Python [72].

5.4 Bad Data Detection Results

Using the GIC estimation bad data detection method outlined in the previous subsection, the ability of the proposed LAV technique to detect and identify bad data is presented in the results

here. First, the sensitivity of the WLS-based method to bad data is shown. The resulting estimate error motivated the development of alternative means. Next, the LAV-based method is shown to better detect and minimize the effect of bad data under a variety of schemes. These scenarios include magnitude of data corruption, varying identification thresholds, and more. Lastly, the LAV-based method performance with multiple bad data is tested.

5.4.1 Test Scenario

The effects and mitigation of bad data in the GIC state estimation context are demonstrated on the synthetic 2000-bus power system set on the footprint of the state of Texas [73]. When a snapshot of the electric field at a moment in time anchored with geographic coordinates is provided, GICs flowing in the system can be found using a power system analysis software with GIC capabilities. The electric field is assumed to be nonuniform across the system, but uniform within each of 20 predefined zones.

To generate noisy, but not outlying, measurements, a subset of 60 of the potentially available neutral GIC results at every transformer are exported from the software. The measurements which comprise the subset are chosen by the geographically based placement algorithm laid out in Section 5.2 and superimposed with random Gaussian noise with zero mean and a particular variance. Outlier measurements are generated by multiplying a particular measurement by a factor ranging from 0.6 to 10. This factor is referred to as the corruption multiplier (CM). Six synthetic magnetic field meters are made available, which combined can be used to calculate local electric fields with knowledge of the earth's conductivity models in that area. If an electric field data point is not available in a particular zone, electric field data from the same regional conductivity region is used as a pseudomeasurement for that zone, with preference given to the geographically closer data when multiple options are present.

5.4.2 WLS Sensitivity to Bad Data

It is known that WLS estimators are sensitive to bad data and that outliers may lead to poor estimates. To demonstrate this effect for GIC estimation, one of the elements of the neutral GIC

measurement vector is corrupted and the WLS-based estimate found. The GIC current magnitudes calculated from this estimate are compared to the actual values and plotted for every transformer in the system in Fig. 5.2. Even though only one transformer was affected with bad data, the resulting skew of estimated electric field state(s) leads to multiple transformers being ineffectively monitored.

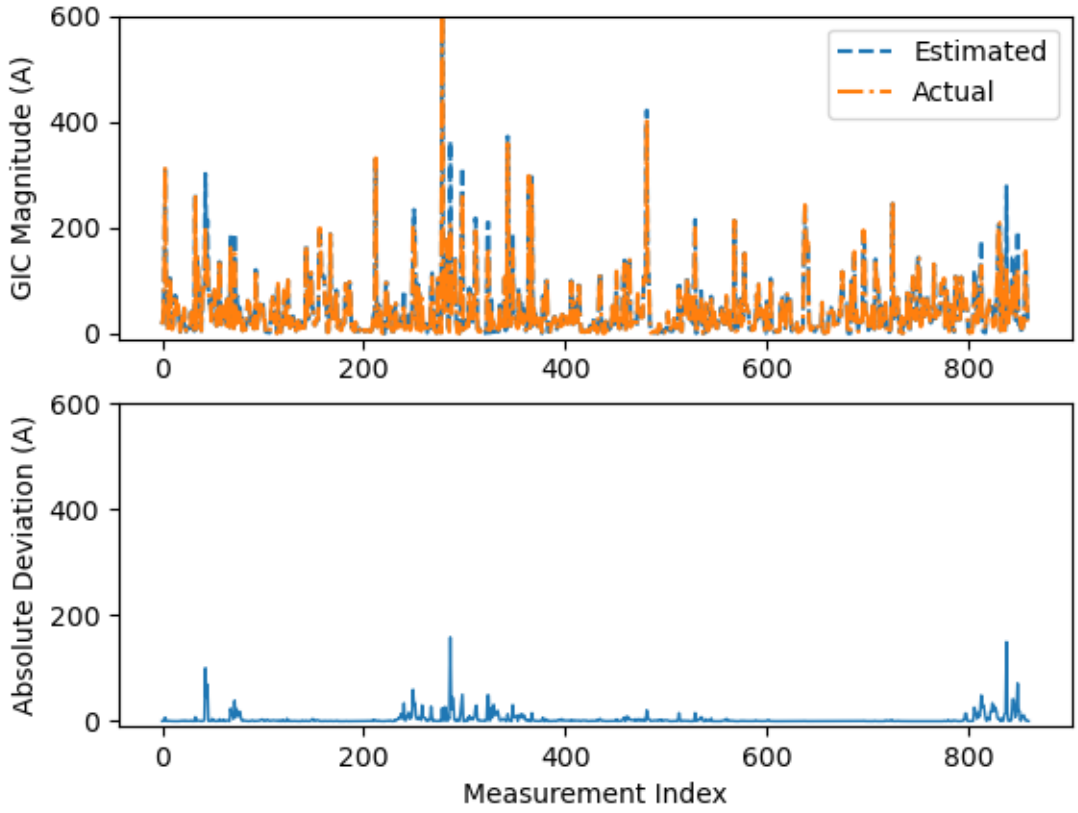

Figure 5.2: WLS-estimated and actual GIC magnitude values at each transformer with one measurement corrupted (multiplied by 1.5). The absolute difference between these values is also shown

To generalize these effects, the extent to which the data is perturbed is varied from CM $= 0.5$ to CM $= 2$. Each GIC measurement out of 60 has a turn being corrupted for 50 Monte Carlo simulations, where the randomness is manifest in the noise of the non-corrupted measurements. From

the resulting electric field estimate the neutral GICs are calculated across the system and compared to the known true value. Fig. 5.3 shows that the more corrupted the bad data measurement, the greater the average GIC error due to estimate error. This can exceed 15A in some simulations, such as the worst case scenario with respect to which measurement is corrupted, denoted by the dashed blue line. On the other hand, only half of the corrupted measurements lead to an average error greater than 3A at CM $= 2.0$. The average across the different corrupted measurements at the different corruption levels is denoted by the solid orange line. For reference, in this particular scenario the system is experiencing a sizeable GMD with an average electric field magnitude of 4V/km and thus the average neutral GIC is greater than 40A. In the remainder of this section, the robustness of the alternative LAV-based estimator to bad data is demonstrated.

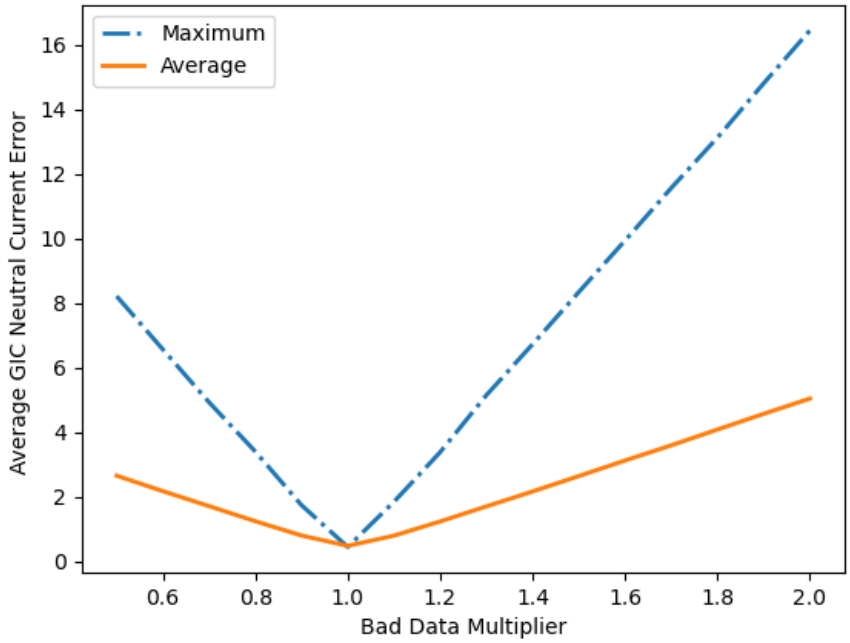

Figure 5.3: WLS estimation deteriorates with increasing data corruption. Each of the 60 measurements are individually corrupted and the average and worst case results shown

5.4.3 LAV Bad Data Identification and Minimization

The LAV-based estimation effectiveness is shown by achieving two objectives:

- the bad data can be identified
- the effects of the bad data are minimized.

The largest absolute deviation between a measurement and resulting estimate is a potential element of bad data, and the bad data is correctly identified when this consistently aligns with the erroneous data. Incorrect identification, or false positives, should also be considered when assessing the the LAV-based estimation's effectiveness. The robustness of LAV estimation is demonstrated by lack of sensitivity of the estimate to the magnitude and placement of the bad data.

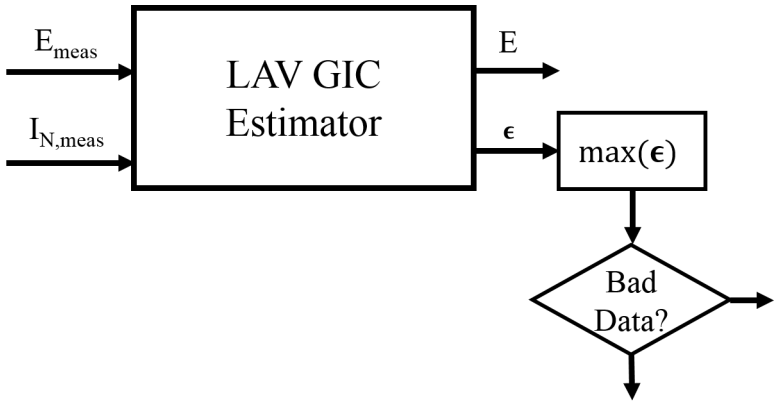

Figure 5.4: Flow chart representing the inputs and post-processing required for bad data identification

The identification, and not just the suppression, of bad data is valuable to the overall process of situational awareness. The difference between the measured and estimated values is equivalent to ϵ, which is easily found from the auxiliary variable results of the LAV estimation linear program. The maximum deviation can then be analyzed to determine if the corresponding measurement should be considered bad data, as seen in Fig. 5.4. To demonstrate this, an introductory example

is provided. Let Measurement 5 experience varying amounts of corruption, from 100% to 130% of its true value, where each level of corruption is depicted in a different subplot of Fig. 5.5. The resulting absolute deviation, or residual, between measurement and estimate is plotted for each bus for 12 random noise simulations and a vertical red dotted line plotted denoting the index of the corrupted measurement. The expectation is that the peaks of the simulation plots will a)

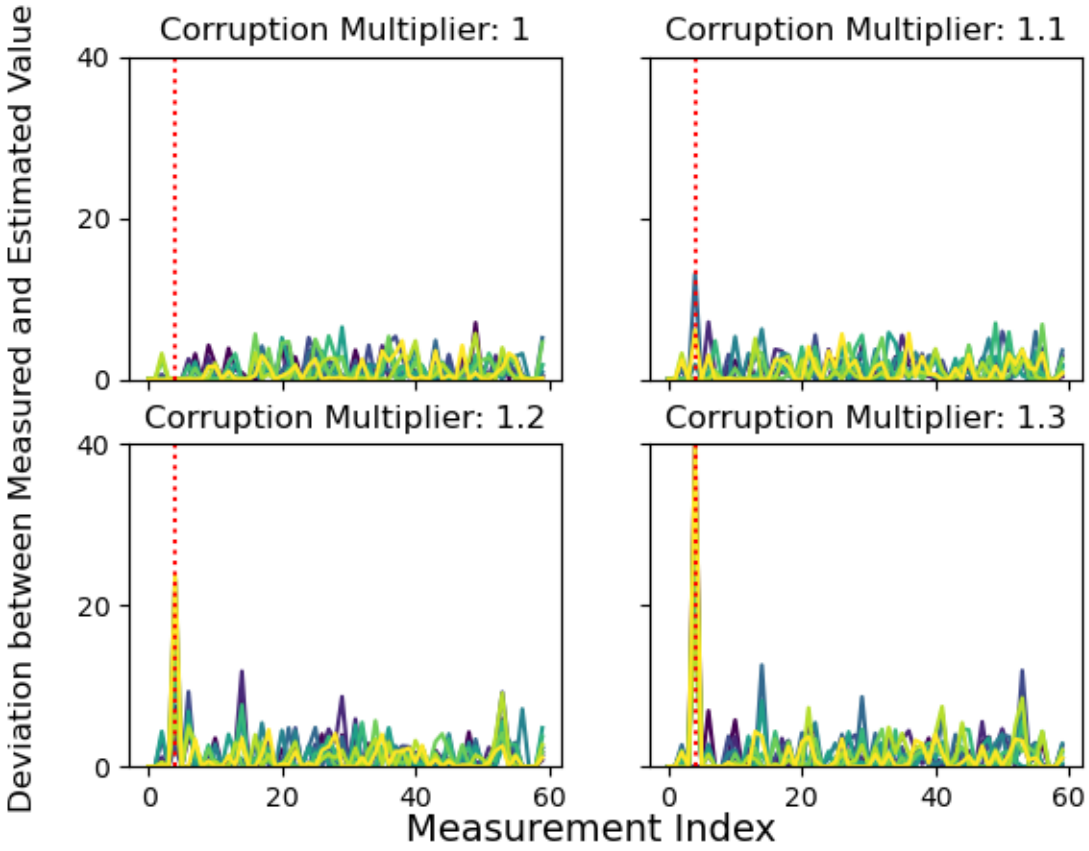

Figure 5.5: Absolute difference between measured and estimated GIC neutral current values for all system buses when the corruption of Measurement 5 is varied from CM=1 to CM=1.3

clearly be the maximum value and b) align with the dotted red line. For the bad data-free scenario (CM $= 1$), there is not a clear outlier among the deviations. This is to be expected in this situation as all the measurement noise follows the expected normal distribution. As the corruption increase

towards CM $= 1.3$ an outlying residual becomes more apparent. This greatest absolute difference coincides with the bad data index (red dotted line) confirming that this can be an effective method of identifying bad data.

To prevent bad data from being incorrectly flagged, a series of thresholds are developed which help distinguish between actual bad data and variations due to expected measurement noise. The use of similar thresholds is commonly employed with normalized residual testing methods to lower the probability of false positives in bad data detection [74]. Consider a variation on the measurement residual, the absolute difference between the measurements, $\mathbf{z}$, and values calculated from the estimated states, $\hat{\mathbf{x}}$, in vector form,

$$\mathbf{r} = |\mathbf{z} - \mathbf{h}\hat{\mathbf{x}}|. \tag{5.7}$$

Let r_i denote the ith greatest value of $\mathbf{r}$; e.g. $r_1 = \max(\mathbf{r})$, r_2 is the second greatest value of $\mathbf{r}$, and so on. The following threshold schemes, summarized in Table 5.1, leverage the elements of $\mathbf{r}$. Threshold schemes can include simple criteria (S), relative bounds (RB), and lower bounds (LB) with a representative subset of possibilities shown here. Threshold S employs the most basic

Threshold	**Bounds**
S	none
RB $= \alpha$	$r_1 > (\alpha \times r_2)$
LB $= \beta$	$r_1 > \beta$
RB $= \alpha$ LB $= \beta$	$r_1 > (\alpha \times r_2), \quad r_1 > \beta$

Table 5.1: Summary of residual threshold schemes for bad data identification

algorithm; the index with the largest deviation is tagged as “bad data," as shown in Fig. 5.6.

Assuming the same system, storm, measurement network, and noise characteristics (for non-corrupt data) from before, Fig. 5.7 shows that when this method is used there is the potential for excessive identification of the wrong measurement, denoted by the orange area. This overzealous

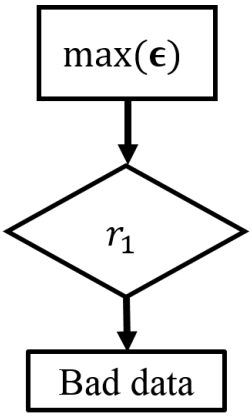

Figure 5.6: Flow chart showing the simple threshold method for bad data identification

method is not very useful on its own, but could be used in conjunction with other post-processing tools for analysis of potentially bad data.

To improve upon this scheme, a relative bound is instated, as seen in Fig. 5.8a. This restricts the identification of bad data unless the largest difference is at least a certain multiplier α greater than the second largest difference, i.e. $r_1 > (\alpha \times r_2)$. In Fig. 5.9, a relative bound is instated of 1.5 (Threshold RB=1.5). Note that the rate of wrong identification drops in most situations, though the rate of false positives is still rampant when there is no bad data input, i.e. CM=1. One trade-off of using this threshold is that some buses which previously experienced a nearly 100% rate of correct identification are now in in the 60%-90% range. Depending on the next step when bad data is identified, a lower rate of false positives or a higher rates of correct identification may be more desirable.

To further minimize false positives, a lower bound is added, as seen in Fig. 5.8b. This considers whether the difference between measured and estimated values is significantly large, regardless of the relative largeness of the greatest difference. Lower bounds of 5, 10, and 15 are tested, the results of which are shown in Figs. 5.10, 5.11 and 5.12, respectively.

In these particular scenarios, Threshold LB=5 greatly improves the bad data detection performance when CM $= 1$ without noticeable loss of performance when bad data is present. A lower bound of 15 nearly eliminates false positive identification, but also removes the ability to identify

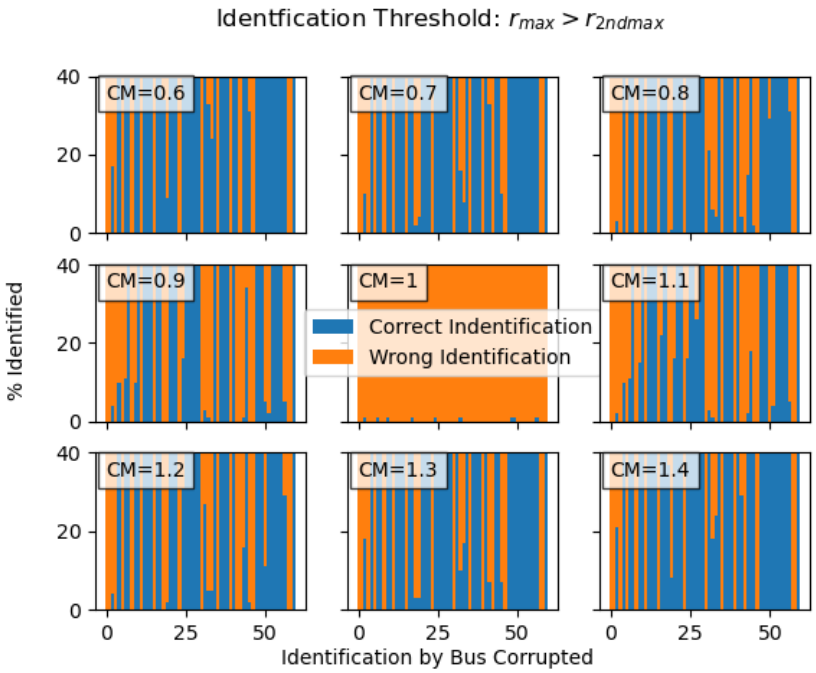

Figure 5.7: Percent of bad data correctly and incorrectly identified for each of 60 measurements (x-axis) with varying corruption (60% to 140% of true value) using Threshold S

nearly all bad data when $0.90 <$ CM < 1.10. Threshold RB $= 1.5$ LB $= 10$ appears to provide a good compromise, performing well when there is no bad data yet still able to identify some bad data in the $0.90 <$ CM < 1.10 range. Again, depending on the application of the knowledge of the presence of bad data (or lack thereof) there may be motivation for the system monitoring designers to be more or less aggressive with one or both of the thresholds. For practical applications, threshold parameters may be system and even storm dependent. One way to minimize threshold dependence on the underlying storm and an area for future work could be to determine the lower bound based on a function of the average measurement GIC. Further research and extensive offline studies will be needed to inform these ounds when used in the real world.

As might be noticed in Fig. 5.7, even with the simplest threshold some buses are not able to be identified when corrupted using this particular measurement set chosen using a geographically based algorithm. While the system is technically observable there is insufficient redundancy in some regions to isolate the bad data. Bad data in critical measurements is not able to identified from

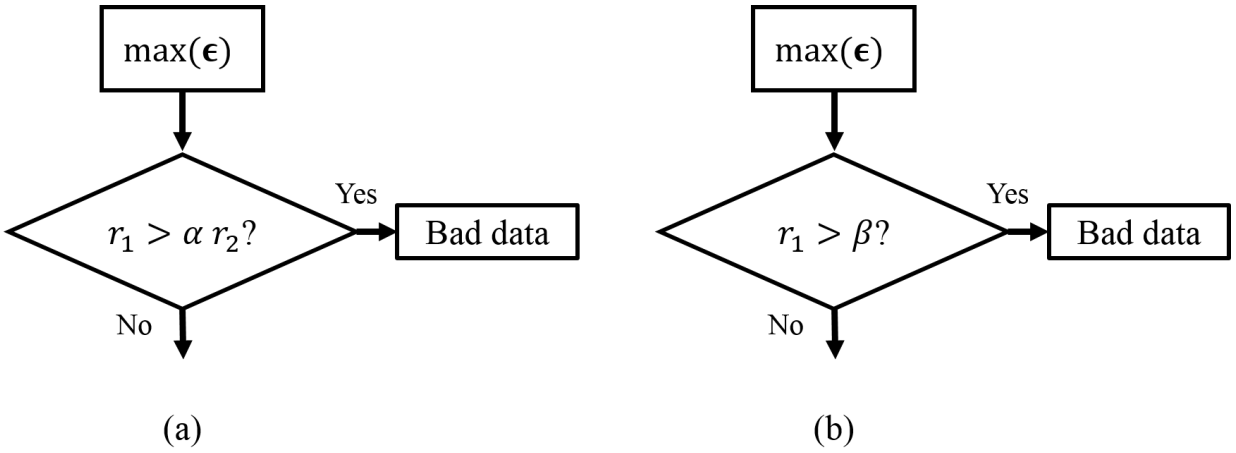

Figure 5.8: Flow charts showing the bounded threshold methods for bad data identification. (a) Threshold RB $= \alpha$ (b) Threshold LB $= \beta$

these methods. A closer look at this effect is demonstrated in the following example. Assuming the same system, storm, measurement network, and noise characteristics (for non-corrupt data) from before, each of the 60 measurements is given CM $= 1.5$. The LAV estimation is performed and the resulting absolute deviation for all measurements for 10 random Monte Carlo simulations plotted, see Fig. 5.13. The index of the measurement that has been corrupted is indicated by the vertical dotted red line. Sometimes the maximum deviation is clear, see Measurements 17-20. When these buses are corrupted they would be likely to be correctly identified as such regardless of the previously discussed threshold used. For Measurement 21, r_1 does coincide with the expected bus index, but the difference is subtle and would be excluded depending on the lower bound chosen. Measurement 16 is not able to be identified as bad data. Analysis of similarly unidentifiable buses shows that they are likely to be on the edges of the system, where the states have fewer transformers and lines available to provide redundancy.

The LAV-based estimator performs well in terms of average error of the resulting estimates and calculated GICs. For $1 <$ CM < 10 the average absolute GIC neutral current error is found over 50 Monte Carlo simulations at each corruption level for each measurement corrupted using LAV estimation. The average error is always less than 0.25 A, regardless of which measurement is corrupted. Compared to the WLS method, LAV estimation error does not increase with increasing

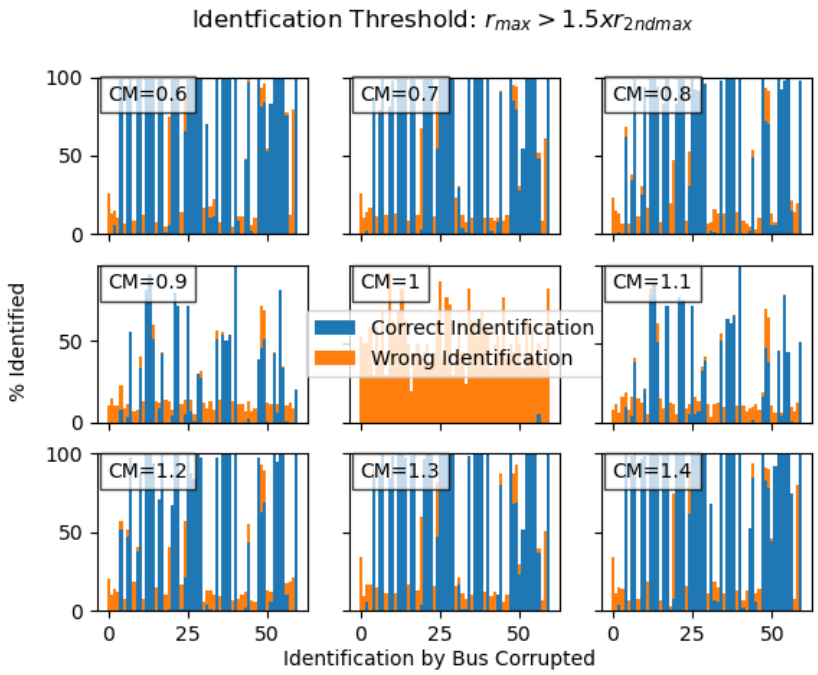

Figure 5.9: Percent of bad data correctly and incorrectly identified for each of 60 measurements (x-axis) with varying corruption (60% to 140% of true value) using Threshold RB=1.5

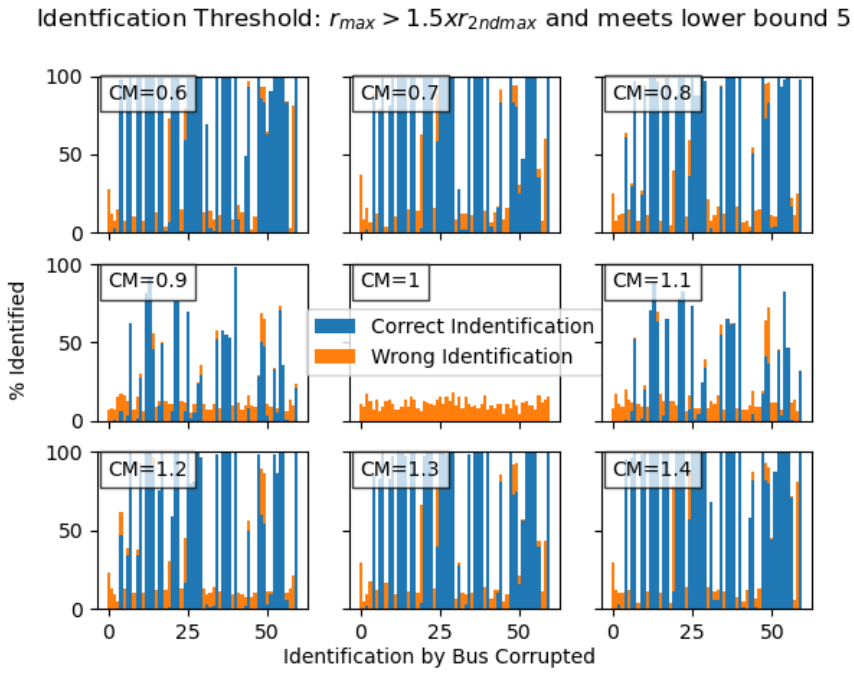

Figure 5.10: Percent of bad data correctly and incorrectly identified for each of 60 measurements (x-axis) with varying corruption (60% to 140% of true value) using Threshold RB=1.5 LB=5

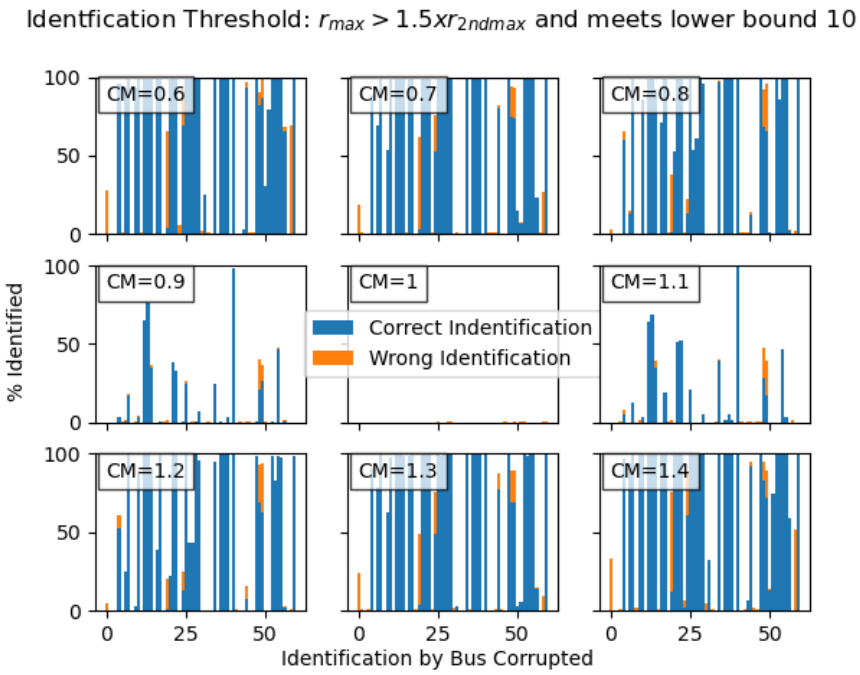

Figure 5.11: Percent of bad data correctly and incorrectly identified for each of 60 measurements (x-axis) with varying corruption (60% to 140% of true value) using Threshold RB=1.5 LB=10

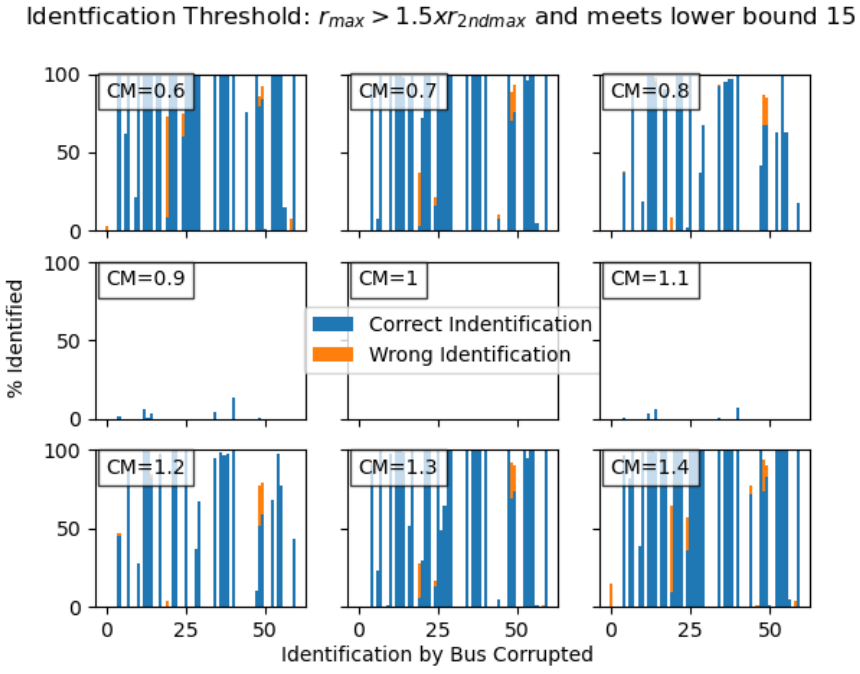

Figure 5.12: Percent of bad data correctly and incorrectly identified for each of 60 measurements (x-axis) with varying corruption (60% to 140% of true value) using Threshold RB=1.5 LB=15

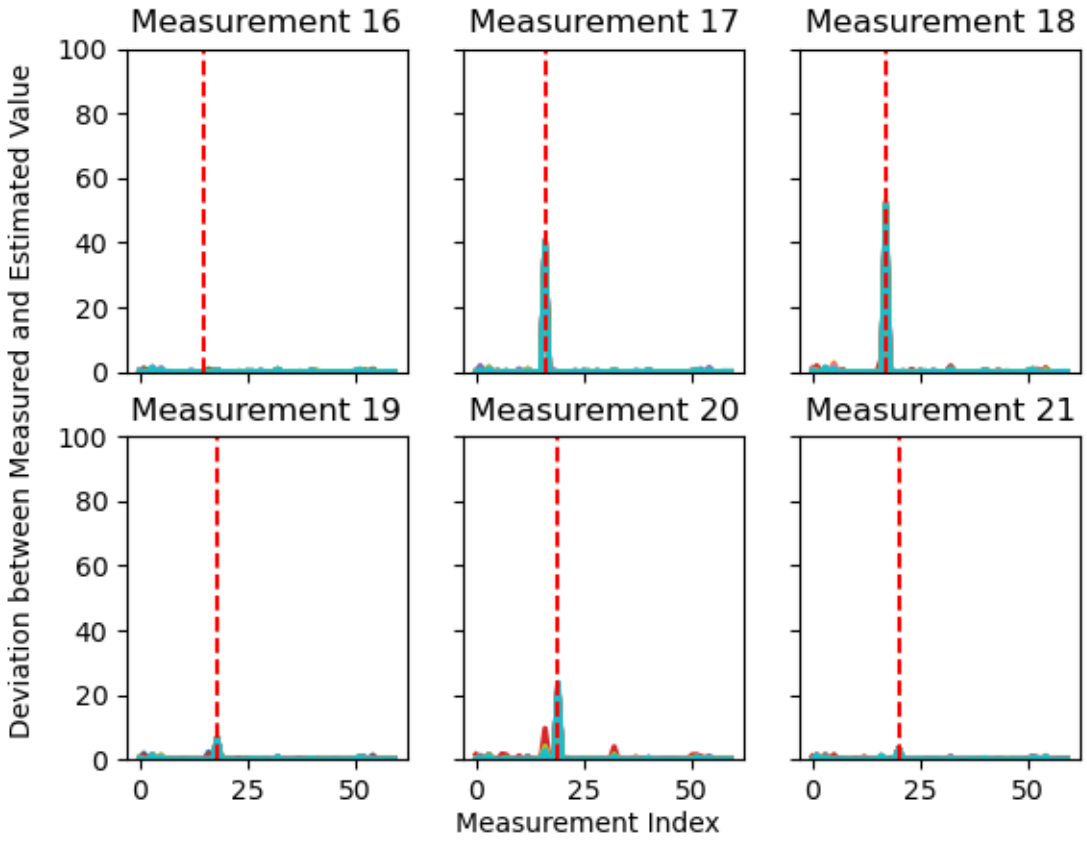

Figure 5.13: Measurement residuals when measurement indices 16-21 (of 60) are corrupted

corruption multiplier applied to generate bad data. In Fig. 5.14 the average error across the different measurements and worst case measurement corruption error are shown. While the WLS results deteriorate with increasing CM, the LAV results are unaffected in the general and worst case sense.

Furthermore, while LAV estimation has been shown to better identify and not be swayed by bad data, its major drawback is computational inefficiency. For this particular scenario, the WLS method takes on average less than 0.023 seconds to solve. Meanwhile, the LAV method takes an average of 4.66 seconds to solve.

5.4.4 Multiple Bad Data

Up until this point, the focus has been on single pieces of bad data. In practice, there may be multiple sources of bad data, interacting and non-interacting. For non-interacting bad data,

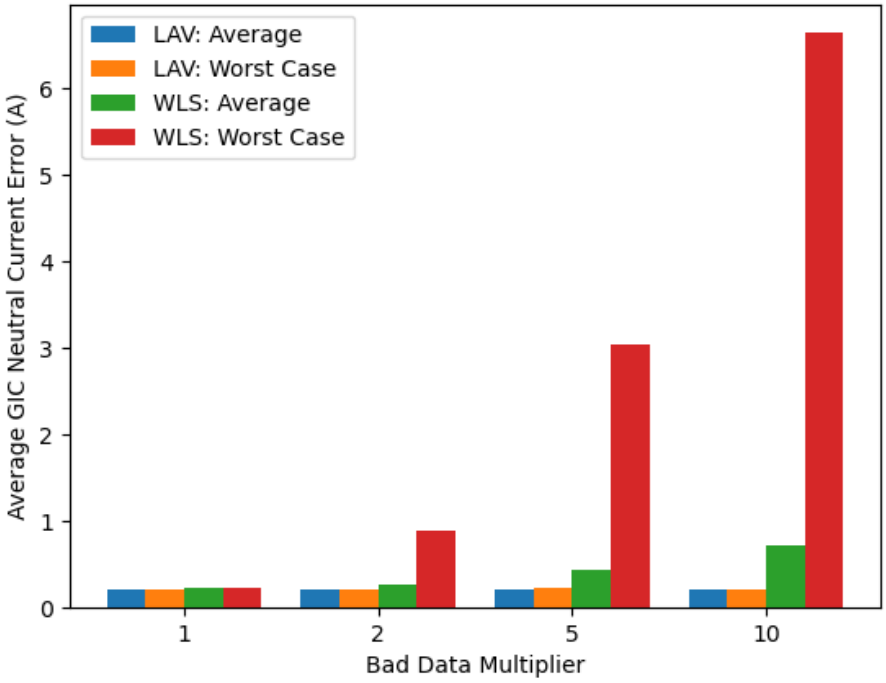

Figure 5.14: Compared with WLS estimation, LAV estimation does not deteriorate in terms of average GIC error with increasing corruption of bad data

the previously described residual based methods are still valid. As seen in Fig. 5.15, the bad data elements, with indices denoted by vertical red dotted lines, clearly align with the likely-to-be-identified elements, denoted by deviation peaks, in more than half of the multiple bad data simulations shown. Noting the similar magnitude of the residuals for both bad data elements in Measurements 17 and 18, using a relative bound threshold would not detect bad data in this measurement set. To counter this, one of two strategies can be employed. The first is an iterative method, where the largest residual is compared to a lower bound threshold, but is not checked by a relative bound. This accounts for the potential situation as seen for Measurements 17 and 18. Then this measurement is thrown out of the measurement set and LAV estimation run again, assuming system observability is maintained. The process can be repeated until r_1 fails a bad data threshold check or the system becomes unobservable. One drawback to this method is that without leveraging a relative bound, iterations may continue to test for bad data even if there is

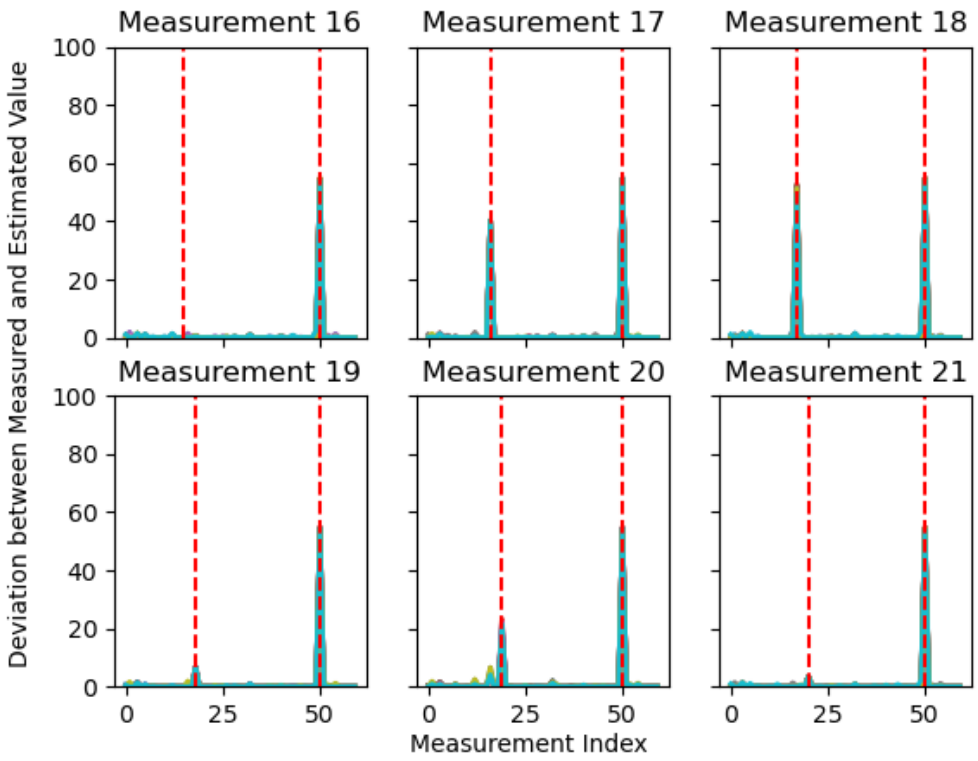

Figure 5.15: Measurement residuals when measurement indices 16-21 (of 60) and Measurement 50 are corrupted

none, leading to false positives.

A second strategy involves looking at $\Delta r_{ij} = r_i - r_{i+1}$. The largest Δr_{ij} will be the bad data threshold such that the bad data corresponds to $r_1, ..., r_k$ where

$$k = \arg\max_i \Delta r_{ij}. \tag{5.8}$$

In terms of performance, this method will not be as thorough as the iterative method. For example, it would not be able to identify Measurement 20 as bad data in Fig. 5.15 because its residual is closer in magnitude to the largest residual less than it than it is to the smallest residual greater than it. The benefit of this method is that it only requires one LAV solution, making it a potentially quicker identification method than the iterative method. Exploring interacting bad data is an area

for future work, as the present lack of measurement redundancy may prove a challenge to the identification especially of conforming bad data.

5.5 Measurement Noise Considerations

A commonly held assumption in power systems state estimation is that the measurement noise follows the Gaussian distribution. This in part allows for the equivalence of the maximum likelihood and weighted least squares estimates. In recent years, this assumptions has been revisited, especially with respect to PMU and distribution system related measurements [75, 76, 77]. It has been shown that these measurements' errors potentially follow thick-tailed non-Gaussian probability distributions. In this section, real GIC data is analyzed for error distribution insight and the GIC estimation performance assessed when using synthetic measurements affected by non-Gaussian noise.

Real GIC data measured from 12 substations in the Bonneville Power Administration (BPA) footprint in the Pacific Northwest is available at [78]. The data, available at 5 minute increments, is sampled over the course of a few days in November 2019 and plotted in Fig. 5.16. Unfortunately, at least a third of meters provide irrelevant data, as seen in Fig. 5.16, and likely need to be serviced or checked on. This illustrates previously discussed metering challenges and the importance of developing useful applications which leverage this data to motivate the increased installation and upkeep of such meters. During November 29 through December 5 it was relatively quiet, geomagnetically speaking, after some Kp4 activity the previous week; the Kp index during this period is shown in Table 5.2 [79].

11/29	11/30	12/1	12/2	12/3	12/4	12/5
Kp3-	Kp1+	Kp2-	Kp1	Kp0+	Kp2-	Kp1-

Table 5.2: Kp index for November 29-December 5, 2019

In [75], measurement error was determined using redundant measurements and then statisti-

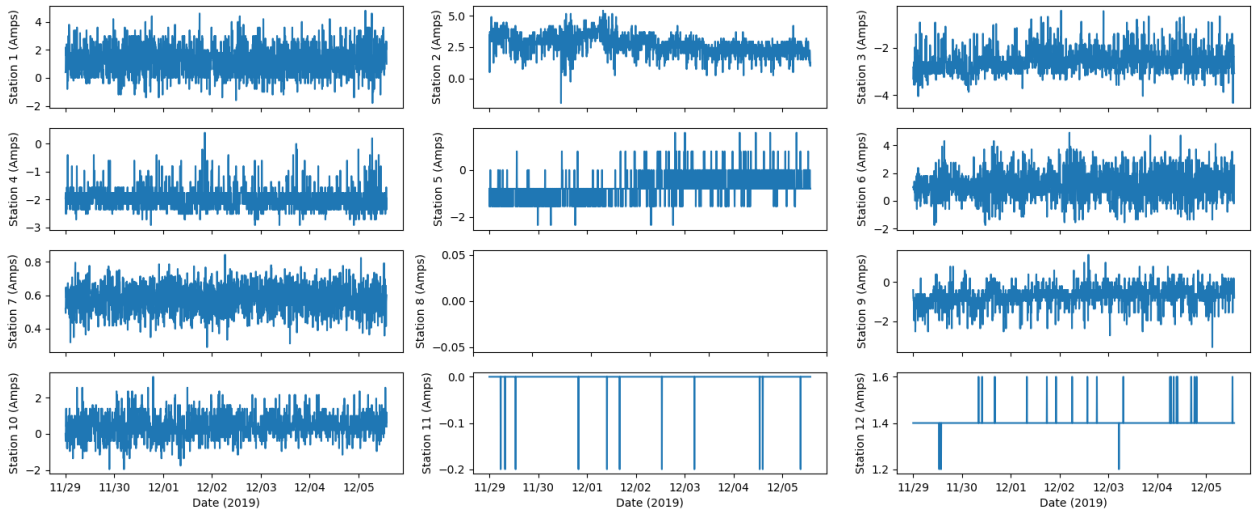

Figure 5.16: 5-minute GIC data from BPA from November 29 to December 5, 2019

cally analyzed using the Shapiro-Wilks test. The Shapiro-Wilks test is used to determine whether a sample came from a normally distributed population. The result is a p value that indicates rejection or not of the null-hypothesis that the population is normally distributed. Without redundancy in the BPA measurement set, it is assumed that because of the low geomagnetic activity on December 2-3 the GIC readings should be essentially 0. Therefore the measurement error analogous to that used in [75] is the BPA GIC signal itself. A Shapiro-Wilks test is applied to each meter's data set and p is found to be less than $\alpha = 0.05$ and the null hypothesis rejected. To see if the data is thick-tailed, as was found for PMU data, the probability density function (PDF) is approximated by binning and plotting a normalized histogram of the data. The mean and standard deviation of the data from each meter is found and the Gaussian, Laplace, and Cauchy PDFs with those characteristics also shown in Fig. 5.17. To this end, the Laplace distribution does appear to be a good fit for the data. As this preliminary analysis is dependent on the assumption that the expected GIC was 0 during this period, additional real world data, especially closely located magnetometer and/or GIC data, could shed more definitive light on the actual noise characteristics.

Next, non-Gaussian (Laplacian) noise is superimposed on the synthetically developed measurements and the performance of the GIC estimation methods demonstrated. The same parameters,

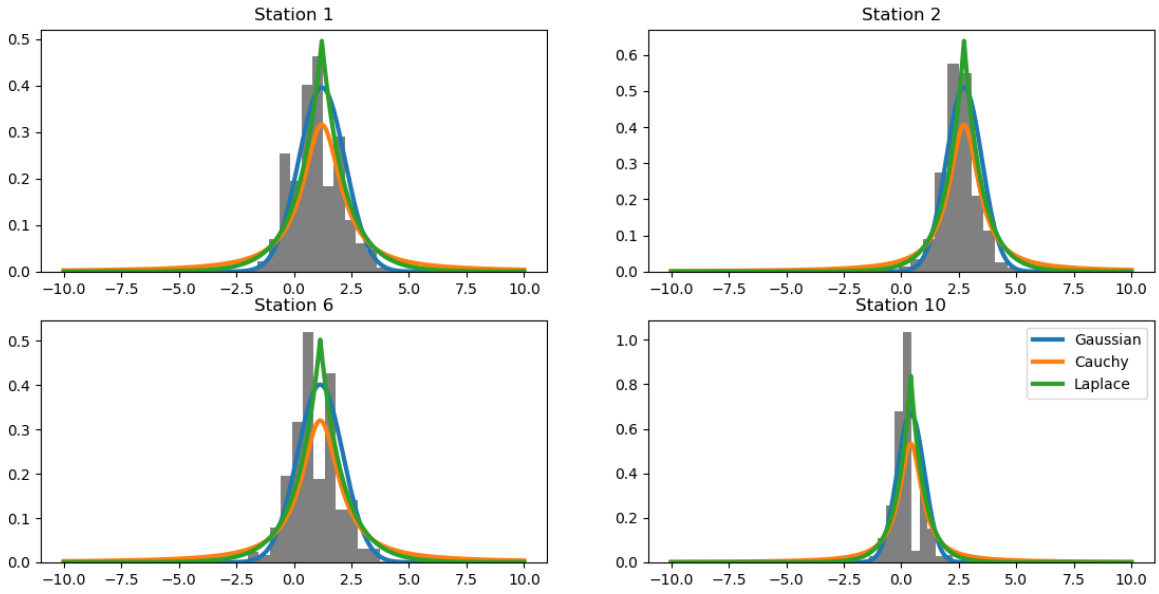

Figure 5.17: Estimated PDF of real GIC data (gray) compared to Gaussian, Laplace, and Cauchy PDFs with the same mean and standard deviation

variance for Gaussian and scale for Laplace, are used and 50 Monte Carlo simulations run at each noise level and the WLS results compared in Fig. 5.18. As is to be expected, the WLS GIC estimation method experiences better performance when the measurement noise follows a normal distribution. Future work can leverage increasingly available data to better understand GIC measurement noise and address necessary improvements to the estimations methods accordingly.

5.6 Summary

In this chapter, extensions to the GIC estimation problem are investigated. A brief overview of bad data detection methods in power system state estimation is provided and an equivalent LAV-based process with respect to GIC estimation designed and tested. To achieve this goal, the concepts of observability, redundancy, and measurement placement are defined with special considerations for the GIC estimation context. The proposed detection and identification methods are tested on the synthetic Texas 2000 bus case and the LAV-based estimation performance shown under a variety of corruption levels, with a variety of identification thresholds, and with multiple bad data. Real GIC data is analyzed and the sensitivity of the estimation methods to non-Gaussian

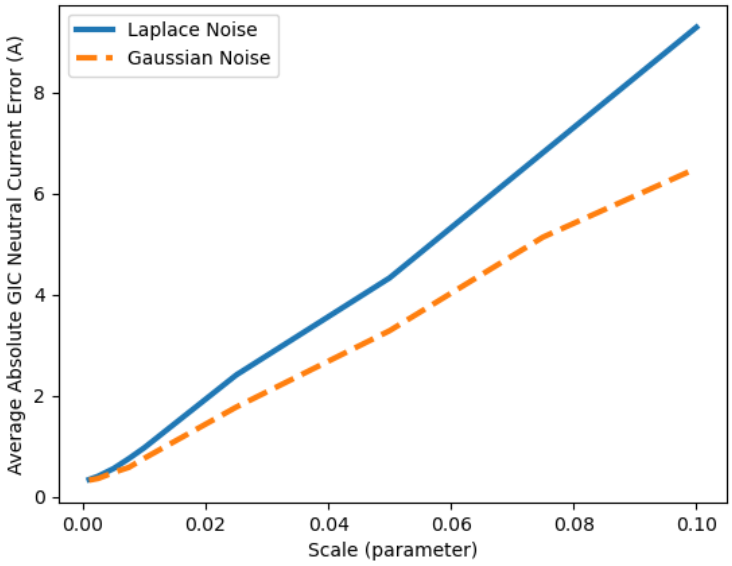

Figure 5.18: WLS estimation GIC error when the measurements are subject to Laplace and Gaussian noise

measurement noise assessed.

Although the performance of these methods can be shown in the idealized settings where the underlying electric field follows certain rules, recall that in reality the electric field may vary more than is assumed. “Bad data" found in a situation with an assumed low granularity of states may actually be good data, but marked as wrong because the assumed state should actually be two or three different states due to the spatially varying nature of the electric field. For data to be definitely thrown out as bad, an operator or analyst should consider changing the zones to see if the data is still identified as bad. There may indeed be a faulty meter, or it could be merely a modeling error or poor assumption. Another caveat that could be considered in future research is the possibility of a local electric field enhancement zone. This may cause what appears to be an instance of bad data, but is actually the result of localized disturbances that can cause increased GICs [80]. Bad data detection can be difficult when the states are not as clearly defined as in traditional estimation and when the system is less metered. But with sufficient metering and tuning, LAV estimation can be a useful tool for dealing with non-normal data.

6. OTHER GIC MONITORING APPLICATIONS *

In this chapter, additional applications leveraging GIC estimation and monitoring methods and results are covered, for the benefit of widespread system monitoring and visualization. First, the need for a state estimator that explicitly incorporates GIC modeling is presented and a GIC-inclusive alternative designed. This method leverages the electric field data provided by the previously proposed GIC estimation methods for state initialization and tuning of model parameters. Next, as real-time electric field information is increasingly desired, entities like the National Oceanic and Atmospheric Administration (NOAA) and Computational Physics, Inc. (CPI) are developing models to provide near real-time electric field estimate maps. These two methods are compared from a power systems perspective by applying the fields to the same synthetic case and analyzing the resulting GICs. These inputs are vital for comprehensive GIC monitoring tools so being aware of differences in their methods and the resulting GICs is useful as applications are developed and improved.

6.1 A GIC-Inclusive AC State Estimator

The purpose of traditional state estimation is to obtain the statistically optimal states, voltage magnitude and angle at every bus, from the system topology and some set of system measurements. This process is highly dependent on the model; without accurate models error can be incurred in the estimate. Without modeling the additional reactive power losses in transformers resulting from GICs, the resulting estimate may be unreliable if used in additional applications or algorithms. In this section, an improved ac state estimator, which is augmented to include neutral GIC states, is proposed to enhance traditional estimation performance during a GMD. It utilizes neutral GIC measurements as well as pseudomeasurements and initialization based on the results of a GIC estimator or other electric field data procurement.

*Part of this section is reprinted with permission from “The Potential for a GIC-Inclusive State Estimator," by C. Klauber, G.P. Juvekar, K. Davis, T. J. Overbye, and K. Shetye, Sept. 2018, North American Power Symposium (NAPS) 2018, ©2018 IEEE, with permission from IEEE

6.1.1 Motivation

Additional reactive power absorption due to GICs in transformers results in lower voltage at many buses. In traditional state estimation, these deviations may be masked by or incorrectly attributed to trying to match measurements to models that do not represent the actual system and GMD condition. State estimation is firmly dependent on the system model; if the measurement model $\mathbf{z} = h(\mathbf{x}) + \mathbf{e}$ no longer holds then the resulting estimate will incur error. Consider the situation illustrated in Fig. 6.1 where the load at Bus 3 is metered. In the presence of GIC losses, typically modeled at the transformer high side, $z_{q,3} \neq h(\mathbf{x})$ where $z_{q,3}$ is the reactive power injection at Bus 3. The effects of this incomplete model and motivation for a GIC-aware state estimator are demonstrated on the 500/230kV 150-bus synthetic system [73].

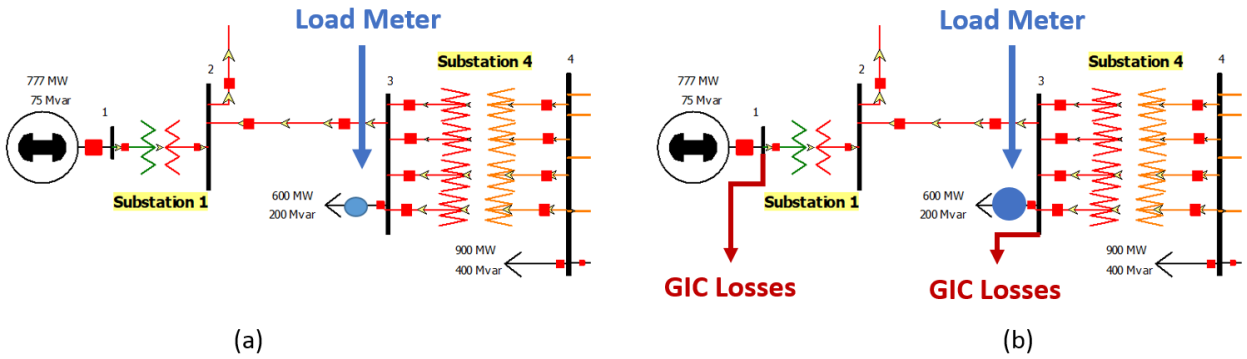

Figure 6.1: Power system model and metering during (a) normal conditions and (b) a geomagnetic disturbance

Uniform electric fields of varying magnitude and direction are applied to the system using a power flow program with GIC capabilities. Artificially noisy measurements are generated from the power flow results such that 55-80% of power flow, 65-100% of power injection, and up to 50% of the voltage magnitudes are metered. Using a typical GIC-agnostic estimator, the magnitude of the electric field is increased with a fixed direction and the average absolute error, as a function of storm magnitude and averaged over 100 Monte Carlo simulations, is shown in Fig. 6.2. The

average error increases with storm magnitude as the mismatch between the measurements and model increases with reactive power losses. Maintaining a constant electric field magnitude and varying the direction from 0 to 360 degrees produces error that follows a sinusoidal trend. This follows from the fact that induced dc voltages are dependent on the lines' alignment with the storm direction. Holding the storm magnitude and direction constant, 4 V/km at 50 degrees), the ratio of power flow to power injection measurements is varied. Fig. 6.3 illustrates that including more power flow measurements, as opposed to power injections, improves the state estimator accuracy. This is because a bus reactive power injection measurement is expected to be the summation of all branch reactive power flows, including the transformer losses due to GICs, but the expectation does not always equal the reality and error is incurred. The consequences of not including GIC

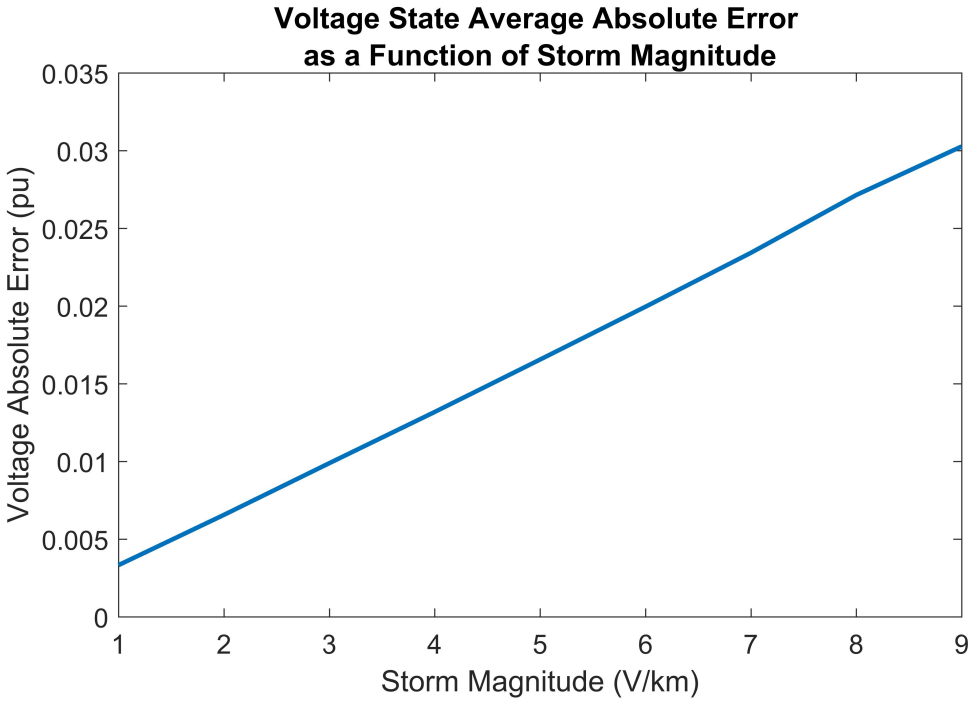

Figure 6.2: Traditional estimator average absolute voltage error increases with increasing storm magnitude. Reprinted with permission from [12]

effects in the state estimation model are errors that can misguide operators and propagate through

other operational tools. To address the need for a state estimator that appropriately models the system during a GMD, a GIC-inclusive estimator is developed in the following section.

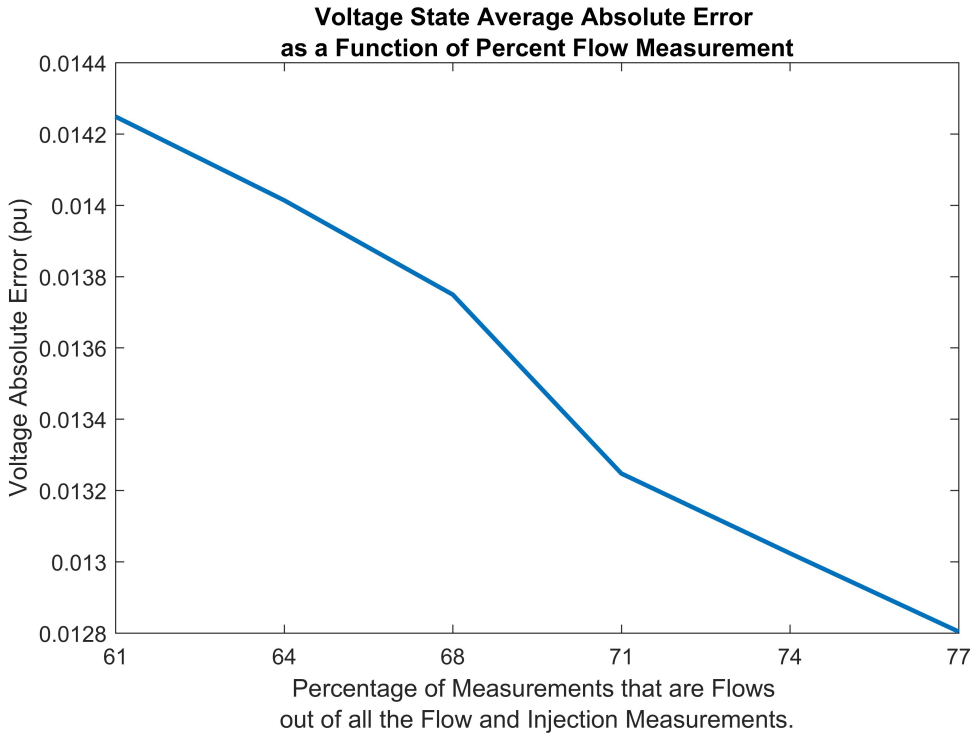

Figure 6.3: Traditional estimator average absolute voltage error decreases as the percentage of the measurements which are power flow measurements increases during a GMD. Reprinted with permission from [12]

6.1.2 Updating the Model

First, the state and measurement vectors are augmented to incorporate relevant GIC elements. Available GIC neutral measurements are appended to the measurement vector such that

$$\mathbf{z} = [\mathbf{P}_f, \mathbf{P}_{inj}, \boldsymbol{\theta}_{meas}, \mathbf{Q}_f, \mathbf{Q}_{inj}, \mathbf{V}_{meas}, \mathbf{I}_{meas}]^T \tag{6.1}$$

where $\mathbf{P}_f$, $\mathbf{Q}_f$, $\mathbf{P}_{inj}$ and $\mathbf{Q}_{inj}$ are the measured real and reactive power flows and injections, respectively. The measured voltage magnitudes and angles, $\mathbf{V}_{meas}$ and $\boldsymbol{\theta}_{meas}$, and the set of measured

transformer neutral GICs, $\mathbf{I}_{meas}$, are also included. The state vector is augmented such that

$$\mathbf{x} = [\boldsymbol{\theta}, \mathbf{V}_{pu}, \mathbf{I}_{n,pu}]^T \tag{6.2}$$

where $\mathbf{I}_{n,pu}$ is all the transformer neutral GICs in the system. As electric field information becomes more widely available for real-time applications it will be leveraged not directly in the measurement set but indirectly through the initialization of the new GIC states and certain modeling parameters which will be discussed.

In traditional estimation, the Jacobian matrix, $\mathbf{H}$, is a function of the measurement model, $h(\mathbf{x})$, and the state, $\mathbf{x}$. When the state and measurement vectors are extended, the size of $\mathbf{H}$ increases. To incorporate the reactive power losses in the model, the expressions $h_i(\mathbf{x})$ for reactive power flows and injections must be appended to include the value as a function of the states, $mathbfx$. The losses are assumed to be linearly dependent on the transformer (t) effective GICs, expressed by

$$Q_{loss,t} = k_t V_{pu,t} \mathcal{I}_t \tag{6.3}$$

where k_t is a transformer-dependent scalar [52], $V_{pu,t}$ is the pu ac voltage at the transformer high side, and $\mathcal{I}_t$ is the effective GIC given by 3.10. To include these losses in the measurement model, the original expression for the reactive power injection at bus i (when bus i is the high side of a transformer) is augmented to include Eq. 6.3:

$$Q_{i,new} = Q_{i,orig} + Q_{loss,i} \tag{6.4}$$

The resulting new partial differentiation terms in $\mathbf{H}$ with respect to the new GIC neutral current state, $\mathbf{I}_n$, is

$$\frac{\partial Q_i}{\partial I_{n,t}} = V_{pu,t} k_t \frac{\partial I_{eff,t}}{\partial I_{n,k}}. \tag{6.5}$$

Since the original reactive power injection term is not a function of the induced neutral current, there is only one term. A similar derivation is undertaken to update the reactive power flow terms

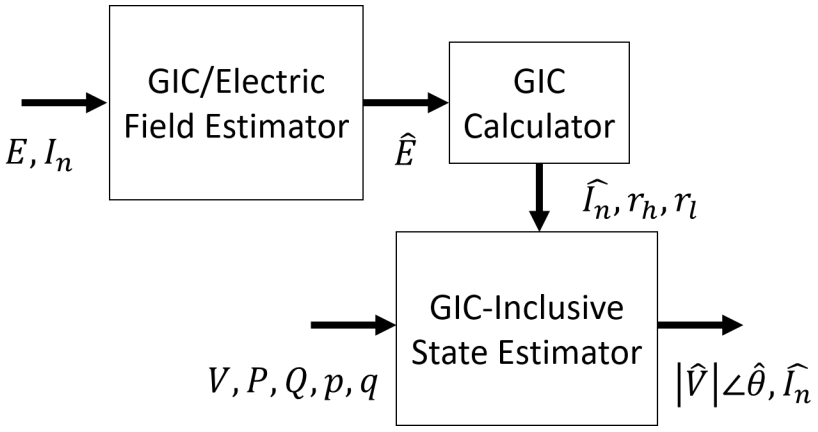

Figure 6.4: Flow chart showing how a GIC estimator/calculator can be used as input for a GIC-inclusive state estimator to inform and improve the resulting state estimate

in the Jacobian. The partial derivative of the effective GIC with respect to the neutral current at the same transformer is dependent on the ratios of the high and low side winding currents to the neutral currents, $r_{h,k}$ and $r_{l,k}$, resulting in

$$\frac{\partial I_{eff,k}}{\partial I_{n,k}} = \pm(r_{h,k} + r_{l,k}/a_k) \tag{6.6}$$

where a_k is transformer k's turn ratio. The ratios of the high side and low side GICs with respect to the neutral GICs, $r_{h,k}$ and $r_{l,k}$, can be determined analytically based on the GIC estimation prior step. New terms coming from the partial derivative of the new GIC neutral measurements with respect to new GIC neutral states can also be found using the values calculated from the GIC estimation; if the pre-estimation is trusted, this term is expected to be good enough and can be considered a constant in subsequent iterations. In addition to these values, the pre-ac estimation electric field estimation results can be used to compute initial guess values for the more traditional methods. As there can be a lot of variability in GICs due to storm magnitude and direction, there is no obvious "flat start" value for the new GIC states and including these values improves convergence and computation time of the extended state estimation model. The overall process is illustrated in Fig. 6.4

6.1.3 GIC-Inclusive Results

The proposed inclusive estimator was tested on the synthetic UIUC 150-bus system under uniform and non-uniform electric fields with varying electric field direction and magnitude. An electric field is applied to the system and the values taken from the simulation results affected by artificial Gaussian noise. A summary of the measurements is found in Table 6.1. The true state solution is retained for validation purposes.

Measurement Type	**Noise (Variance)**	**% Metered**
Power flows	0.01	70-85%
Power injection	0.02	70-95%
Voltage magnitude	0.01	up to 80%
Neutral GICs	0.005	50-70%

Table 6.1: Summary of measurement noise and availability for GIC-inlusive state estimation

The key result is that the average voltage estimate error is less when using the inclusive measurement model, as seen in Fig. 6.5. The neutral GIC states are also estimated with reasonable accuracy. Where traditional estimation methods are prone to convergence issues under GMD conditions, each of the 100 Monte Carlo simulations at each storm magnitude level converged. Furthermore, the proposed estimator is unaffected by storm magnitude, reinforcing the fact that the deterioration of traditional methods is due to lack of GIC modeling and addressed by this work. Regarding computation efficiency, the GIC-inclusive estimator takes about 2 seconds to solve the 150 bus system on an Intel Core i7-650U @ 2.5 GHz.

By adding GIC measurements and models, the difference between the pu voltage magnitude estimates and known states is diminished and the convergence properties improved. This improvement is keenly dependent on additional metering and future work will explore concepts of minimum measurements for IC-inclusive observability and sensitivity to the prior step GIC estimation accuracy.

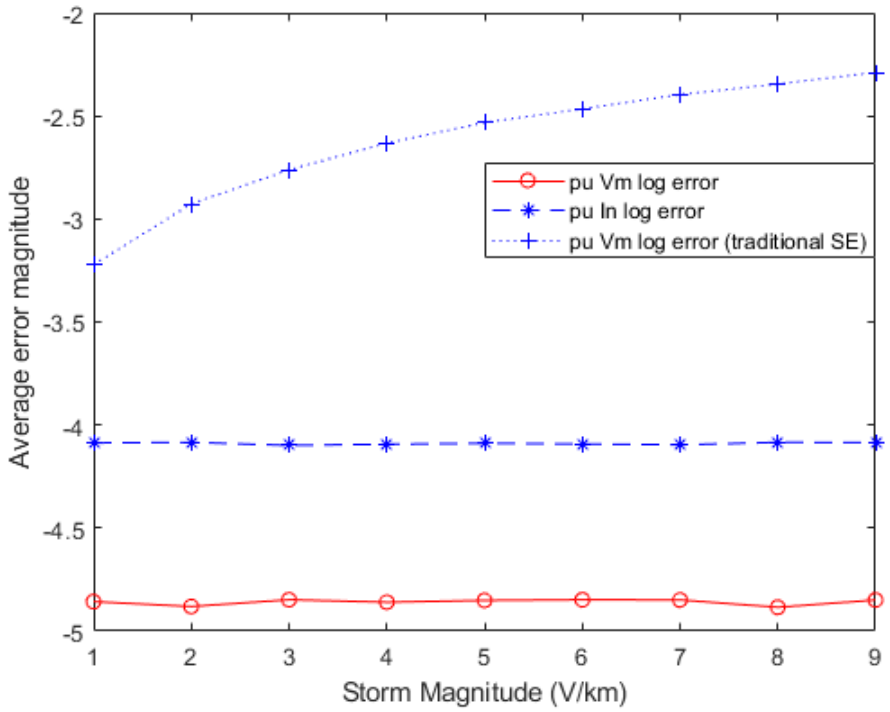

Figure 6.5: Decimal logarithmic absolute error for the states (voltage magnitude and neutral GICs) from the traditional and GIC-inclusive state estimators as a function of storm magnitude

6.2 Comparison of Electric Field Calculation Methods

As more GMD-related data and improved electric field models become available, it is important to validate different methods and processes by comparing data and model quality. Currently, there are at least two organizations that produce 1-minute electric field maps, providing vital inputs for GIC estimation and other monitoring methods. AVERT is a cloud-based commercial software developed by Computational Physics, Inc. [81] which uses real-time regional and local data such as time-varying magnetometer measurements to calculate the electric field. The calculation method is derived from standard frequency domain techniques and the ground response is derived from the NERC TPL-007-1 regional one-dimensional models [82, 83, 3]. The electric field maps are produced with 0.2 degree latitude by 0.2 degree longitude specificity in the B3D (binary 3D) format, which is compatible with PowerWorld and other power system modeling tools. At the moment, the 6 magnetometers of the Texas A&M Magnetometer Network provide input to the AVERT model

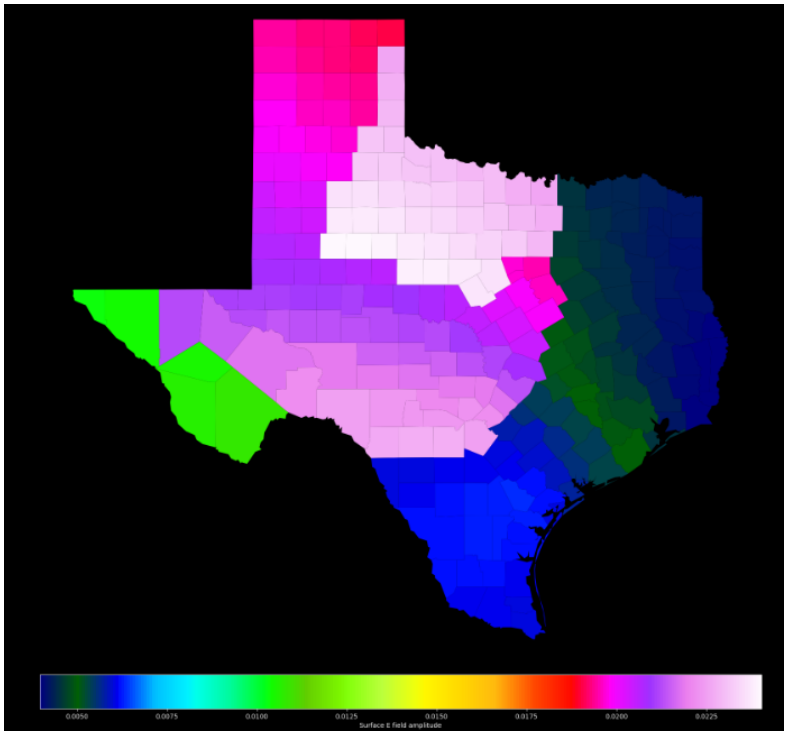

Figure 6.6: Snapshot of AVERT electric field estimate output. Maximum Efield: 26 mV/km

for the state of Texas. A snapshot of the resulting electric field map is shown in Fig. 6.6, where the electric field amplitude scale is from 5 mV/km (forest green) to 25 mV/km (white).

Meanwhile, the National Oceanic and Atmospheric Administration (NOAA) also provides data and tools for addressing space weather events. Their real-time electric field data uses USGS geomagnetic data reported from up to 13 stations and the Fernberg 1D conductivity models [84]. The SECS interpolation method is used, as there are so few stations to cover the entire country. The data is also near real-time, updated on the minute, and geographically mapped to the United States, or portions thereof, with gridded data files, see Fig. 6.7. While the AVERT method primarily outputs data in the B3D format, the NOAA 1-minute geoelectric field data is provided in geoJSON format. Both formats can be used in industry and read by power system analysis softwares, such as PowerWorld. It should be noted that NOAA is about to release an upgraded version of their geoelectric field maps, which leverage the empirical magnetotelluric transfer functions (EMTFs) to derive the values. These models include more complex earth conductivity models.

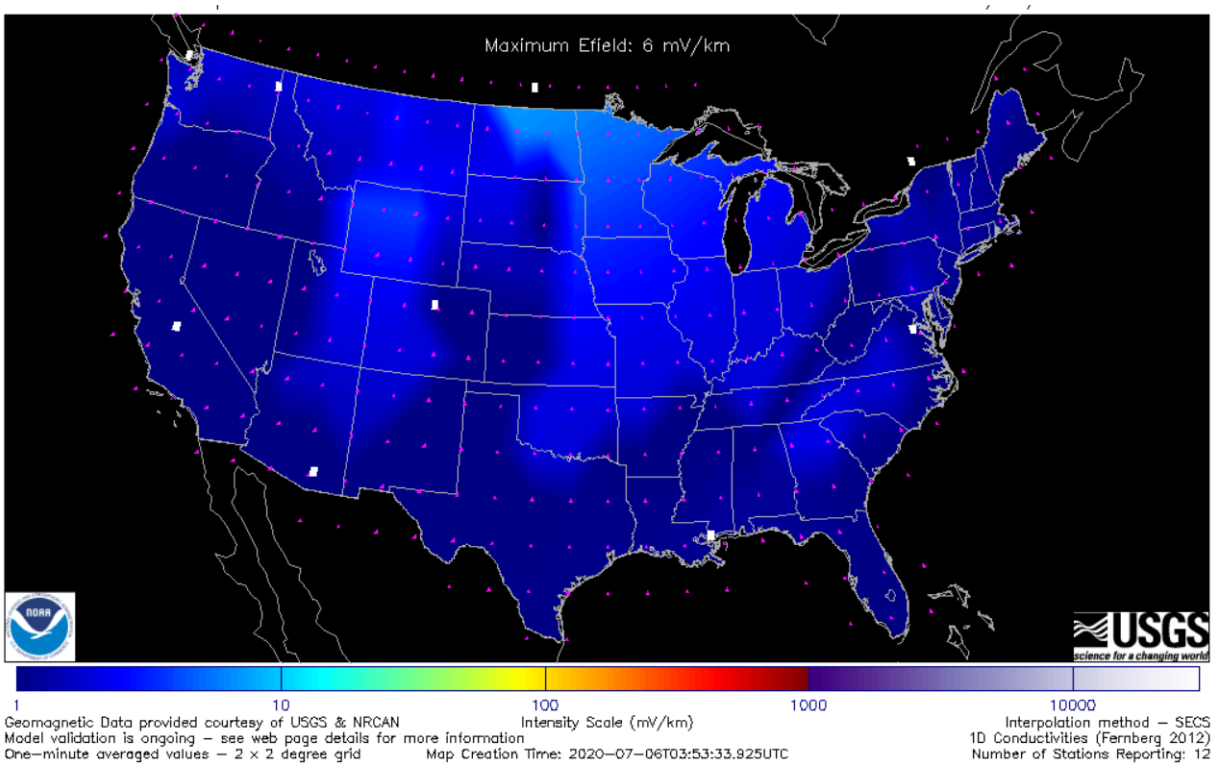

Figure 6.7: Snapshot of NOAA electric field estimate output

Key differences to note include that NOAA is using up to 13 stations over the continental United States, while AVERT is using 7 stations over a much smaller area, i.e., the state of Texas. The NOAA data is mapped to points on a 2 x 2 degree grid, while the AVERT data is provided with a granularity of 0.2 x 0.2 degrees. In the future, geomagnetically induced current and electric field measurements, continually improving conductivity models, and actual grid models can be used to validate one or both methods, but in the meantime the results of the two methods can be compared applied to a synthetic system.

For a 20 minute period during a low geomagnetic activity (Kp 0+) day, the time series data provided by both methods are applied to the synthetic Texas 2000 bus system in a power system analysis software. Maximum and average electric field magnitude for both sets of fields are saved, as well as the effective and neutral GIC, at each transformer. In Figs. 6.8 and 6.9 each line represents the response over time of a particular transformer (effective and neutral GICs) or substation

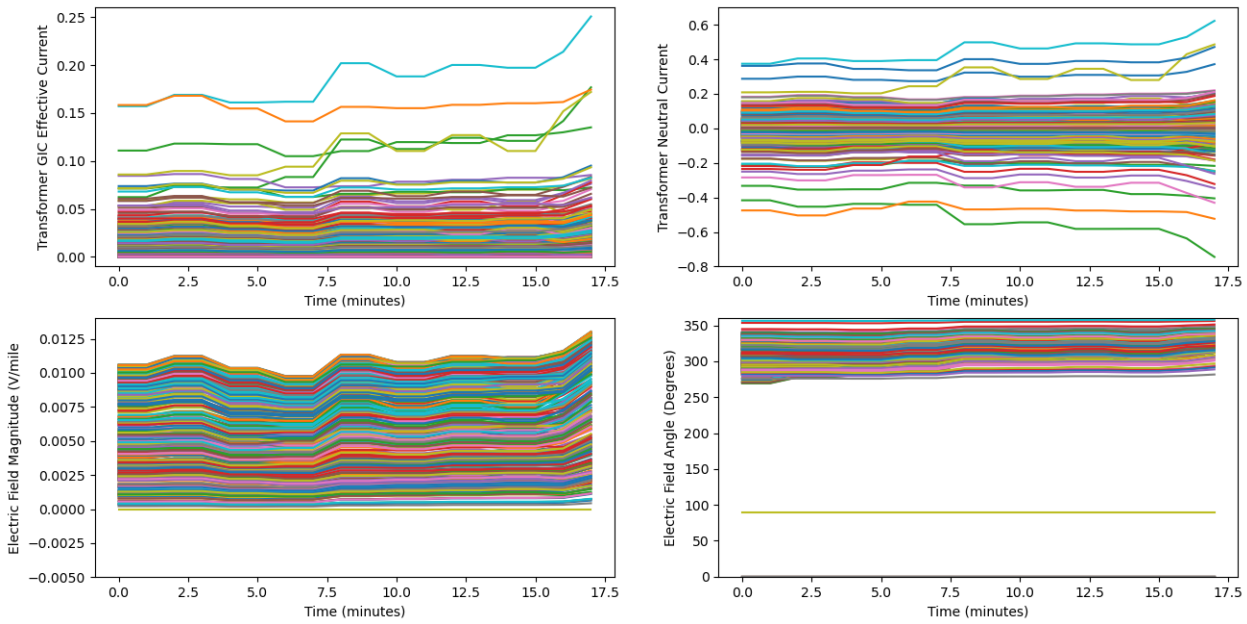

Figure 6.8: Transformer GICs (top) and substation electric field (bottom) over time using AVERT models on May 14, 2020

(electric field, magnitude and direction). One observation is that the AVERT electric field magnitude is on average 10 times greater than the NOAA electric field magnitude. Both wave forms appear to rise slightly around the 2 minute, 8 minute and 16 minute marks. This indicates that the methods do share some similarity of response. Additional analysis at other quiet times leads to similar conclusions, that the AVERT fields are a factor of 4 to 20 times greater but that both models produce similar shapes at the same times. Because there has not been a sizable GMD event since this comparison functionality was developed, these results may be marginally significant as this behaviour may be the manifestation of over-sensitivity to noise in the absence of a more interesting signal. Regardless, this comparison process, including pulling the data from the internet, sending it to a power systems analysis software, and plotting the results, has been semi-automated and is available in the event of future geomagnetic activity. As debate continues among the different geoelectric field calculation perspectives, it is important to consider the power system effects, i.e., GICs, especially as this information becomes increasingly leveraged in real-time analysis.

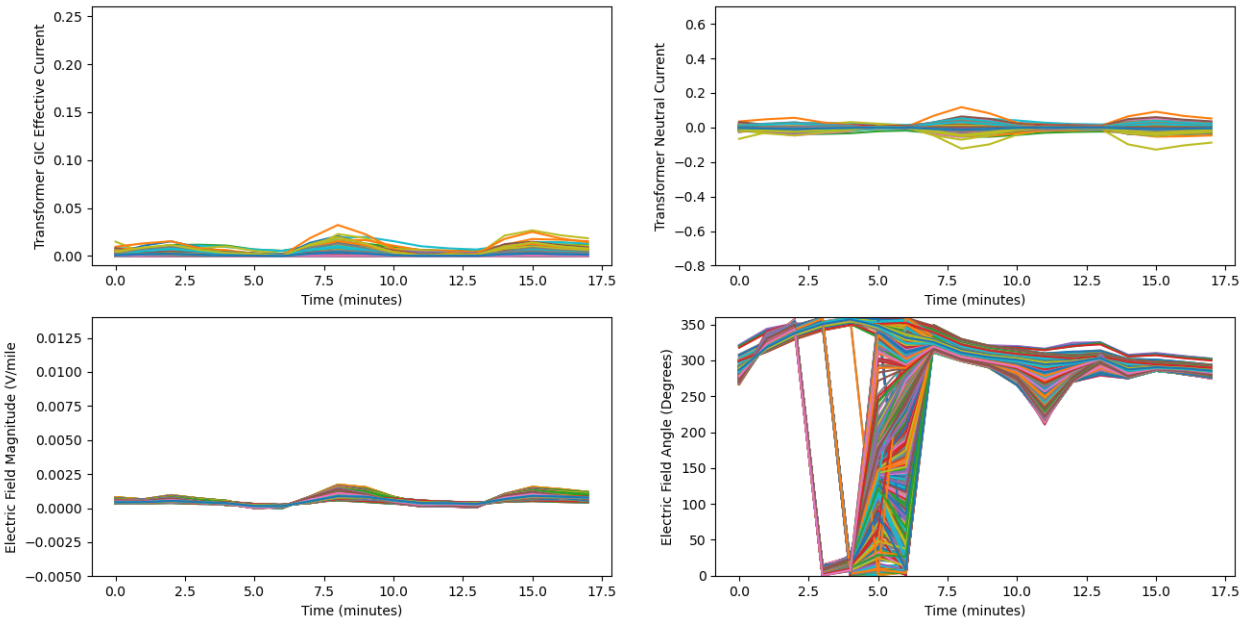

Figure 6.9: Transformer GICs (top) and substation electric field (bottom) over time using NOAA models on May 14, 2020

7. VISUALIZATION OF GMD EFFECTS ON POWER SYSTEMS

Prior research on GMD grid impacts has led to many improved methods for off-line analysis. Due to recent industry interest in real-time monitoring and specifically the installation of six magnetometers in the state of Texas, enhanced monitoring and visualization applications are increasingly feasible. While the full potential of GIC estimation is dependent on future improved metering infrastructure, the purpose of this chapter on real-time GIC visualization answers the question of what can be done with the information already available.

In this chapter, data available from the Texas A&M University Magnetometer Network will be utilized and examples of GIC visualizations using existing power flow simulation software provided. Leveraging and integrating GIC estimation and real data from the state of Texas with PowerWorld Dynamics Studio [85, 86] enables real-time solutions and visualization for future operations and control research.

7.1 GIC Visualization

Power system control center visualization is not a new topic in industry. Typical schemes include incorporating color contours to show value variation and animating arrows to show power flow directions. These large displays may be geographically-based, enabling a consistent and intuitive overview, or not, to more clearly show lots of information in dense areas. Regardless, the intention is to inspire and aid in rapid responses to changes in the system. Geographic data views (GDVs) are designed to provide dynamic visualization of changing system values anchored in static geographic information [87]. Symbols representing the particular information of interest are placed on the display according to the corresponding geographic information. Symbol size, color, and shape are used to communicate specifics of the chosen information. For example, generator output and limits can be visualized by using circles that increase in size as the generator outputs more MW, that change color as the generator gets closer to its reactive power limits, and are placed on a one line with realistic geographical spacing. As GICs are inherently location-sensitive and the

corresponding geographic data is already required for modeling purposes, GDVs can be effectively used for GIC visualization.

Power system software options that can be used to model GICs now include EPRI OpenGIC and GIC add-ons for GE PSLF, PowerWorld Simulator, and Siemens PTI PSS/E. Primarily, these are used for off-line analysis and a limited but growing number of accounts of power system simulation tools for real-time, on-line monitoring and control exist in the literature. Some examples, not included in literature, may not be disclosed due to proprietary methods and tools. The purpose of the remainder of this chapter is to describe the utilization of real-time measurements to show how GICs can be calculated and visualized in real-time, with the long-term intent of enabling utility operations and GMD mitigation.

7.2 Using Real Magnetometer Data to Visualize GICs in PowerWorld DS

Previously, synthetic data was used to estimate electric field and the resulting induced dc line voltages in the system. This information could be sent to the simulation software PowerWorld DS [85, 86] for integrated ac analysis and visualization. Now the real-time data from the six new magnetometer sites in the state of Texas can be used as input for research and education purposes. Earth's magnetic field, in three dimensions, can be measured using magnetometers. As installed per Fig. 2.1, each magnetometer station is a continually operating system, currently live and transmitting the magnetic field data, once per second to a central server. The magnetic field data is stored in a database and visualized on a dashboard. Meanwhile, the surface electric field, calculated using the AVERT model from real-time magnetometer measurements and with county level granularity, is provided via web link in downloadable B3D format, a binary format that enables the compact transfer of cubes of data. In this case, the three dimension are latitude, longitude, and time. The area covered by the system of interest is broken down into a grid defined in the B3D file, with a northward and eastward component of electric field for each point in the grid. PowerWorld Simulator can read B3D files and when a GIC simulation is run using the B3D file as input on a system with geographic coordinates, a variety of calculated values are now available, including dc line voltages, substation GIC current injections, transformer neutral GICs

and effective GICs. When a full power flow simulation is run, reactive power losses in transformers and the resulting voltage changes can be found as well. Other commercially available software can also do similar GIC analysis; other common electric field input formats are CSV or geoJSON files. PowerWorld DS can incorporate B3D files as well, but once the simulation starts, the provided information cannot change or be updated.

To provide regularly updating data to PowerWorld DS requires regular communication via DS protocol and a server. This element of communication is required regardless of the power system simulation platform chosen, the specifics of which are detailed here using PowerWorld software. To automate this process, the Python package Easy SimAuto (ESA) [88] is used to apply the new B3D input, run the GIC simulation, and procure the resulting dc line voltage values for every line in the system in PowerWorld Simulator. This information is then passed to DS using the DS protocol and from there the ac simulation incorporates those values and provides the resulting GIC flows and integrated power flow results, as outlined in Fig. 7.1.

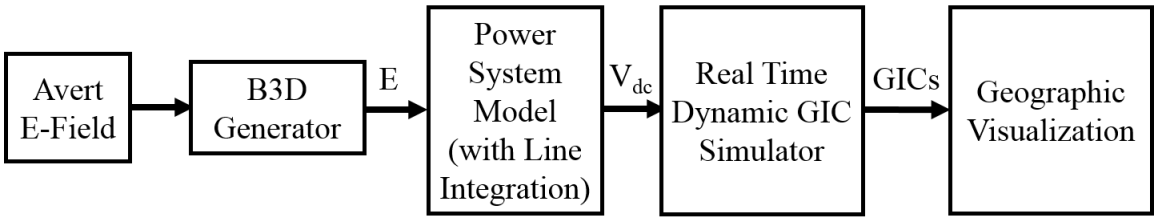

Figure 7.1: Flow chart showing the GIC visualization process using real data

The DS can run a full transient stability (time domain) simulation of the system in real-time and can scale up for thousands of buses. Based on a client-server system, it also enables interactive simulations. Leveraging the capabilities of the PowerWorld DS environment, operator clients can issue control commands, informed by visualization of the estimation or calculation results, to mitigate GIC impacts. To send the dc line voltage values to DS first requires a server connection and that the simulation is running. These initializing steps can be done programmatically using the

DS Protocol [85, 86]. A new command in the DS Protocol, "`SET GMDDCVOLT xxx`", enables the setting of the GMD-induced dc voltage for a particular branch to be set to `xxx` volts. To identify the appropriate branch, the From and To bus numbers must be identified with the command, as well as the Circuit number. It is assumed that positive polarity is on the To terminal and that setting this value removes any existing schedule for this value that may be saved with the case. As long as the "Include GIC in Power Flow and Transient Stability" box is checked in the GIC Analysis Form for the case (.PWB), these values will be used to calculate reactive power losses which will be included in the simulations that follow in each time step in the DS.

Though the time step of the underlying dynamic simulation is on the order of milliseconds, the electric field does not vary on the same time scale. Therefore, the aim is to update the electric field input every 60 seconds, per the current electric field data availability. As the DS `tcmCommand` command does not currently support the changing of multiple objects with one command, to update the dc line voltage of all 2345 lines in the Texas 2000 system requires numerous iterations, as demonstrated in the code snippet shown in Fig. 7.2. The latency between the client and the DS is dependent on the computational complexity of the running DS visualizations and the rate of simulation checking in Dynamic Simulator Options. For example, visualizing line flows on the Texas 2000 oneline while trying to update 2345 line voltages can take minutes, but it takes just a few seconds when the oneline is closed, as demonstrated by the DS output shown in Fig. 7.3. This trade off between the DS's computing and visualizing power may motivate the development of a separate visualization client, such that the DS can continue to be leveraged for its transient stability simulation abilities without sacrificing speed because of the intensive visualization.

If GDVs have been set up for the case ahead of time the display will update as the new information is provided or other changes happen in the system. For the display in 7.4, GIC currents are represented by circles with size that scale linearly with magnitude and color that represents direction. Red fill means negative current (out of the transformer and into the system) and blue fill means positive current (from the system into the transformer). The display begins to update every minute in correspondence with the update rate of the electric field information. Information

```
for i in range(len(L)):
    userid = userid + 1
    opt2 = [userid,soc,fracsec]
    deviceid = id_list[i]
    actio = "SET GMDDCVOLT {}"
    action = actio.format(round(val_list[i],3))
    txt ="{}"
    jsondata = {
        'Branch': {
            'ID': [int(id_mat[i][0]),int(id_mat[i][1]),str(id_mat[i][2])],
            'Action': action
        }
    }
    opt2.append(jsondata)
    ds.msgtypes[13](opt2)
    dsrec = ds.receive(16)
```

Figure 7.2: Code segment showing the for loop which oversees the updating of all dc line voltages in the system

transfer and display re-rendering take less than 10 seconds, so a faster refresh rate is feasible if the input could match. The substation name and current value are also printed with the shape, providing additional insight when the currents are large enough. Additionally, since grid operators may not have the same intuition about GMD effects as they do normal operations, a table of substations ranked by largest transformer GIC magnitude is provided. It also shows the last update time, which can be used to detect issues with some part of the data flow. Furthermore, an electric field multiplier option can be enabled. As the resulting currents can be very small during normal/quiet periods, an electric field multiplier can be invoked for demonstration purposes. Fig. 7.4 shows a GDV display over the synthetic Texas 2000 bus case at a snapshot in time during a quiet period with an electric field multiplier of 10. The substations with the transformers with the largest currents are shown in the accompanying table. A new method for wide-area visualization of power grid information known as pseudo-geographic mosaic displays (PGMDs) is also employed [89]. This method leverages dynamically created GDVs and arranges them to maximize the usage of the display space while maintaining some semblance of the geographic anchoring of the information. Similar to the GDVs, the color of the shape indicates the direction of the current flow, while the

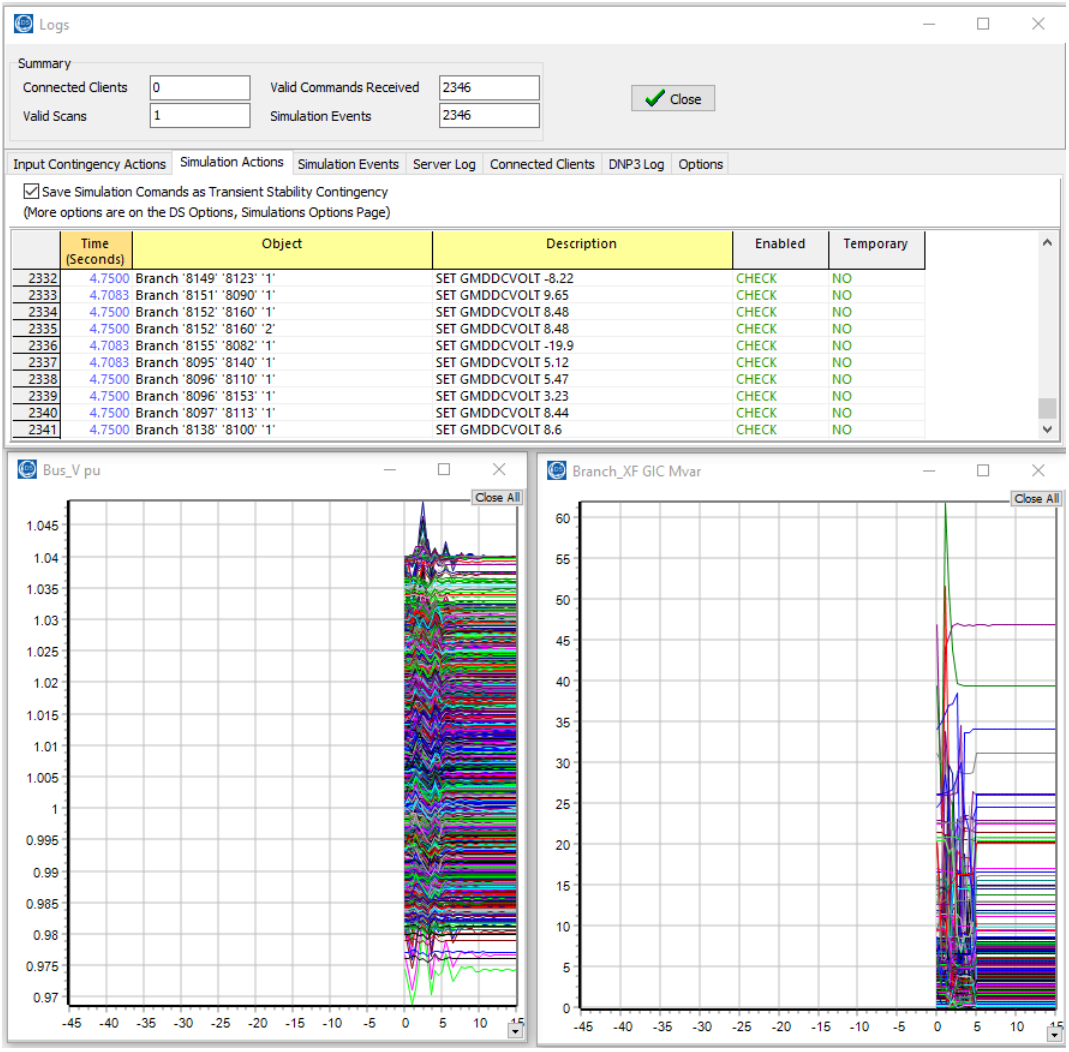

Figure 7.3: PowerWorld DS output (predefined pu bus voltage and transformer GIC Mvar losses strip charts and log) for a step (1 V/km N) electric field input on the Texas 2000 system. The corresponding oneline was not open and the line voltages were updated within seconds

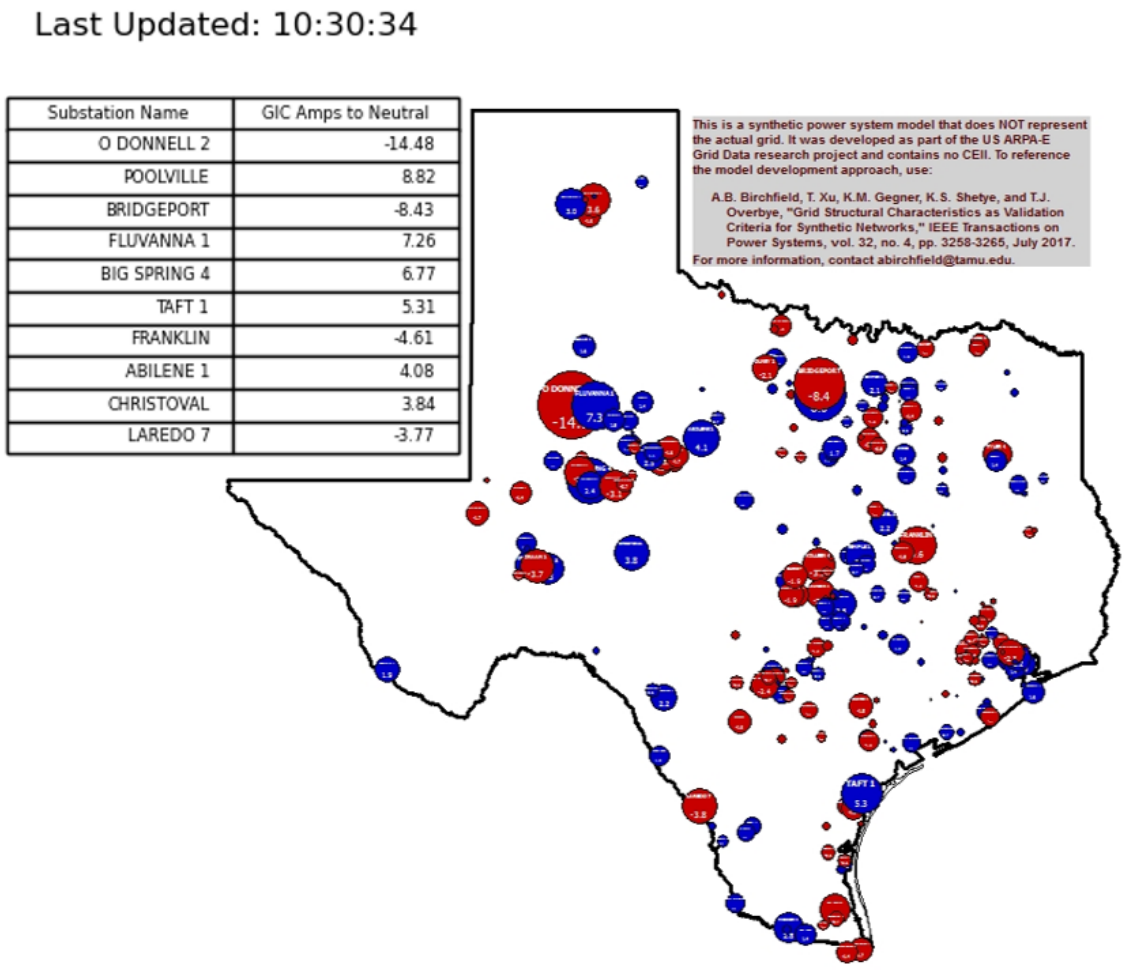

Figure 7.4: Real-time GIC magnitude and direction visualization for the Texas footprint using geographic data views (Geoelectric Field Multiplier=10)

size and color indicates the magnitude. The PGMD for the same instant shown in Fig. 7.4 is shown in Fig. 7.5.

This application which provides the ability to update GIC-related values in real time enables the development of more realistic simulated real-time user experiences, or “rides", with GMD scenarios. More work will be done with respect to these experiences, especially optimizing the information transfer while using the DS for visualization. There is much potential for this application and visualization to be used in educational and informative settings, providing avenues to advertise the Texas A&M Magnetometer Network data. In the near future, the plan is that the various capabilities developed in this project will come together to provide interesting and engaging

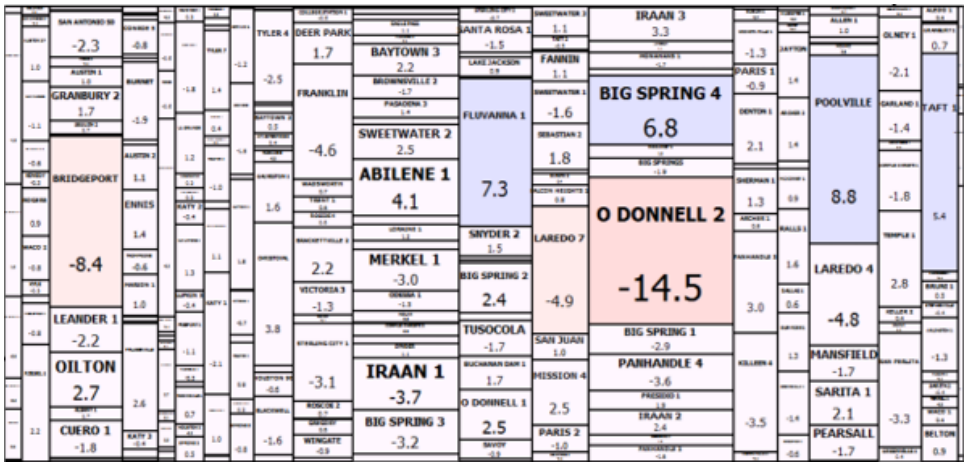

Figure 7.5: Real-time GIC magnitude and direction visualization for the Texas footprint using pseudo-geographic mosaic displays (Geoelectric Field Multiplier=10)

visualizations and experiences for the general public and potential collaborators that will maintain interest and investment in this important area of work.

8. CONCLUSIONS

In this chapter, a summary of this thesis is presented and the main contributions highlighted. The chapter also includes concluding remarks and areas for future research.

8.1 Summary and Contributions

Chapter 3 In this chapter, a GIC estimation method is proposed which leverages available GIC-related measurements to provide a best-guess estimate of the GIC state which can be used to improve situational awareness during a GMD. The states are defined to be the electric field in pre-defined zones, from which GICs across the system can be quickly calculated. The GIC estimator leverages a WLS objective and is computationally efficient due to the linear GIC relationship.

Chapter 4 In this chapter, the previously described WLS GIC estimation method is tested on a large case. Accuracy of the method depends on measurement availability, measurement noise, and size of the electric field zones. The method is shown to provide useful information using simple visualizations and as an input to basic analysis tools.

Chapter 5 In this chapter, additional GIC estimation topics are covered, including a novel discussion on the meaning of observability and redundancy in the GIC estimation context. This also enables the development of a measurement placement algorithm. A LAV-based estimation method is created and identification thresholds designed which are used to identify and minimize the effects of bad data on GIC estimation performance. Additionally, preliminary analysis of real GIC data considers the potential for and effect of non-Gaussian noise when using these estimation methods.

Chapter 6 In this chapter, additional system monitoring applications are developed and tested. First, the need for a GIC-aware ac state estimator is presented and addressed via the design of a GIC-inclusive ac state estimator. This estimator leverages available electric field information, such as that estimated directly from magnetometer data or via GIC estimation, as well as a more comprehensive system model to improve the traditional state estimate during a GMD. By augmenting

the measurement vector, state vector, and model equations, the true nature of the system is better captured resulting in a more accurate estimate provided sufficient metering. Second, two methods of providing real-time non-uniform electric field data are contrasted by comparing the GICs resulting from the application of the alternative fields to a synthetic case. The semi-automated comparison tool can provide useful post-event analysis with modeling implications after the next sizeable GMD activity.

Chapter 7 In this chapter, real-time GIC visualizations for power system situational awareness are discussed. Real electric field data is streamed in near real-time to a power system analysis program which pushes line voltages to a power systems dynamics simulator. Using specially designed geographic and pseudo-geographic data visualizations and tables, this tool can provide powerful insight to grid operators and even casual observers. The integration with existing analysis tools also enables this to be used as a foundation for research involving how visualization and integrated analysis clients can be used to influence and improve operator response during a GMD.

8.2 Future Work

The work of this thesis opens up several directions for future research for improving the monitoring and visualization of GMDs on power systems.

With regards to the WLS and LAV based GIC estimation methods, future work includes optimization of the number and boundaries of electric field zones, larger case testing, and validation using real data and cases. Fine-tuning of the bad data detection thresholds and additional considerations for realistic measurement noise characteristics could also be undertaken. The bad data detection methods could also be leveraged to identify local electric field enhancements. Additionally, the same GIC/electric field relationship can be re-purposed for parameter estimation. By leveraging the data over time, the GIC models can be improved through updating and validation of substation grounding resistance, earth conductivity, and transformer constants.

With respect to the integration of GIC estimation with other applications in Chapter 6, additional extensions of the GIC-inclusive state estimator can include bad data and topology detection. More comprehensive analysis of the dependence on electric field input will clarify what the true

measurement input needs of this method are. It is also of interest to develop a single-step combined estimator and further study the effects of noise variance on the estimators' performance. Additional analysis and comparison of readily available real-time electric field data can inform continuing work in geoelectric field calculation methods.

Regarding the visualization work of Chapter 7, future work can enhance the functionality to include suggested operator actions and additional decision making information. Integrating monitoring and control aspects enables the testing of automated and guided-user mitigation research, including but not limited to line switching, generation redispatch, reactive power management, and transformer thermal limit monitoring. It also provides a basis for human factors research. As the program is already implemented in PowerWorld Dynamic Simulator, there is significant potential for an interactive GMD simulation using real-time or past event data and a real time feedback loop. This can be used for training, research, and educational reasons for the purpose of improving situational awareness and decision making for large and complex systems during a GMD.

REFERENCES

[1] V. D. Albertson, J. M. Thorson, R. E. Clayton, and S. C. Tripathy, "Solar-Induced-Currents in Power Systems: Cause and Effects," *IEEE Transactions on Power Apparatus and Systems*, vol. PAS-92, pp. 471–477, March 1973.

[2] H. Zell, "The Day the Sun Brought Darkness," *NASA*, 2009.

[3] "TPL-007-2 Transmission System Planned Performance for Geomagnetic Disturbance Events," *North American Electric Reliability Corporation (NERC)*, Oct 2017.

[4] D. H. Boteler and R. J. Pirjola, "Modelling geomagnetically induced currents produced by realistic and uniform electric fields," *IEEE Transactions on Power Delivery*, vol. 13, pp. 1303–1308, Oct 1998.

[5] T. J. Overbye, K. S. Shetye, T. R. Hutchins, Q. Qiu, and J. D. Weber, "Power grid sensitivity analysis of geomagnetically induced currents," *IEEE Transactions on Power Systems*, vol. 28, pp. 4821–4828, Nov 2013.

[6] M. Kazerooni, H. Zhu, T. J. Overbye, and D. A. Wojtczak, "Transmission system geomagnetically induced current model validation," *IEEE Transactions on Power Systems*, vol. 32, pp. 2183–2192, May 2017.

[7] C. Klauber and H. Zhu, "Power network topology control for mitigating the effects of geomagnetically induced currents," in *2016 50th Asilomar Conference on Signals, Systems and Computers*, pp. 313–317, Nov 2016.

[8] M. Kazerooni, H. Zhu, and T. J. Overbye, "Mitigation of geomagnetically induced currents using corrective line switching," *IEEE Transactions on Power Systems*, vol. 33, pp. 2563–2571, May 2018.

[9] H. Zhu and T. Overbye, "Blocking device placement for mitigating the effects of geomagnetically induced currents," in *2016 IEEE Power and Energy Society General Meeting (PESGM)*,

pp. 1–1, July 2016.

[10] L. Marti and C. Yin, "Real-Time Management of Geomagnetic Disturbances: Hydro One's eXtreme Space Weather control room tools," *IEEE Electrification Magazine*, vol. 3, pp. 46–51, Dec 2015.

[11] L. Marti, A. Rezaei-Zare, and A. Yan, "Modelling considerations for the Hydro One real-time GMD management system," in *2013 IEEE Power Energy Society General Meeting*, pp. 1–6, July 2013.

[12] C. Klauber, G. P. Juvekar, K. Davis, T. Overbye, and K. Shetye, "The Potential for a GIC-inclusive State Estimator," in *2018 North American Power Symposium (NAPS)*, pp. 1–6, Sep. 2018.

[13] V. D. Albertson, B. Bozoki, J. G. Kappenman, E. Larsen, D. E. Nordell, J. Ponder, F. S. Prabhakara, K. Thompson, and R. Walling, "Geomagnetic disturbance effects on power systems," *IEEE Transactions on Power Delivery*, vol. 8, pp. 1206–1216, July 1993.

[14] J. Berge, L. Marti, and R. K. Varma, "Modeling and mitigation of geomagnetically induced currents on a realistic power system network," in *2011 IEEE Electrical Power and Energy Conference*, pp. 485–490, Oct 2011.

[15] "Effects of geomagnetic disturbances on the bulk power system," *North American Electric Reliability Corporation (NERC)*, Feb 2012.

[16] V. D. Albertson, J. G. Kappenman, N. Mohan, and G. A. Skarbakka, "Load-flow studies in the presence of geomagnetically-induced currents," *IEEE Transactions on Power Apparatus and Systems*, vol. PAS-100, pp. 594–607, Feb 1981.

[17] K. Shetye and T. Overbye, "Modeling and analysis of GMD effects on power systems: An overview of the impact on large-scale power systems.," *IEEE Electrification Magazine*, vol. 3, pp. 13–21, Dec 2015.

[18] "High-Impact, Low-Frequency Event Risk to the North American Bulk Power System," *North American Electric Reliability Corporation (NERC)*, June 2010.

[19] B. Obama, "Executive Order- Coordinating Efforts to Prepare the Nation for Space Weather Events," *Office of the Press Secretary*, 2016.

[20] T. Phillips, "Near Miss: The Solar Superstorm of July 2012," *NASA Science*, 2014.

[21] D. H. Boteler and R. J. Pirjola, "Modeling geomagnetically induced currents," *Space Weather*, vol. 15, pp. 258–276, Jan 2017.

[22] K. S. Shetye, T. J. Overbye, Q. Qiu, and J. Fleeman, "Geomagnetic disturbance modeling results for the AEP system: A case study," in *2013 IEEE Power Energy Society General Meeting*, pp. 1–5, July 2013.

[23] K. Zheng, D. Boteler, R. J. Pirjola, L. Liu, R. Becker, L. Marti, S. Boutilier, and S. Guillon, "Effects of system characteristics on geomagnetically induced currents," *IEEE Transactions on Power Delivery*, vol. 29, pp. 890–898, April 2014.

[24] C. Basu, M. Padmanaban, S. Guillon, M. de Montigny, and I. Kamwa, "Combining multiple sources of data for situational awareness of geomagnetic disturbances," in *2015 IEEE Power Energy Society General Meeting*, pp. 1–5, July 2015.

[25] M. Lu, H. Nagarajan, E. Yamangil, R. Bent, S. Backhaus, and A. Barnes, "Optimal transmission line switching under geomagnetic disturbances," *IEEE Transactions on Power Systems*, vol. 33, pp. 2539–2550, May 2018.

[26] A. Yan, D. Zhou, and L. Marti, "Analysis of geomagnetically induced currents," in *2013 IEEE Power Energy Society General Meeting*, pp. 1–6, July 2013.

[27] V. D. Albertson and J. A. Van Baelen, "Electric and magnetic fields at the earth's surface due to auroral currents," *IEEE Transactions on Power Apparatus and Systems*, vol. PAS-89, pp. 578–584, April 1970.

[28] K. S. Shetve, A. B. Birchfield, R. H. Lee, T. J. Overbye, and J. L. Gannon, "Impact of 1D vs 3D earth conductivity based electric fields on geomagnetically induced currents," in *2018 IEEE PES Innovative Smart Grid Technologies Conference Europe (ISGT-Europe)*, pp. 1–6, Oct 2018.

[29] US Array, "Magnetotelluric array," *http://www.usarray.org/researchers/obs/magnetotelluric*. Last accessed on 06/26/20.

[30] L. Marti, C. Yiu, A. Rezaei-Zare, and D. Boteler, "Simulation of Geomagnetically Induced Currents With Piecewise Layered-Earth Models," *IEEE Transactions on Power Delivery*, vol. 29, pp. 1886–1893, Aug 2014.

[31] S. Cuttler, J. J. Love, and A. Swidinsky, "Geoelectric hazard assessment: the differences of geoelectric responses during magnetic storms within common physiographic zones," *Earth, Planets, Space*, Mar 2018.

[32] A. Abur and A. Gomez, *Power System State Estimation-Theory and Implementations*. Marcel Dekker, Inc., 2004.

[33] A. Monticelli, "Electric power system state estimation," *Proceedings of the IEEE*, vol. 88, pp. 262–282, Feb 2000.

[34] F. C. Schweppe and J. Wildes, "Power system static-state estimation, part I: Exact model," *IEEE Transactions on Power Apparatus and Systems*, vol. PAS-89, pp. 120–125, Jan 1970.

[35] F. C. Schweppe and D. B. Rom, "Power system static-state estimation, part II: Approximate model," *IEEE Transactions on Power Apparatus and Systems*, vol. PAS-89, pp. 125–130, Jan 1970.

[36] F. C. Schweppe, "Power system static-state estimation, part III: Implementation," *IEEE Transactions on Power Apparatus and Systems*, vol. PAS-89, pp. 130–135, Jan 1970.

[37] F. F. Wu, "Power system state estimation: a survey," *International Journal of Electrical Power & Energy Systems*, vol. 12, no. 2, pp. 80 – 87, 1990.

[38] A. Simoes-Costa and V. H. Quintana, "A robust numerical technique for power system state estimation," *IEEE Transactions on Power Apparatus and Systems*, vol. PAS-100, pp. 691–698, Feb 1981.

[39] J. W. Gu, K. A. Clements, G. R. Krumpholz, and P. W. Davis, "The Solution of Ill-Conditioned Power System State Estimation Problems Via the Method of Peters and Wilkinson," *IEEE Power Engineering Review*, vol. PER-3, pp. 43–44, Oct 1983.

[40] F. F. Wu, W. E. Liu, and S. Lun, "Observability analysis and bad data processing for state estimation with equality constraints," *IEEE Transactions on Power Systems*, vol. 3, pp. 541–548, May 1988.

[41] J. J. Allemong, L. Radu, and A. M. Sasson, "A Fast and Reliable State Estimation Algorithm for AEP's New Control Center," *IEEE Transactions on Power Apparatus and Systems*, vol. PAS-101, pp. 933–944, April 1982.

[42] A. Monticelli and A. Garcia, "Fast decoupled state estimators," *IEEE Transactions on Power Systems*, vol. 5, pp. 556–564, May 1990.

[43] J. Zhao, L. Mili, and R. C. Pires, "Statistical and numerical robust state estimator for heavily loaded power systems," *IEEE Transactions on Power Systems*, vol. 33, pp. 6904–6914, Nov 2018.

[44] S. Soltan, M. Yannakakis, and G. Zussman, "Power Grid State Estimation Following a Joint Cyber and Physical Attack," *IEEE Transactions on Control of Network Systems*, vol. 5, pp. 499–512, March 2018.

[45] M. D. Butala, M. Kazerooni, J. J. Makela, F. Kamalabadi, J. L. Gannon, H. Zhu, and T. J. Overbye, "Modeling geomagnetically induced currents from magnetometer measurements: Spatial scale assessed with reference measurements," *Space Weather*, vol. 15, pp. 1357–1372, Oct 2017.

[46] J. W. Gjerloev, "The SuperMAG data processing technique," *Journal of Geophysical Research: Space Physics*, vol. 117, no. A9, 2012.

[47] D. H. Boteler, L. Trichtchenko, R. Pirjola, J. Parmelee, S. Souksaly, A. Foss, and L. Marti, "Real-time simulation of geomagnetically induced currents," in *2007 7th International Sym-*

posium on Electromagnetic Compatibility and Electromagnetic Ecology, pp. 261–264, June 2007.

[48] J. Qiao, Q. Liu, and Y. Zhang, "Design of geomagnetic induction current monitoring and early warning system based on cloud server," in *2019 14th IEEE Conference on Industrial Electronics and Applications (ICIEA)*, pp. 1552–1556, June 2019.

[49] S. Watari, "Estimation of geomagnetically induced currents based on the measurement data of a transformer in a Japanese power network and geoelectric field observations," *Earth, Planets and Space*, vol. 67, p. 77, May 2015.

[50] M. Kazerooni, H. Zhu, K. Shetye, and T. J. Overbye, "Estimation of geoelectric field for validating geomagnetic disturbance modeling," in *2013 IEEE Power and Energy Conference at Illinois (PECI)*, pp. 218–224, Feb 2013.

[51] A. Rezaei-Zare, "Reactive Power Loss Versus GIC Characteristic of Single-Phase Transformers," *IEEE Transactions on Power Delivery*, vol. 30, no. 3, pp. 1639–1640, 2015.

[52] X. Dong, Y. Liu, and J. G. Kappenman, "Comparative analysis of exciting current harmonics and reactive power consumption from GIC saturated transformers," in *2001 IEEE Power Engineering Society Winter Meeting. Conference Proceedings (Cat. No.01CH37194)*, vol. 1, pp. 318–322 vol.1, Jan 2001.

[53] P. Ren and A. Abur, "Obtaining partial solutions for divergent state estimation problems in large power systems," in *2018 IEEE International Symposium on Circuits and Systems (ISCAS)*, pp. 1–5, May 2018.

[54] S. Pajic and K. A. Clements, "Power system state estimation via globally convergent methods," *IEEE Transactions on Power Systems*, vol. 20, pp. 1683–1689, Nov 2005.

[55] K. D. Jones, J. S. Thorp, and R. M. Gardner, "Three-phase linear state estimation using phasor measurements," in *2013 IEEE Power Energy Society General Meeting*, pp. 1–5, July 2013.

[56] L. Zhang, A. Bose, A. Jampala, V. Madani, and J. Giri, "Design, testing, and implementation of a linear state estimator in a real power system," *IEEE Transactions on Smart Grid*, vol. 8, pp. 1782–1789, July 2017.

[57] T. Yang, H. Sun, and A. Bose, "Transition to a two-level linear state estimator—part II: Algorithm," *IEEE Transactions on Power Systems*, vol. 26, pp. 54–62, Feb 2011.

[58] Boteler, David, "Methodology for simulation of geomagnetically induced currents in power systems," *J. Space Weather Space Clim.*, vol. 4, p. A21, 2014.

[59] J. L. Gannon, A. B. Birchfield, K. S. Shetye, and T. J. Overbye, "A Comparison of Peak Electric Fields and GICs in the Pacific Northwest Using 1-D and 3-D Conductivity," *Space Weather*, vol. 15, no. 11, pp. 1535–1547, 2017.

[60] United States Geological Survey, "Regional conductivity maps," *https://geomag.usgs.gov/conductivity/*. Last accessed on 04/30/20.

[61] C. Klauber, K. Shetye, T. J. Overbye, and K. Davis, "A GIC Estimator for Electric Grid Monitoring During Geomagnetic Disturbances," *IEEE Transactions on Power Systems*, pp. 1–9, 2020.

[62] "Texas 2000-Bus System," *https://electricgrids.engr.tamu.edu/electric-grid-test-cases*. Last accessed on 03/01/20.

[63] T. V. Cutsem, M. Ribbens-Pavella, and L. Mili, "Bad Data Identification Methods In Power System State Estimation-A Comparative Study," *IEEE Transactions on Power Apparatus and Systems*, vol. PAS-104, no. 11, pp. 3037–3049, 1985.

[64] E. Handschin, F. C. Schweppe, J. Kohlas, and A. Fiechter, "Bad data analysis for power system state estimation," *IEEE Transactions on Power Apparatus and Systems*, vol. 94, no. 2, pp. 329–337, 1975.

[65] A. Garcia, A. Monticelli, and P. Abreu, "Fast decoupled state estimation and bad data processing," *IEEE Transactions on Power Apparatus and Systems*, vol. PAS-98, no. 5, pp. 1645–1652, 1979.

[66] T. V. Cutsem, M. Ribbens-Pavella, and L. Mili, "Hypothesis testing identification: A new method for bad data analysis in power system state estimation," *IEEE Transactions on Power Apparatus and Systems*, vol. PAS-103, no. 11, pp. 3239–3252, 1984.

[67] H. M. Merrill and F. C. Schweppe, "Bad data suppression in power system static state estimation," *IEEE Transactions on Power Apparatus and Systems*, vol. PAS-90, no. 6, pp. 2718–2725, 1971.

[68] T. L. Baldwin, L. Mili, M. B. Boisen, and R. Adapa, "Power system observability with minimal phasor measurement placement," *IEEE Transactions on Power Systems*, vol. 8, no. 2, pp. 707–715, 1993.

[69] K. A. Clements, "Observability methods and optimal meter placement," *International Journal of Electrical Power & Energy Systems*, vol. 12, no. 2, pp. 88–93, 1990.

[70] G. R. Krumpholz, K. A. Clements, and P. W. Davis, "Power system observability: A practical algorithm using network topology," *IEEE Transactions on Power Apparatus and Systems*, vol. PAS-99, no. 4, pp. 1534–1542, 1980.

[71] M. R. Irving, R. C. Owen, and M. J. H. Sterling, "Power-system state estimation using linear programming," *Proceedings of the Institution of Electrical Engineers*, vol. 125, no. 9, pp. 879–885, 1978.

[72] P. Virtanen, R. Gommers, T. E. Oliphant, M. Haberland, T. Reddy, D. Cournapeau, E. Burovski, P. Peterson, W. Weckesser, J. Bright, S. J. van der Walt, M. Brett, J. Wilson, K. Jarrod Millman, N. Mayorov, A. R. J. Nelson, E. Jones, R. Kern, E. Larson, C. Carey, İ. Polat, Y. Feng, E. W. Moore, J. Vand erPlas, D. Laxalde, J. Perktold, R. Cimrman, I. Henriksen, E. A. Quintero, C. R. Harris, A. M. Archibald, A. H. Ribeiro, F. Pedregosa, P. van Mulbregt, and S. . . Contributors, "SciPy 1.0: Fundamental Algorithms for Scientific Computing in Python," *Nature Methods*, vol. 17, pp. 261–272, 2020.

[73] A. B. Birchfield, T. Xu, K. M. Gegner, K. S. Shetye, and T. J. Overbye, "Grid structural characteristics as validation criteria for synthetic networks," *IEEE Transactions on Power*

Systems, vol. 32, no. 4, pp. 3258–3265, 2017.

[74] A. Monticelli and A. Garcia, "Reliable bad data processing for real-time state estimation," *IEEE Transactions on Power Apparatus and Systems*, vol. PAS-102, no. 5, pp. 1126–1139, 1983.

[75] S. Wang, J. Zhao, Z. Huang, and R. Diao, "Assessing Gaussian Assumption of PMU Measurement Error Using Field Data," *IEEE Transactions on Power Delivery*, vol. 33, no. 6, pp. 3233–3236, 2018.

[76] R. MíDnguez, A. J. Conejo, and A. S. Hadi, *Non Gaussian State Estimation in Power Systems*, pp. 141–156. Boston: Birkhäuser Boston, 2008.

[77] T. Ahmad and N. Senroy, "Statistical Characterization of PMU Error for Robust WAMS Based Analytics," *IEEE Transactions on Power Systems*, vol. 35, no. 2, pp. 920–928, 2020.

[78] D. Goodrich, "Geomagnetically Induced Currents Measured in BPA Transformers, Near-Real-Time," *Bonneville Power Administration/BPA Transmission,* `https://transmission.bpa.gov/Business/Operations/gic/gic.aspx`. Last accessed 05/15/20.

[79] "The aurora and solar activity archive: November 2019." `https://www.spaceweatherlive.com/en/archive/2019/11`, 2019.

[80] C. M. Ngwira, A. A. Pulkkinen, E. Bernabeu, J. Eichner, A. Viljanen, and G. Crowley, "Characteristics of extreme geoelectric fields and their possible causes: Localized peak enhancements," *Geophysical Research Letters*, vol. 42, no. 17, pp. 6916–6921, 2015.

[81] Computation Physics, Inc., "What is AVERT?," `http://gmddev.cpi.com/hazard.html`. Last accessed 07/01/20.

[82] R. Horton and D. H. Boteler, "Calculation of GIC in Bulk Power Systems," in *CIGRE US National Committee 2013 Grid of the Future Symposium*, 2013.

[83] F. Simpson and K. Bahr, *Practical Magnetotellurics*. Cambridge University Press, 2005.

[84] "Current space weather conditions: Geoelectric field 1-minute," *Space Weather Prediction Center,* https://www.swpc.noaa.gov/products/geoelectric-field-1-minute, 2020. Last accessed on 05/15/20.

[85] T. J. Overbye, Z. Mao, K. S. Shetye, and J. D. Weber, "An interactive, extensible environment for power system simulation on the PMU time frame with a cyber security application," in *2017 IEEE Texas Power and Energy Conference (TPEC)*, pp. 1–6, Feb 2017.

[86] T. J. Overbye, Z. Mao, A. Birchfield, J. D. Weber, and M. Davis, "An Interactive, Stand-Alone and Multi-User Power System Simulator for the PMU Time Frame," in *2019 IEEE Texas Power and Energy Conference (TPEC)*, pp. 1–6, Feb 2019.

[87] T. J. Overbye, E. M. Rantanen, and S. Judd, "Electric power control center visualization using geographic data views," in *2007 iREP Symposium - Bulk Power System Dynamics and Control - VII. Revitalizing Operational Reliability*, pp. 1–8, 2007.

[88] Z. Mao and B. Thayer, "Easy SimAuto (ESA)." https://github.com/mzy2240/ESA, 2019.

[89] T. J. Overbye, J. Wert, A. Birchfield, and J. D. Weber, "Wide-Area Electric Grid Visualization Using Pseudo-Geographic Mosaic Displays," in *2019 North American Power Symposium (NAPS)*, pp. 1–6, 2019.